Spectrum Sensing and Occupancy Prediction for Cognitive Machine-to-Machine Wireless Networks

Eleftherios Chatziantoniou

Spectrum Sensing and Occupancy Prediction for Cognitive Machine-to-Machine Wireless Networks

Eleftherios Chatziantoniou

Department of Computer Science & Technology

University of Bedfordshire

A thesis submitted to the University of Bedfordshire, in partial fulfilment of the requirements for the degree of

Doctor of Philosophy (PhD)

December 2014

Abstract

The rapid growth of the Internet of Things (IoT) introduces an additional challenge to the existing spectrum under-utilisation problem as large scale deployments of thousands devices are expected to require wireless connectivity. Dynamic Spectrum Access (DSA) has been proposed as a means of improving the spectrum utilisation of wireless systems. Based on the Cognitive Radio (CR) paradigm, DSA enables unlicensed spectrum users to sense their spectral environment and adapt their operational parameters to opportunistically access any temporally unoccupied bands without causing interference to the primary spectrum users. In the same context, CR inspired Machine-to-Machine (M2M) communications have recently been proposed as a potential solution to the spectrum utilisation problem, which has been driven by the ever increasing number of interconnected devices. M2M communications introduce new challenges for CR in terms of operational environments and design requirements. With spectrum sensing being the key function for CR, this thesis investigates the performance of spectrum sensing and proposes novel sensing approaches and models to address the sensing problem for cognitive M2M deployments.

In this thesis, the behaviour of Energy Detection (ED) spectrum sensing for cognitive M2M nodes is modelled using the two-wave with diffuse power fading model. This channel model can describe a variety of realistic fading conditions including worse than Rayleigh scenarios that are expected to occur within the operational environments of cognitive M2M communication systems. The results suggest that ED based spectrum sensing fails to meet the sensing requirements over worse than Rayleigh conditions and consequently requires the signal-to-noise ratio (SNR) to be increased by up to 137%. However, by employing appropriate diversity and node cooperation techniques, the sensing performance can be improved by up to 11.5 dB in terms of the required SNR. These results are particularly useful in analysing the effects of severe fading in cognitive M2M systems and thus they can be used to design efficient CR transceivers and to quantify the trade-offs between detection performance and energy efficiency.

A novel predictive spectrum sensing scheme that exploits historical data of past sensing events to predict channel occupancy is proposed and analysed. This approach allows CR terminals to sense only the channels that are predicted to be unoccupied rather than the whole band of interest. Based on this approach, a spectrum occupancy predictor is developed and experimentally validated. The proposed scheme achieves a prediction accuracy of up to 93% which in turn can lead to up to 84% reduction of the spectrum sensing cost.

Furthermore, a novel probabilistic model for describing the channel availability in both the vertical and horizontal polarisations is developed. The proposed model is validated based on a measurement campaign for operational scenarios where CR terminals may change their polarisation during their operation. A Gaussian approximation is used to model the empirical channel availability data with more than 95% confidence bounds. The proposed model can be used as a means of improving spectrum sensing performance by using statistical knowledge on the primary users occupancy pattern.

Declaration

Unless otherwise acknowledged, the content of this thesis being submitted for the degree of *Doctor of Philosophy (PhD)* at the University of Bedfordshire is the author's original work. This work has not been submitted before for any other degree at this or any other university.

Eleftherios Chatziantoniou

Signature: .....

Date: .....

Acknowledgements

First of all I would like to thank my supervisor Professor Ben Allen for giving me the opportunity to join the Centre for Wireless Research as a bursary research student. His continuous and consistent guidance, support and valuable suggestions were particularly important to the successful completion of my research. Special thanks go to my second supervisor Dr. Vladan Velisavljvic for attending countless meetings and providing me with crucial feedback. I would also like to express my gratitude to HMGCC for the financial contribution to this project, and Mr. Dene Hedgens in particular, for a number of productive meetings and fruitful discussions.

I would also like to thank Dr. Petros Karadimas for the informal meetings and discussions on different research topics of wireless communications as well as Professor David Gunton for his valuable feedback. Special thanks go to Miss Elena Chatziantoniou for proofreading the final version of this manuscript. Many thanks to all my CWR colleagues in D109 for the relaxing breaks and of course to the University's cafeteria for providing me with more than enough espresso to keep me focused every morning for the last three years.

Last but not least, I am deeply thankful to my family, my father George, my mother Maria, and my sister Elena for being there for me, despite the physical distance between us. I am specially grateful to my parents, for the education they have provided me with, and for teaching me the most important lessons that cannot be taught in any university.

Contents

Abbreviations

2G	Second Generation
3G	Third Generation
3GPP	Third Generation Partnership Project
ACF	Autocorrelation Function
ADC	Analog to Digital Converter
ANN	Artificial Neural Network
AR	Autoregressive
ARMA	Autoregressive Moving Average
AWGN	Additive White Gaussian Noise
BP	Back-propagation
BWA	Baum-Welch Algorithm
CFAR	Constant False Alarm Rate
CFD	Cyclostationary Feature Detection
CLT	Central Limit Theorem
CP	Cyclic Prefix
CR	Cognitive Radio
DC	Duty Cycle
DL	Down-link
DARPA	Defense Advanced Research Projects Agency
DSA	Dynamic Spectrum Access
DTV	Digital Television
EB	Exa Byte
ED	Energy Detection
EGC	Equal Gain Combining

ETSI	European Telecommunications Standards Institute
FCC	Federal Communications Commission
GSM	Global System for Communications
GUI	Graphical User Interface
H2H	Human to Human
HMM	Hidden Markov Model
HMP	Hidden Markov Process
i.i.d	independent and identically distributed
ICT	Information and Communications Technologies
IEEE	Institute of Electrical and Electronic Engineering
IoT	Internet of Things
ISM	Industrial Scientific and Medical
ITS	Intelligent Transportation Systems
LLR	Log Likelihood Ratio
LTE	Long Term Evolution
M2M	Machine-to-Machine
MA	Moving Average
MAC	Medium Access Control
MFD	Matched Filter Detection
MGF	Moment Generation Function
MIMO	Multiple Input Multiple Output
MLE	Maximum Likelihood Estimation
MLP	Multi Layer Perception
MRC	Maximal Ratio Combining
NSF	Maximal Ratio Combining
OFCOM	National Science Foundation
OFDMA	Orthogonal Frequency-Division Multiple Access
OFDM	Orthogonal Frequency-Division Multiplexing
OSI	Open System Interconnection
OSTBC	Orthogonal Space-time Block Codes
PACF	Partial Autocorrelation Function

POMDP	Partial Observable Markov Decision Process
PDF	Probability Density Function
PHY	Physical
PSD	Power Spectral Density
PU	Primary User
QoS	Quality of Service
RF	Radio Frequency
RADAR	Radio Detection and Ranging
RFID	Radio Frequency Identification
ROC	Receiver Operating Characteristics
SDR	Software Defined Radio
SLS	Square Law Selection
SNR	Signal-to-Noise Ratio
SU	Secondary User
TDD	Time Division Duplex
TV	Television
TVBD	Television Band Devices
TWDP	Two Wave with Diffused Power
UL	Uplink
USRP	Universal Software Radio Peripheral
UMTS	Universal Mobile Telecommunications System
UWB	Ultra Wideband
V2V	Vehicle-to-Vehicle
WiFi	Wireless Fidelity
WiMax	Wireless Interoperability for Microwave Access
WLAN	Wireless Local Area Network
WRAN	Wireless Regional Area Network
WSN	Wireless Sensor Network
XG	Next Generation Communications Programm
XPD	Cross-polarisation Discrimination

List of Symbols

a	P_{fa} constraint
a_{ij}	Transition probabilities
$\mathbf{A}$	Transition matrix
b_{ij}	Emission probabilities
$\mathbf{B}$	Emission matrix
b	P_{md} constraint
$C_{sensing}$	Sensing cost
d	Degree of differencing
d	Prediction span in Chapters 4 and 5
e_{sense}	Sensing energy per time unit
f_{start}	Start frequency
f_{stop}	Stop frequency
F	Frequency spectrum
D_i	Binary decision
$erfc$	Complementary Error function
$erfc^{-1}$	Inverse Complementary error function
$\mathbb{E}$	Mathematical expectation
E_p	Pilot signal's energy
E_s	Energy per symbol
$f_r(r)$	PDF of fading envelope
g	Channel gain
h	Impulse response
H_0	Null hypothesis

H_1	Alternative hypothesis
I_0	Zero order modified Bessel function
k	Markov order
k	Number of BWA iterations in Chapter 4
K	Average specular power and diffuse power ratio
L	Number of diversity branches
m	Number of cooperative users
M	TWDP PDF approximation order
M	Number of observable HMM states in Chapter 4
n	Sample index
N	Number of samples
N	Number of hidden HMM states in Chapter 4
N_{cd}	Number of correct detections
N_{ch}	Number of shared frequency channels
N_{fd}	Number of false detections
N_{free}	Number of available channels
N_{H_0}	Number of times under H_0
N_{H_1}	Number of times under H_1
N_{pred}	Number of channels predicted as unoccupied
N_{PU}	Number of PUs
N_{sense}	Number of sensed channels
N_{SU}	Number of SUs
N_{total}	Total number of channels
N_0	Noise power spectral density
$\mathcal{N}$	Gaussian function
O	Observation sequence
o	Observation symbol
p	AR order
$p_{idleness}$	Idleness probability
P	Probability
P_d	Probability of detection

$\bar{P}_{d_{TWDP}}$	Average probability of detection over TWDP fading
P_e	Error probability
P_{fa}	Probability of false alarm
$P_{i,t}$	Received signal's power
P_{md}	Probability of missed detection
q	MA order
Q	Gaussian Q function
Q^{-1}	Inverse Gaussian Q function
$\bar{Q}_d$	Average probability of cooperative detection
$\bar{Q}_f a$	Average probability of cooperative detection
Q_m	Marcum Q function
r	Signal's envelope
r_y	Autocorrelation function
r^2	Coefficient of determination
R	Resolution bandwidth
R_y	Fourier Coefficient
S	State space
$S_{t,i}$	Channel occupancy status
S_y	Cyclic Spectral Density
t	Time index
T	Observation interval
T_{ED}	Energy Detection test statistic
T_{MFD}	Matched Filter Detection test statistic
T_c	CP length
T_d	OFDM signal length
T_x	Test statistic
u	Time-bandwidth product
v	Hidden sequence symbol
V	Voltage magnitude of a specular wave
V	HMM Emission space in Chapter 4
w	Noise

W	Bandwidth
x	Transmitted signal
x_t	Hidden state
$\hat{x}_t$	Predicted state
$\hat{X}_p$	Pilot signal
X_t	Hidden process
y	Received signal
y_i	Observed variable
$\bar{y}_i$	Estimated variable
y_{SLS}	SLS decision statistics
Y_t	Observation process
z	Spectrum occupancy
α	Cyclic frequency
α_i	TWDP PDF approximation coefficient
α_{ij}	Forward probabilities
β_{ij}	Backward probabilities
γ	Instantaneous SNR
$\bar{\gamma}$	Average SNR
Γ	Gamma function
$\delta_t(i)$	Viterbi path
Δ	Relative strength of specular waves
ϵ_t	Error term
ζ	Fusion centre output
η	CFD detection threshold
$\eta_{sensing}$	Sensing efficiency
η_1	Lower LLR bound
η_2	Upper LLR bound
κ	Time-shift
λ	Detection threshold
λ	HMM parameters in Chapters 4 and 5
λ_{CFAR}	CFAR detection threshold

λ_{opt}	Optimal detection threshold
λ^*	Optimal HMM parameters
Λ	LLR test statistic
μ	Time duration of a state
π	Initial state distribution
ρ	Autocorrelation coefficient
σ_N	Equipment noise variance
σ_w	Noise variance
σ_x	Signal variance
σ^2	Average power of the diffused waves
τ	Time lag
τ_{sense}	Sensing time
ϕ	Signal's instantaneous phase
ϕ_i	AR coefficient
χ^2	Chi-squared test statistic
ω	Cyclic spectrum

List of Figures

List of Tables

Publications

Journal Articles

- E. Chatziantoniou, B. Allen, V. Velisavljevic, "Energy detection based spectrum sensing over two-wave and diffuse power fading channels," *IEEE Transactions on Vehicular Technology*, Under review (submitted in May 2015).

- E. Chatziantoniou, B. Allen, V. Velisavljevic, "Threshold Optimization for Energy Detection-Based Spectrum Sensing Over Hyper-Rayleigh Fading Channels," *Communications Letters, IEEE*, vol.19, no.6, pp.1077-1080, Jun. 2015.

- E. Chatziantoniou, B. Allen, V. Velisavljevic, "Performance Analysis of energy detection over hyper-Rayleigh fading channels," *Journal of Engineering, IET*, Jan. 2015.

Conference Papers

- E. Chatziantoniou, B. Allen, V. Velisavljevic, "A spectrum occupancy prediction platform for cognitive radio applications," in *NI days 2014 - Graphical Design Conference*, Nov. 2014.

- E. Chatziantoniou, B. Allen, V. Velisavljevic, "An empirical polarisation domain channel availability model for cognitive radio," in *International Symposium on Personal Indoor and Mobile Communications (PIMRC), 2014 IEEE 25th International Symposium on,* pp. 643-647, Sep. 2014.

- E. Chatziantoniou, B. Allen, V. Velisavljevic, "A statistical framework for channel availability modelling in the polarisation domain," in *Antennas, Wireless and Electromagnetics, 2014 IET 2nd Colloquium on,* pp. 1-16, May 2014.

- E. Chatziantoniou, B. Allen, V. Velisavljevic, "HMM-based spectrum occupancy predictor for energy efficient cognitive radio," in *International Symposium on Personal Indoor and Mobile Communications (PIMRC), 2013 IEEE 24th International Symposium on,* pp. 601-605, Sep. 2013.

- E. Chatziantoniou, V. Velisavljevic, B. Allen, "Spectrum occupancy prediction for cognitive radio using an HMM," in *COST IC1004, 5th MC and Scientific meeting,* no. TD(12)05048, Sep. 2012.

Chapter 1 | *Introduction*

1.1 The Spectrum Utilisation Problem

Since the 1920' s, the assumption that any new wireless transmitter will interfere with existing users has led to a centralised regulation policy for the Radio Frequency (RF) spectrum by governmental authorities such as the Office for Communications (Ofcom) in the United Kingdom and the Federal Commission for Communications (FCC) in the United States [1]. Under such an allocation policy, frequency bands are statically assigned to wireless systems on a long term basis over large geographical areas. As a result, every wireless system, from cellphones to remote garage-door openers, requires an exclusive licence to operate in a particular frequency band. This approach makes the RF spectrum one of the most tightly regulated natural resources of all time.

With reference to the UK frequency allocation chart as in [2], shown in Figure 1.1, a shortage on available frequency bands for new wireless systems is observed. However, spectrum activity measurements have indicated that large portions of the spectrum remain unused for long periods of time especially in the spectrum below 6 GHz [3], [4]. Therefore, in reality, the spectrum scarcity problem lies on the inefficient spectrum usage that stems from both technical and regulatory reasons such as rigid spectrum allocation policies, fixed radio functions and limited network coordination.

On the other hand, according to a recent report the global mobile data traffic is expected to grow exponentially to 15.9 Exa Bytes (EB) per month with nearly a 6-fold increase over 2014, as shown in Figure 1.2 [5]. The main factor for the global mobile traffic growth is the proliferation of mobile devices driven by the advanced services they provide.

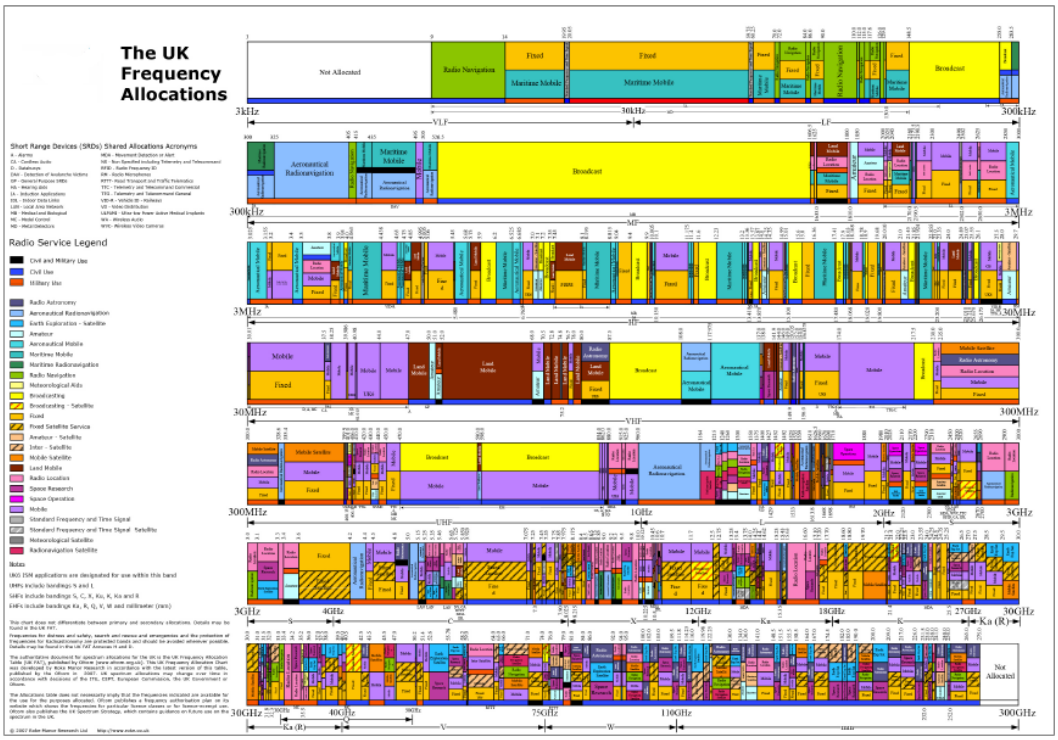

Figure 1.1: UK frequency allocation chart [2].

With the spectrum under-utilisation problem on the one hand and the increasing demand for bandwidth on the other, efficient spectrum utilisation has become even more essential. To date, several techniques have already been used to improve spectrum utilisation such as Multiple Input Multiple Output (MIMO) technology and Orthogonal Frequency-Division Multiple Access (OFDMA) [6], [7]. However, these techniques are being applied within existing frequency allocation policies and thus, their performance is still limited by spectrum availability.

To this end, Dynamic Spectrum Access (DSA) [8] has been proposed as a new paradigm for accessing the RF spectrum. DSA is expected to improve spectrum utilisation and increase the spectrum efficiency of wireless systems by allowing unlicensed users to opportunistically access the licensed frequency bands that are temporally unoccupied. This can be achieved by allowing two different types of users to co-exist in the same network:

- Primary Users (PUs)
- Secondary Users (SUs).

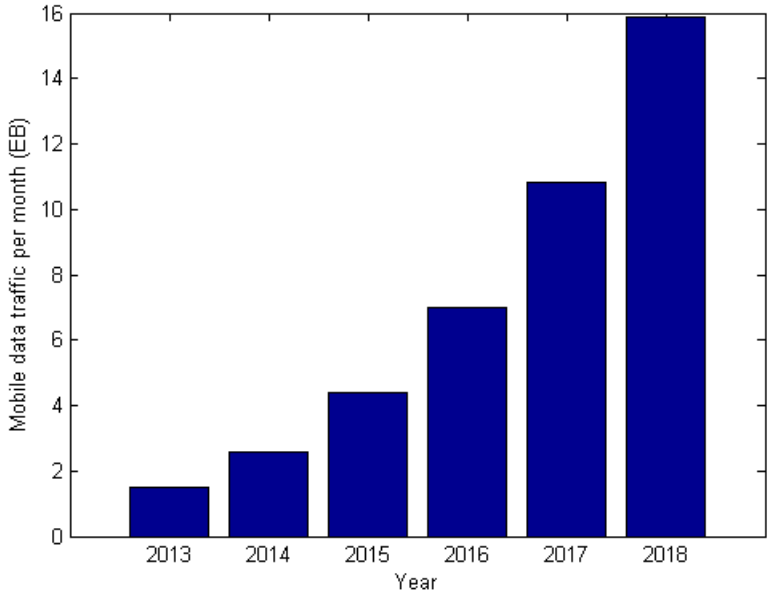

Figure 1.2: Mobile data traffic prediction from 2013 to 2018 [4].

PUs are conventional radios, with higher priority on accessing the licensed RF spectrum. Such users may operate within any wireless technology such as Global System for Mobile Communications (GSM), Worldwide Interoperability for Microwave Access (WiMax), Long Term Evolution (LTE) as well as wireless microphone systems and Wireless Local Area Network (WLAN), etc. On the other hand, SUs are "smart" radios able to opportunistically access any temporally available band within the licensed spectrum and vacate it as soon as a PU needs to access it. An example of the DSA concept is illustrated in Figure 1.3 where the SU is shown to transmit within different temporally available frequency bands of a given spectrum.

Cognitive Radio (CR) is the key enabling technology for DSA systems [9]. CR technology is considered to be an advancement of Software Defined Radio (SDR) [9] as it enables the SUs to monitor their spectral environment, adjust their operating parameters (e.g. frequency, transmission power, modulation

scheme) in real-time and access any available channels subject to their Quality of Service (QoS) requirements.

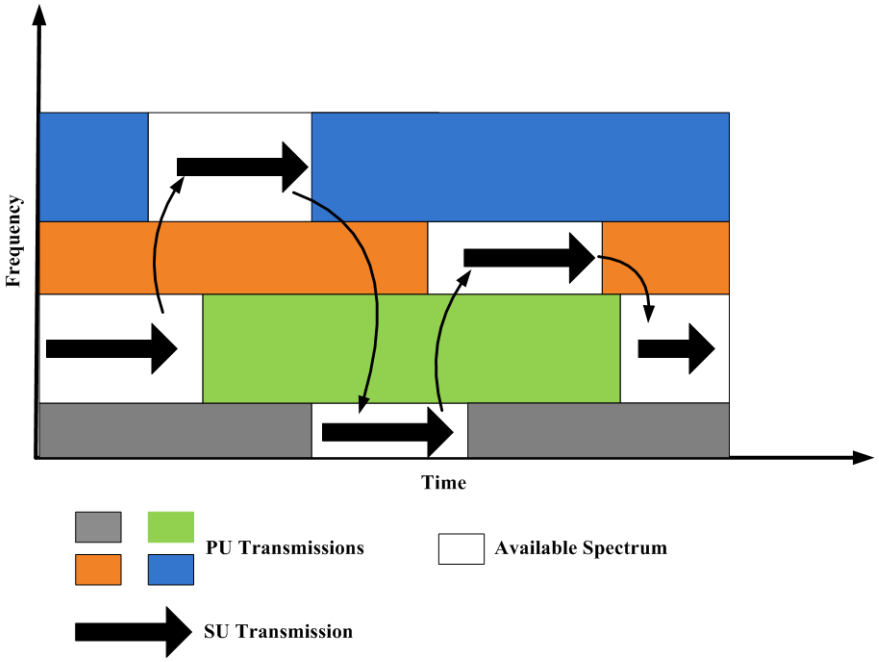

Figure 1.3: Example of the DSA concept.

1.2 Cognitive Radio and Machine-to-Machine Communications

Machine-to-machine (M2M) communication systems are expected to enable devices to communicate autonomously without any human interaction. In thins context, M2M are systems are considered as the practical realisation of the Internet of Things (IoT). The IoT concept is envisioned as an extended network of heterogeneous "things" where physical and virtual objects are interconnected. Such deployments are expected to provide intelligent wireless services in a wide range of smart sensing applications such as smart buildings, vehicular automation, public health, manufacturing etc. For example, the concept of smart city suggests that intelligent buildings will use M2M technology for automation and energy management. More specifically, a number of "smart" objects within the building will monitor the energy consumption

and control the functionality of home appliances such as Television (TV) sets, air conditioners, etc. Furthermore, wireless M2M communications are being used by Intelligent Transportation Systems (ITS) to exchange information from road-based and vehicle-based sensors for traffic monitoring and electronic tolling. Therefore, given the increasing interest in IoT, M2M communications are envisioned as a very important sector of the future Information and Communications Technologies (ICT) market. However, with 50 billion devices to be interconnected by 2020, an additional challenge will be posed to the existing spectrum utilisation problem [10]. In this context, CR technology has been proposed for improving the spectrum efficiency of future M2M systems.

Different from traditional wireless systems M2M communications introduce new challenges and requirements owing to their operational environments and design specifications. Sensing and monitoring is considered as the main application space of M2M systems. Therefore, such schemes typically consist of statically deployed sensors, on or within the environment being monitored. More specifically, the use of sensing devices inside enclosed structures such as aircraft, vehicles, and shipping containers has been explored as a means of proactive maintenance and security. One of the basic issues of such environments is that their wave propagation properties are fundamentally different because of their small dimensions and metallic structure, which result in high number of multipath components. Hence, the performance of CR technology needs to be analysed over such non-traditional fading environments.

Furthermore, M2M nodes are characterised as low-cost, energy-constrained devices with high energy efficiency requirements. However, cognitive M2M system's energy consumption is expected to increase because of the additional cognitive functions including: spectrum sensing; spectrum decision; spectrum sharing; and spectrum mobility. Thus, given that energy consumption will be further increased as CR functions are going to be integrated in M2M devices, energy efficiency is a key feature of cognitive M2M systems.

1.3 Scope of Thesis

CR is a broad and multidisciplinary technology that involves different research aspects of wireless communications such as antenna design, information theory, Medium Access Control (MAC) protocol design, routing and SDR architectures. As a result, cognition can be integrated in all layers of a protocol stack such as the Open Systems Interconnection (OSI) model. Hence, efficiency can be achieved through any level of the OSI model. However, the focus of this thesis lies on the PHY-layer of CR and more specifically on spectrum sensing. Spectrum sensing is one of the most essential components of CR and refers to the process of monitoring the radio spectrum in order to dynamically access it without interfering with the primary system.

Spectrum sensing is fundamentally influenced by the fading characteristics of the wireless channel. For example, due to the effects of multipath or shadowing, an SU may not distinguish between a deeply faded channel and an unoccupied one. In this context, the performance analysis of spectrum sensing and the investigation of potential mitigation techniques for fading is the first step of determining the spectrum sensing requirements and designing efficient CR receivers. Hence, the study of spectrum sensing over fading channels that best describe the new landscape of M2M deployments, i.e. short range communications in enclosed structures and confined environment, is essential.

Another solution to energy efficient CR lies in minimising the time and energy expenditure of the spectrum sensing process. This can be achieved by using appropriate knowledge of the PU occupancy statistics in order to learn and predict the channel availability at future time instants. To this end, the use of prior knowledge of the spectrum occupancy statistics and PU occupancy patterns is used to determine the channels to be sensed in future sensing events. Therefore, by adjusting the sensing parameters according to spectrum occupancy prediction, the sensing task can be avoided for channels that are predicted to be occupied. This in turn can reduce the sensing time and energy consumption, hence, maximise battery life of cognitive M2M nodes.

In this context, the main objective of this thesis is to investigate fading conditions that affect the sensing performance and propose sensing methods that can improve the sensing performance in terms of energy efficiency for future wireless systems such as cognitive M2M communications. The objectives of this study can be summarised as follows:

- To analyse the detection performance of different spectrum sensing schemes over fading conditions that are expected to occur in confined environments and enclosed structures.
- To develop a predictive spectrum sensing scheme that combines PHY-layer spectrum sensing and PU occupancy statistics as a means of improving the sensing performance in terms of sensing time and energy consumption.
- To develop a channel availability model for the polarisation domain that can describe the perceived channel availability by mobile CR nodes.

1.4 Key Contributions

The main contributions of this thesis are summarised as follows:

- In Chapter 3 a novel closed form expression for the average probability of single user detection for Energy Detection (ED)-based spectrum sensing over Two-Wave with Diffuse Power (TWDP) fading channels is derived and validated. This expression provides a new insight into the performance of spectrum sensing over worse than Rayleigh fading conditions. The derived expression can be used to model the behaviour of ED-based spectrum sensing over fading conditions that occur in enclosed environments for a variety of emerging communication systems such as cognitive sensor and wireless M2M deployments.
- By extending the derived expression, simple yet accurate closed form expressions for cooperative spectrum sensing and Square Law Selection

(SLS) diversity reception are deduced in Chapter 3. Based on these expressions, the performance of diversity reception and cooperative spectrum sensing are analysed over different fading scenarios. Furthermore, the optimal detection threshold for ED-based spectrum sensing is analytically determined for improving the performance over hyper-Rayleigh fading channels.

- The framework of a Hidden Markov Model (HMM) for spectrum sensing and occupancy prediction in the temporal domain is described in Chapter 4. More specifically, it is shown how the spectrum sensing problem can be formulated as an HMM and how the proposed model can be further exploited to model and predict spectrum occupancy for CR based on historical spectrum sensing data.

- The occupancy model is evaluated experimentally using real-world data over cellular and the Industrial Scientific and Medical (ISM)frequency bands in Chapter 5. Furthermore, a smart spectrum sensing scheme based on the HMM-based spectrum occupancy predictor is proposed. The predictive spectrum sensing scheme is proposed as a means of improving the sensing performance and reducing the sensing time and energy consumption by enabling the CR nodes to sense the channels that are predicted to be unoccupied rather than the entire band of interest. The performance of the proposed is analysed in terms of its prediction performance for one-step and multi-step ahead predictions.

- An empirical channel availability model for the polarisation domain is developed in Chapter 6. The proposed model forms a statistical framework for the channel availability in both the vertical and horizontal polarisation for CR systems .

1.5 Thesis outline

The structure of this thesis is organised as follows:

- **Chapter 2:** A literature review on CR technology as a realisation of the DSA concept is proved. Key functions, current and emerging applications, and standarisation efforts of CR technology are presented. State-of-the-art spectrum sensing and spectrum occupancy prediction algorithms are introduced and compared. Finally, the need for efficient CR and hence spectrum sensing for future application spaces is discussed.

- **Chapter 3:** Closed form expressions for the average probability of detection for energy detection based spectrum sensing over Two Wave with diffused power fading channels are derived. Such fading channels can model the sensing behaviour of CR nodes that operate in enclosed environments. The TWDP fading statistics are described followed by the derivation of novel closed form expressions for the average probability of detection for ED-based spectrum sensing. The accuracy of the derived expressions is evaluated through simulations.

- **Chapter 4:** An HMM model for spectrum occupancy prediction is introduced. The fundamentals of HMM are presented, including relevant estimation and prediction algorithms that will form the basis of the proposed predictive spectrum sensing approach.

- **Chapter 5:** A smart sensing scheme based on spectrum occupancy prediction is introduced and evaluated. The performance of the HMM-based spectrum occupancy prediction method and the predictive spectrum sensing is analysed based on real-world spectrum activity measurements.

- **Chapter 6:** An empirical channel availability model for the polarisation domain is developed. The proposed model is developed and evaluated based on real-world spectrum occupancy data obtained through a spectrum activity campaign.

- **Chapter 7** A chapter by chapter synopsis of this manuscript provided and the conclusion of this work are drawn. The limitations of this research are discussed and further research directions are proposed.

Chapter 2

Cognitive Radio - A Literature Review

2.1 Introduction

The term "Cognitive Radio" was first introduced in 1999 by Mitola to describe an intelligent radio that can autonomously make decisions through model-based reasoning grounded on information about the radio environment [9]. Since then, the CR paradigm has been adopted as the key enabling technology for DSA [8]. Contrary to the current static spectrum access policy, which allows licensed users to use the radio spectrum exclusively, DSA enables unlicensed users to opportunistically access any unused portions of spectrum within the licensed frequency bands. The DSA concept requires SUs with cognitive capabilities able to monitor their spectral surroundings, adjust their operation parameters, and access the available spectrum whilst causing minimal interference to the primary system. The remainder of this chapter is organised as follows. The CR functions are described in Section 2.2 whereas in Section 2.3 current standarisation efforts and future application of CR to M2M communication systems are discussed. A literature review on state-of-the-art spectrum sensing techniques as well as on energy efficient spectrum sensing methods is presented in Section 2.4 and Section 2.5, respectively. Furthermore, an overview of spectrum occupancy prediction methods is presented in Section 2.6.

2.2 Cognitive Radio

Cognitive capability and reconfigurability are the two distinctive characteristics of CR. Cognitive capability enables CR to be aware and interact with the RF environment, while reconfigurability allows real-time adaptation of its operational parameters in order to efficiently utilise the available spectrum. More specifically, cognitive capability refers to a set of tasks that are performed periodically by the CR, known as the "cognition cycle". This cognition cycle consists of four functions: spectrum sensing; spectrum analysis; spectrum decision; and data transmission [11]. On the other hand, reconfigurability refers to the ability of CR to adjust its operational parameters such as operating frequency, modulation scheme and transmission power in real-time, subject to channel conditions and QoS requirements.

These characteristics can clearly describe the operation of a CR as an autonomous entity. However, the operation of an integrated CR system at network level is described effectively by the CR protocol stack as introduced by [8]. In this context, the operation of a CR system involves four main functions that span from the lowest (PHY-layer) to the highest layer (Application layer) of the OSI model. These four functions include: spectrum sensing; spectrum decision; spectrum sharing; and spectrum mobility.

An illustration of a typical CR system's operation cycle is presented in Figure 2.1. Spectrum sensing enables the CR to monitor the spectrum activity within its surroundings to determine whether a frequency band of interest is occupied or unoccupied by a PU. Then, based on the spectrum sensing result, the SU selects the "best" channel and adjusts its operational parameters accordingly through spectrum decision. The aim of spectrum sharing is to fairly and efficiently share the available spectrum between the SUs based on their QoS requirements. Finally, spectrum mobility refers to the process of vacating and switching to a different channel when the current channel becomes unavailable to the SU.

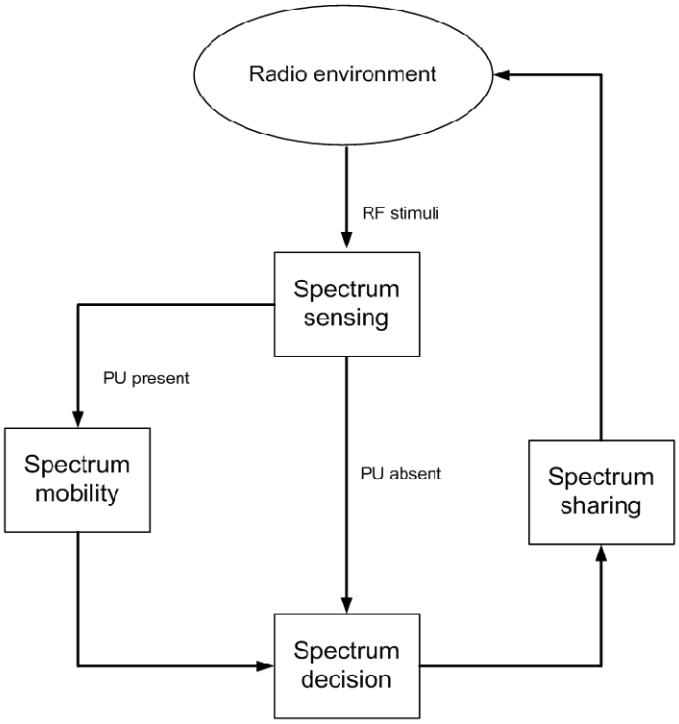

Figure 2.1: CR operation cycle.

2.3 Cognitive Radio Applications

Due to its inherent flexibility and capability of efficient spectrum utilisation, industrial use and standarisation of CR technology have already been initiated by research-funding and defence organisations. More specifically, the Next Generation Communications Program (XG) developed by the Defense Advanced Research Projects Agency (DARPA), focuses on spectrum awareness and adaptive transmission. Both the European Union and the National Science Foundation (NSF) have funded several projects, such as E^3, GENI, ORACLE, SOCRATES and $WINNER+$ that focus on different aspects of CR, DSA and SDR [12]. Furthermore, companies such as Microsoft, Apple, and Google have recently started working on the industrialisation and standardisation of DSA after the release of analogue TV channels by the US government.

2.3.1 Current Cognitive Radio Applications

The Institute of Electrical and Electronic Engineering (IEEE) 802.22 Wireless Regional Area Network (WRAN) standard has been the first attempt to commercialise CR technology [13]. The WRAN standard was finalised in 2011 and designed to deliver wireless broadband services in wide rural areas through opportunistic access within the TV bands in the frequency range of 54-862 MHz. In this standard, TV transmitters and wireless microphones are considered as PUs, while the SUs are known as TV Band Devices (TVBDs). TVBDs are either fixed terminals that operate from known locations or mobile terminals. Fixed TVBDs are required to use a geo-location database, with spectrum sensing as an optional capability, whereas mobile TVBDs are sensing-only devices [14].

CR technology has already been introduced in the form of cognitive femtocells in cellular systems as a means of improving the mobile network's coverage and capacity [15]. Femtocells are low-power basestations that are used to improve the coverage of mobile networks in small indoor environments. However, as the licensed spectrum is shared between femtocells and macrocells, CR technology is employed to minimise the effects of interference to the macrocell network by enabling femtocells to sense and adjust their parameters accordingly [16].

Apart from commercial applications, CR technology has been found to be particularly useful for military and public safety communication systems. Public safety workers and soldiers typically use a number of different wireless devices including: radios; laptops; and mobile cameras along with services that span from voice to text messaging, email, web browsing, database access, and real-time video streaming. Given the public safety bands' spectrum congestion, especially in urban areas, CR technology is used to increase the spectrum efficiency of public safety networks [17]. Military communication systems also make use of CR technology since it facilitates the use of multiple frequency bands and different waveforms in a single device. In addition, CR-enabled devices are used to improve the efficiency of military communications in the

warfare by avoiding jammed frequencies [18].

2.3.2 Future Cognitive Radio Applications

Although there are several communication systems in which CR technology has already been introduced, they are all focused on traditional Human-to-Human (H2H) connectivity. However, as technology evolves, there is a growing interest in a new communication regime that enables machines to communicate autonomously, termed as M2M communications.

It is envisaged that typical M2M systems would involve a large number of "smart" devices with diverse functionalities that generate, exchange and process data without human intervention [19]. M2M communications are considered as the key enabling technology for the practical realisation of the IoT. According to [20], the IoT is envisaged as a network of "things", especially everyday objects such as home appliances, clothes, furniture and vehicles deployed in the physical world for sensing and controlling purposes. Such deployments are expected to be widely utilised in the future for various pervasive applications including: automated manufacturing; healthcare monitoring; intelligent transportation systems; smart power grids; and home multimedia sharing.

Currently, different standardisation activities associated with M2M are in progress, initiated mainly from the Third Generation Partnership Project (3GPP), the European Telecommunications Standards Institute (ETSI), and the IEEE [21] with Weightless being the first standard for white space M2M communication systems. Weightless is a standard designed specifically for machine communications within white space and is expected to enable billions of connected devices worldwide overcoming the traditional problems associated with current wireless standards such as capacity, cost, power consumption and coverage [22]. Weightless standard has been specifically optimised for the requirements of M2M applications. In this context, Weightless standard proposes: Time Division Duplex (TDD) access since it may be challenging to detect a pair of available channels with appropriate duplex separation; rela-

tively long frame duration of the order of 2 seconds; frequency hopping for interference avoidance; broadband downlink (DL); narrowband uplink (UL); and highly efficient MAC-layer protocols to reduce overheads.

M2M nodes are expected to be deployed in a large scale, perhaps with thousands of devices exchanging information [10]. To this end, by allowing opportunistic data transmission, CR technology is expected to alleviate the spectrum congestion problem created by the ever increasing number of communicating devices and innovative services. Additionally, the CR reconfigurability is expected to enable efficient communication between heterogeneous devices with different communication protocols and data formats that are expected to coexist in M2M systems [23].

However, different from traditional wireless communication systems, M2M introduces a new wireless landscape which poses a number of new technical challenges. These challenges include: low power consumption requirements; and reliable and efficient spectrum utilisation within operating environments that significantly differ from those of current wireless technologies.

Energy efficiency will be a key feature for M2M wireless communication systems as M2M nodes are expected to be low-cost, energy-constrained devices able to operate for several years without any need of replacing or recharging batteries. Thus, by introducing CR technology in wireless M2M systems design of energy efficient CR functions, i.e. spectrum sensing, access and transmission, will be a very critical aspect of their success.

2.4 Spectrum Sensing

Spectrum awareness is one the cornerstone of CR as it enables the SUs to access unused frequency bands without interfering with the PUs. This awareness can be obtained by means of either geo-location database, or by spectrum sensing. In the former method the SU queries a geo-location database and then accesses the available spectrum based on the database's response. On the other hand, spectrum sensing allows the SU to actively monitor its spectral environment

in real-time and access the spectrum autonomously.

A geo-location database contains a list of potentially available frequency channels with their corresponding power level within a given geographical area. However, the channels' power level is estimated using propagation and terrain models, which result in underestimated channel availability and hence results in conservative spectrum usage [24]. In addition, the infrastructure requirements and the need of SUs with localisation capabilities increases the complexity and limits the operational environments. Thus, spectrum sensing provides a better solution for dynamic spectral environments as well as for scenarios with mobile users [25]. This thesis focuses on the spectrum sensing approach because of its flexibility and no infrastructure requirements.

Spectrum sensing can be described as a PHY and MAC cross-layer mechanism. PHY-layer sensing focuses on the signal processing aspects of spectrum sensing. Several PHY-layer spectrum sensing techniques have been proposed in the literature, with ED: Matched Filter Detection (MFD); and Cyclostationary Feature Detection (CFD) being the most commonly proposed [26], [27], [28].

On the other hand, MAC-layer sensing focuses on scheduling and coordination when multiple SUs are used. The use of multiple cooperative SUs that sense their spectral environment and share the spectrum sensing results has been proposed as a means of mitigating the effects of multipath and shadowing by exploiting spatial diversity [29]. Furthermore, it has been found to alleviate the hidden PU problem and reduce the requirements on sensing time and receiver sensitivity. Cooperative spectrum sensing can be implemented using either a centralised or a non-centralised (distributed) architecture. The centralised architecture requires a fusion centre that collects the SUs' sensing outputs and controls the spectrum sensing process. On the other hand, in the distributed architecture the SUs share sensing information and make decisions individually. A tree diagram showing the relation between state-of-the-art spectrum sensing methods is presented in Figure 2.2.

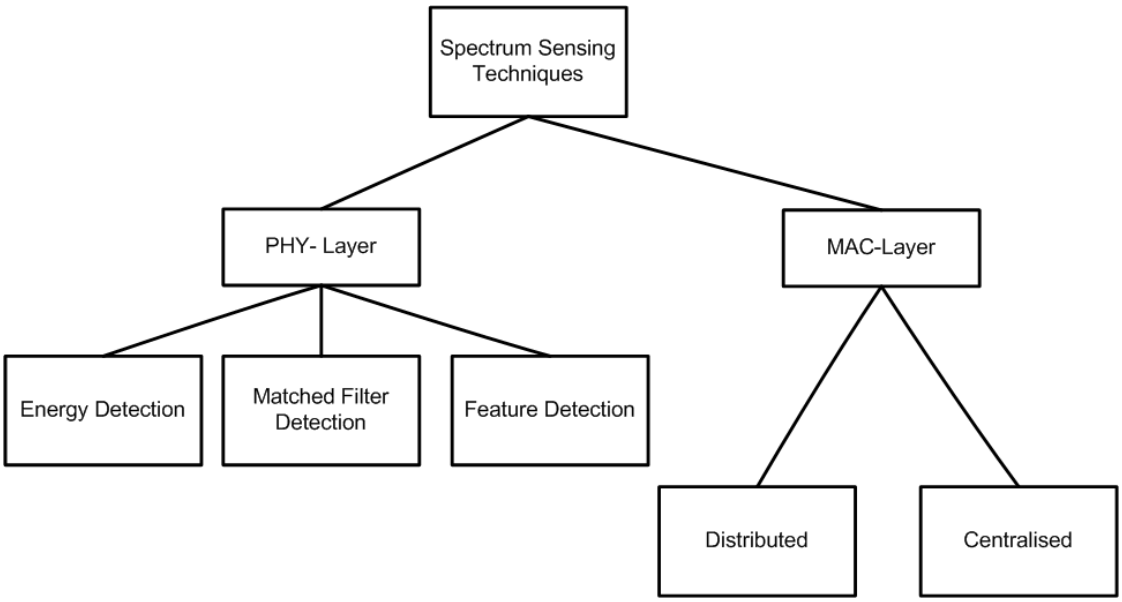

Figure 2.2: Classification of spectrum sensing techniques.

Spectrum sensing can be described as a method for identifying the presence of a signal in a noisy environment and can be described in its simplest form as a binary hypothesis problem as,

$$\begin{aligned} H_0 : y[n] = w[n] \quad n = 1, ...N \\ H_1 : y[n] = x[n] + w[n] \quad n = 1, ...N, \end{aligned} \tag{2.1}$$

where $y[n]$ denotes the received signal, $x[n]$ expresses the primary signal, $w[n]$ is noise and n is the sample index. The null hypothesis, H_0, corresponds to the absence of a primary signal, whereas the alternative hypothesis, H_1, indicates the presence of a primary signal [30]. In order for the SU to distinguish between hypotheses H_0 and H_1, a test statistic, T_x, is compared with a detection threshold, λ, as follows,

$$T_x \underset{H_0}{\overset{H_1}{\gtrless}} \lambda. \tag{2.2}$$

The sensing accuracy can be evaluated using three probabilistic metrics known as the: probability of detection, (P_d); probability of missed detection, (P_{md}); and probability of false alarm, (P_{fa}). P_d expresses the rate of correct signal detections, while P_{fa} expresses the rate of incorrectly detecting a signal which is actually not present. P_{md} expresses the rate of detection failures.

These metrics are expressed as conditional probabilities by [31],

$$P_d = P(T_x > \lambda \mid H_1) \tag{2.3}$$

$$P_{fa} = P(T_x > \lambda \mid H_0) \tag{2.4}$$

$$P_{md} = P(T_x < \lambda \mid H_1). \tag{2.5}$$

Selecting the detection threshold is one of the most important challenges in spectrum sensing as it determines the trade-offs between the probabilities of detection and false alarm and hence the overall sensing accuracy. In the classical deterministic framework, (H_0 and H_1 are true or false) the detection threshold, λ, is selected in order to maximise P_d subject to a given P_{fa} constraint [31]. The detection accuracy is then quantified using the Receiver Operation Characteristics (ROC) curve or the complementary ROC curve. ROC and complementary ROC curves describe the performance of binary decision making systems in terms of the relation between P_{fa} and P_d or P_{md} respectively. The ROC curve is generated by varying the detection threshold from $-\infty$ to ∞ which makes the curve to move from the upper right point $(1, 1)$ to the origin $(0, 0)$. Figure 2.3 describes how the detection performance is interpreted based on the position of the ROC curve within the ROC space. The ROC space is defined by P_{fa} and P_d as x and y axis. The ideal detection performance with $P_d = 1$ and $P_{fa} = 0$ would yield a point in the upper left corner (0,1) of the ROC space whereas a random guess would result in a point along a diagonal line from the lower left corner (0,0) to the upper right corner (1,1). The resulting diagonal line divides the ROC space, with points above it suggesting a better detection performance and points below it suggesting a deteriorated one.

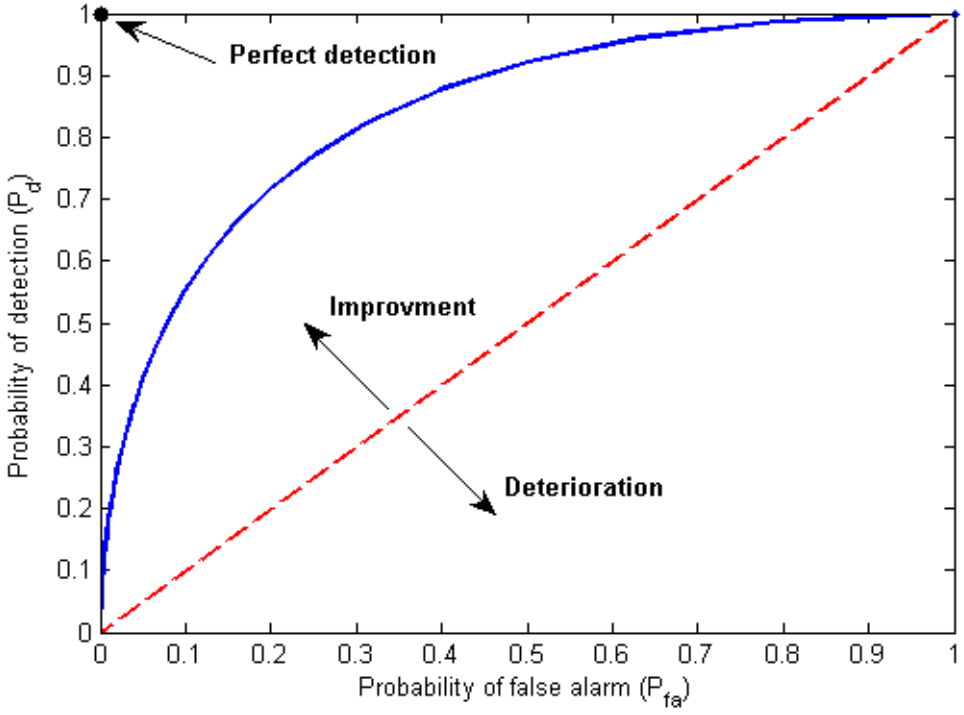

Figure 2.3: ROC space.

In the context of CR, a high probability of missed-detection results in detection failures which in turn causes unwanted interference to the PUs. Nevertheless, a high P_{fa} results in inefficient spectrum utilisation and hence, an overall performance degradation. Thus, for optimal spectrum sensing, high detection probability is required, while false alarm probability must be kept as low as possible to prevent spectrum under-utilisation. As a result, a pair of high P_d and low P_{fa}, which in turn leads ROC curves to move towards the upper left corner within the ROC space, indicates superior detection performance. Being a system level parameter, the P_{fa} target values may vary depending on the application. However, P_{fa} values between 10^{-2} and 10^{-1} are considered in the literature, whereas the IEEE 802.22 standard recommends a $P_{fa} \leq 10^{-1}$ [13].

In addition to the aforementioned metrics, spectrum sensing performance can be further evaluated with respect to the following parameters:

- **Required SNR**: This figure expresses the minimum required Signal to Noise Ratio (SNR) of the received PU signal in order for the SU to achieve

a target sensing accuracy. The received SNR depends on the PU transmit power and propagation environment and it can significantly affect the detection performance in terms of P_d, P_{fa} and P_{md}. As expected, the detection performance improves as the SNR increases. Thus, achieving a target sensing accuracy at low SNR regions suggests superior detection performance.

- **Sensing time**: This figure expresses the minimum required time or samples in order to achieve a target detection accuracy. As the transceiver chain is typically used for sensing and transmission, shorter sensing durations result in longer data transmission slots. Therefore, reliable sensing within a short sensing time results in increased data rates of the secondary system.

- **Complexity**: This figure refers to the computational and implementation complexity of the sensing algorithm. It depends on the statistics that are used for signal detection and on the required knowledge on the primary signal's parameters. Complexity is directly related to the energy consumption of the spectrum sensing technique. Thus, estimation and optimisation of the complexity requirements can lead to improved sensing performance in terms of energy efficiency.

2.4.1 Energy Detection

ED, also known as the radiometre, is a non-coherent detection method that measures the energy of the received signal and compares it with a predefined threshold that depends on the noise floor [32]. ED has been widely used in a number of wireless applications such as Radio Detection and Ranging (RADAR) systems and Ultra-Wideband (UWB) communications [33], [34]. Recently, ED has shown high applicability as a spectrum sensing technique in the emerging CR technology [35]. In ED-based spectrum sensing, the received signal is filtered within the bandwidth of interest, squared and integrated over a given observation interval in order to measure the received signal's energy

level and then compare it with a detection threshold. Figure 2.4 presents the block diagram of ED-based spectrum sensing.

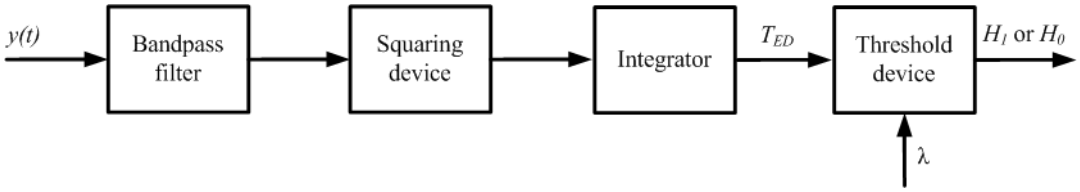

Figure 2.4: Energy detection [12].

A received signal can be mathematically described as,

$$y(n) = x(n) + w(n), \tag{2.6}$$

where $x(n)$ is the transmitted signal, $w(n)$ is the Additive White Gaussian Noise (AWGN), and n is the sample index. In ED-based spectrum sensing the test statistic is obtained by the received signal's energy as,

$$T_{ED} = \sum_{n=0}^{N} |x(n)|^2, \tag{2.7}$$

where N represents the number of samples, which can be related to the sensing time. For simplicity, both the noise and the signal term are modelled as zero-mean, independent Gaussian random variables with variance σ_x^2, i.e. $x(n) \approx \mathcal{N}(0, \sigma_x^2)$ and σ_w^2, i.e. $w(n) = \mathcal{N}(0, \sigma_w^2)$, respectively [26]. However, in practice, the signal term, $x(n)$, is more complicated due to the added impact of channel fading that needs to be taken into account. The topic of ED-based spectrum sensing over fading channels is presented in detail in Chapter 3.

Given that the test statistic, T_{ED}, is a sum of N Gaussian random variables, the Probability Density Function (PDF) follows a chi-squared distribution. Hence, based on the Central Limit Theorem (CLT), the test statistic can be approximated by a Gaussian distribution as,

$$T_{ED} \approx \begin{cases} \mathcal{N}(N\sigma_w^2, 2N\sigma_w^4) & ,H_0 \\ \mathcal{N}(N(\sigma_w^2 + \sigma_x^2), 2N(\sigma_w^2 + \sigma_x^2)^2) & ,H_1. \end{cases} \tag{2.8}$$

After hypothesis testing, the closed-form expressions for the probabilities P_{fa} and P_d over AWGN are evaluated as,

$$P_{fa} = Q\left(\frac{\frac{\lambda}{\sigma_w^2} - N}{\sqrt{2N}}\right) \tag{2.9}$$

$$P_d = Q\left(\frac{\frac{\lambda}{\sigma_w^2+\sigma_x^2} - N}{\sqrt{2N}}\right), \tag{2.10}$$

where λ is the detection threshold and $SNR = \sigma_x^2/\sigma_w^2$.

By solving (2.9) for λ, and replacing in (2.10), the complexity of ED-based spectrum sensing, in terms of the minimum required number of samples N to achieve a target pair of P_{fa} and P_d, is given by,

$$N_{ED} = 2[Q^{-1}(P_{fa} - Q^{-1}(P_d)SNR^{-1} - Q^{-1}(P_d)]^2. \tag{2.11}$$

The ROC curve for ED-based spectrum sensing is obtained by plotting expressions (2.9) and (2.10) as shown in Figure 2.5. These curves describe the performance of ED-based spectrum sensing over AWGN for a range of a SNR values and $N = 100$. It is evident that the detection performance is improved as the received signal's SNR increases since the ROC curves move towards the upper left corner of the ROC space.

ED-based spectrum sensing is the most commonly used sensing technique because of its low computational and implementation complexities. In addition, it is considered as a more generic spectrum sensing technique as it does not require any prior knowledge on the received signal. Although ED-based spectrum sensing is considered as the most popular spectrum sensing method, it has several limitations including: poor detection performance in low SNR regions; need for accurate noise variance estimation; and inability to differentiate between different types of PU signals.

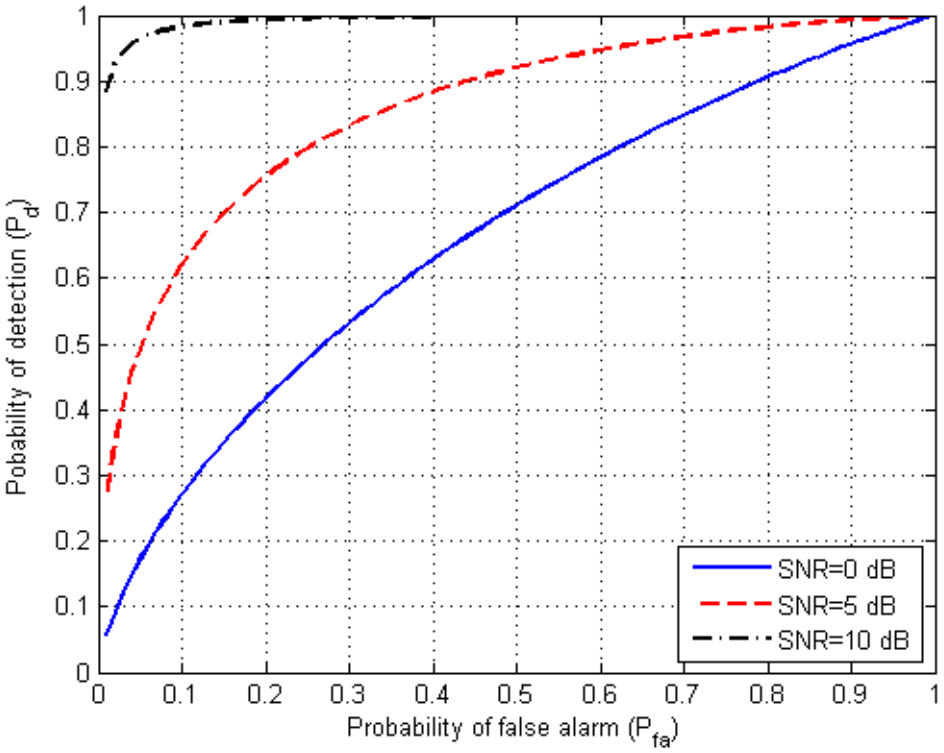

Figure 2.5: ROC curves for ED-based spectrum sensing over AWGN for different SNR values.

2.4.2 Matched filter Detection

In the context of signal processing, matched filters are known as linear filters that are used to maximise the output SNR of a given input signal in the presence of additive stochastic noise [36]. In the context of CR, MFD-based spectrum sensing exploits pilot signals that are embedded to the primary signal in order to detect the presence of a PU. Such pilot signals are used in communication systems for synchronisation and typically account for 1% to 10% of the total transmitted signal power [37].

In MFD-based spectrum sensing the unknown primary signal is convolved with a time-reversed version of the pilot signal. If the template signal exists in the unknown signal then the PU is denoted as present, or absent otherwise. The block diagram of MFD-based spectrum sensing is shown in Figure 2.6.

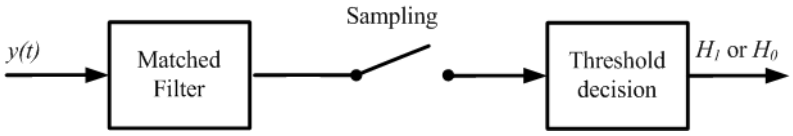

Figure 2.6: Matched filter detection [12].

Given the received signal (2.6), the operation of MFD is mathematically described as,

$$Y[n] = \sum_{\kappa=-\infty}^{\infty} h[n-\kappa]y[\kappa], \tag{2.12}$$

where $y(n)$ is the received signal, $h(n)$ is the matched filter's impulse response and κ indicates the time shifts.

By correlating the received signal with a time shifted version of the pilot signal, $\hat{X}_p$, the test statistic is obtained by [37],

$$T_{MFD} = \frac{1}{N}\sum_{n=1}^{N} Y[n]\hat{X}_p[n]. \tag{2.13}$$

Having determined the detection threshold, P_{fa} and P_d can be evaluated after hypothesis testing as [37],

$$P_{fa} = Q\left(\frac{\lambda}{\sqrt{\sigma_w^2 E_p}}\right) \tag{2.14}$$

$$P_d = Q\left(\frac{\lambda - E_p}{\sqrt{E_p\sigma_w^2}}\right), \tag{2.15}$$

where $E_p = \frac{1}{N}\sum_{n=1}^{N}(\hat{X}_p[n])^2$ denotes the pilot signal's energy and σ_w^2 is the noise variance.

By using the same methodology as in Subsection 2.4.1 and expressions (2.14) and (2.15), the complexity of MFD-based spectrum sensing in terms of the minimum required number of samples, N, for a target pair of P_{fa} and P_d is given as [37],

$$N_{MFD} = [Q^{-1}(P_{fa} - Q^{-1}(P_d)]^2 SNR^{-1}. \tag{2.16}$$

Figure 2.7 presents the ROC curves for MFD-based spectrum sensing obtained by plotting expressions (2.14) and (2.15). The performance of MFD-based spectrum sensing is analysed for three different SNR regimes with $N = 100$ and E equal to 10% of the total signal's energy. It is shown that as the received signal's SNR increases the ROC curves move towards the upper left corner of the ROC space which in turn indicates improved detection performance.

The fact that a matched filter is primarily designed to maximise the SNR of the received signal results in robust detection performance in low SNR regimes. Moreover, due to the high processing gain of coherent detection, the required number of samples scales to $O(1/SNR^{-1})$, which in turn reduces the observation time. However, due to the coherent nature of matched filtering, perfect timing and synchronisation between the PUs and SUs is required. Furthermore, it has been shown that MFD-based spectrum sensing results in high power consumption because of the signal processing algorithms that are needed in the receiver's end [18].

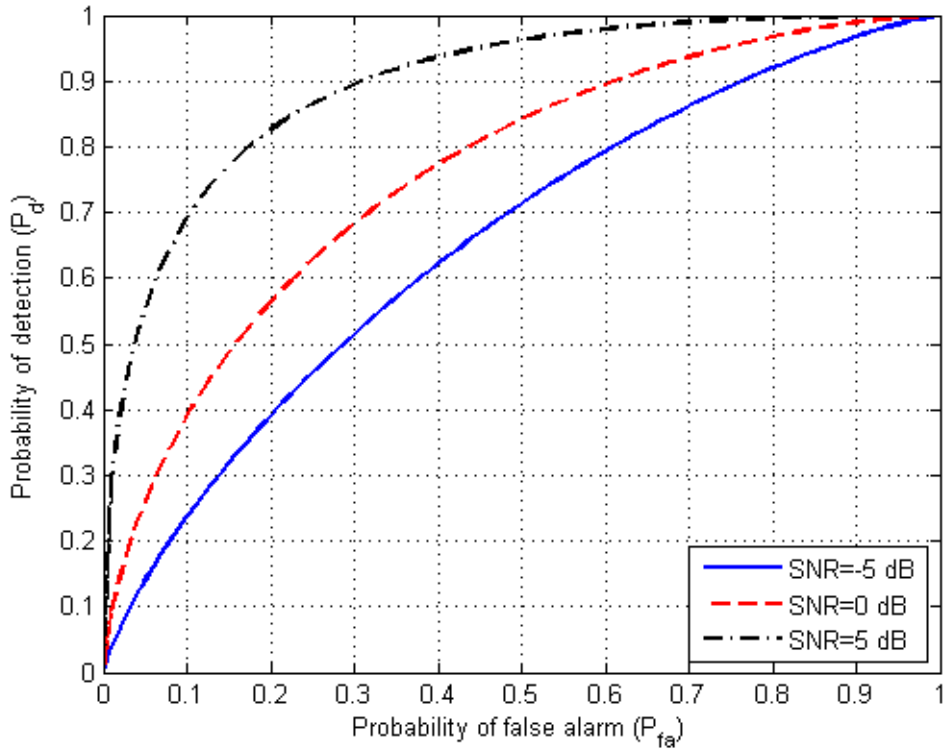

Figure 2.7: ROC curves for MFD-based spectrum sensing over AWGN for different SNR values.

2.4.3 Cyclostationary Feature Detection

Information theory suggests that communication signals with maximal information content (entropy) are statistically white Gaussian. Thus, one would expect signals used in wireless communications systems to be nearly white Gaussian. Based on this assumption, no spectrum sensing technique could outperform ED. However, real-world signals contain distinctive cyclostationary features that can be further exploited for signal detection [38]. Such features are generated by multiplexing the transmitted signals with chirp codes, pulse trains, hopping sequences, spreading functions, and Cyclic Prefixes (CP). In the context of CR, CFD refers to a spectrum sensing technique that exploits known statistical properties of the primary signal in order to determine the presence or absence of PUs.

The Autocorrelation Function (ACF) of a stohastic process $y[n]$ is given by,

$$r_y[n,\tau] = \mathbb{E}[y[n]y*[n+\tau]], \tag{2.17}$$

where $\mathbb{E}$ denotes the mathematical expectation, n the sample index and τ the time lag.

This processes can be characterised as second-order cyclostationary if the ACF (2.17) is periodic in n and can be expressed by a Fourier series as,

$$r_y[n,\tau] = \sum_{\alpha} R_y(\alpha,\tau)e^{jan}. \tag{2.18}$$

The Fourier coefficient $R_y(\alpha,\tau)$, also known as the cyclic autocorrelation, at cyclic frequency α on the time lag τ is given by,

$$R_y(\alpha,\tau) = \frac{1}{N}\sum_{n=0}^{N-1} r_y[n,\tau]e^{-jan}. \tag{2.19}$$

The cyclic spectral density of $y[n]$ for the cyclic frequency α is represented by the cyclic spectrum which can be expressed as a Fourier coefficient given by,

$$S_y[\alpha,\omega] = \sum_{\tau} R_y(\alpha,\tau)e^{-j\omega\tau}. \tag{2.20}$$

Based on the cyclic features of a signal, CFD-based methods that exploit spectral correlation can be developed. A block diagram of a typical CFD-based spectrum sensing method is depicted in Figure 2.8.

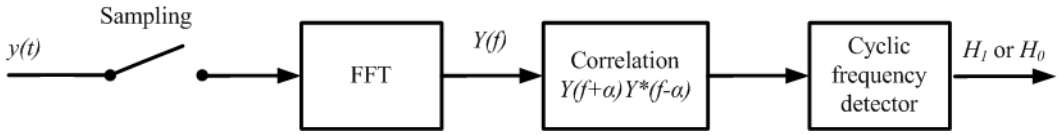

Figure 2.8: Cyclostationary feature detection [12].

A CFD-based spectrum sensing technique based on the cyclic autocorrelation of one cyclic frequency is proposed in [28]. This method was later extended to use multiple frequencies in [39]. In addition, a CFD-based spectrum sensing method that exploits second-order statistics of CP-based orthogonal frequency division multiplexing (OFDM) signals is developed in [40]. Based on the autocorrelation statistics, for CP-based OFDM signal of T_d length with a CP of T_c length and an autocorrelation coefficient $\rho(\tau)$ that corresponds to lags $\tau = \pm T_d$, the detector has to distinguish between the following hypotheses,

$$\begin{aligned} H_0 &: \rho(\pm T_d) = 0 \\ H_1 &: \rho(\pm T_d) = \rho_1, \end{aligned} \tag{2.21}$$

where $\rho_1 = \frac{T_c}{T_d+T_c}\frac{SNR}{1+SNR}$.

After Neyman-Peasron hypothesis testing, the probability of false alarm is obtained as,

$$P_{fa} = \frac{1}{2} erfc\Big(\sqrt{N}\eta\Big), \tag{2.22}$$

where N is the number of samples that are required to calculate the autocorrelation coefficient and $erfc$ denotes the complementary error function.

By solving (2.22) for η the detection threshold is obtained by,

$$\eta = \frac{1}{\sqrt{N}} erfc^{-1}(2P_{fa}). \tag{2.23}$$

Similarly, the probability of detection can be expressed as,

$$P_d = \frac{1}{2} erfc\left(\sqrt{N}\frac{\eta - \rho_1}{1-\rho_1^2}\right). \tag{2.24}$$

By applying the same methodology as in Subsections 2.4.1 and 2.4.2, the number of samples required for CFD to achieve a target detection performance is given by,

$$N_{CFD} = [erfc^{-1}(2P_{fa}) - 1 - \rho_1^2) erfc^{-1}(2P_d)]\rho_1^{-2}. \tag{2.25}$$

A performance analysis of CFD-based spectrum sensing in terms of ROC curves is presented in Figure 2.9. These curves are obtained by plotting expressions (2.22) and (2.24) for a range of SNR values over AWGN. The obtained results indicate that the performance of CFD-based spectrum sensing improves as the received signal's SNR increases.

The main advantage of CFD-based spectrum sensing is the ability to distinguish between different types of primary signals, noise, and interference in scenarios with low SNR. On the other hand, the main disadvantages of CFD-based spectrum sensing are the high implementation complexity and the large number of samples required for accurate feature estimation.

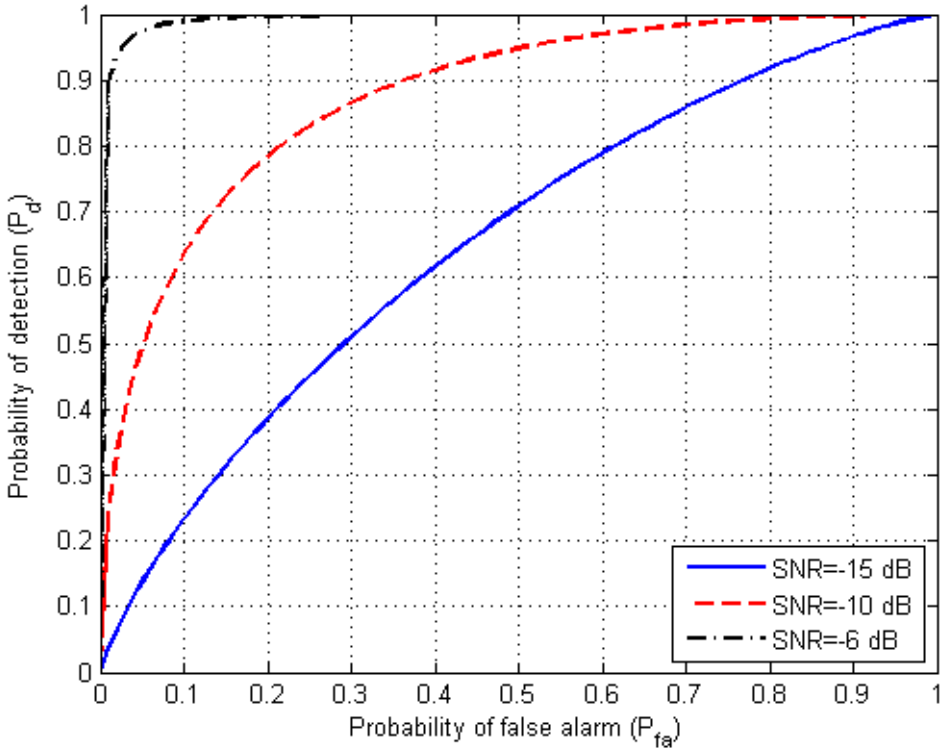

Figure 2.9: ROC curves for CFD-based spectrum sensing over AWGN for different SNR values.

2.4.4 Performance Comparison

The previous section described the state-of-the-art spectrum sensing techniques for CR. Based on the features of each sensing method and the performance metrics as presented in Section 2.4, a performance comparison follows. MFD-based spectrum sensing is the optimal detector with a more robust detection performance, when compared with ED and CFD based methods due to coherent processing gain. However, it requires perfect knowledge on PU signal characteristics and additional operations on the receiver end such as synchronisation and demodulation, which makes it impractical for CR applications. The performance of ED-based spectrum sensing is limited in the cases of non-stationary noise and unknown noise variance. ED-based spectrum sensing has also been found to be affected by baseband filter effects and suprious tones [41]. ED-based spectrum sensing is considered as the optimal detection method in the case of stationary noise [42]. However, in the presence of co-channel or adjacent channel interference when noise becomes non-stationary, CFD-based methods outperform ED-based spectrum sensing [43]. On the other hand, CFD-based spectrum sensing is known to be vulnerable due to channel fading as cyclostationary features are lost when fading occurs [44]. An overview of the most popular spectrum sensing techniques is presented in Table 2.1.

Table 2.1: Spectrum sensing techniques overview.

Technique	Advantages	Disadvantages
ED	Low complexity No prior knowledge required	Poor performance in low SNR Cannot differentiate between PUs
MFD	Optimal detection Low complexity	Requires prior knowledge and synchronisation
CFD	Robust in low SNR Differentiates between PUs	Requires prior knowledge High complexity

The selection of the appropriate spectrum sensing technique requires some trade-offs to be considered regarding the application requirements and constraints. The key factors for selecting a spectrum sensing method include: the sensing accuracy; the SNR requirements; the sensing duration; and the computational complexity. To this end, Figure 2.10 presents the sensing performance with respect to the required SNR for ED, MFD and CFD based spectrum sensing. These curves are obtained by plotting expressions (2.10), (2.15) and (2.24) as a function of SNR. It can be observed that for a target $P_{fa} = 0.01$ ED and MDF require higher SNR to obtain a performance comparable to CFD. Indicatively, ED and MFD-based spectrum sensing require an SNR of 9 dB and 8 dB respectively in order to achieve a target $P_d = 0.9$, while CFD-based spectrum sensing achieves the same detection performance for an SNR value of -6 dB.

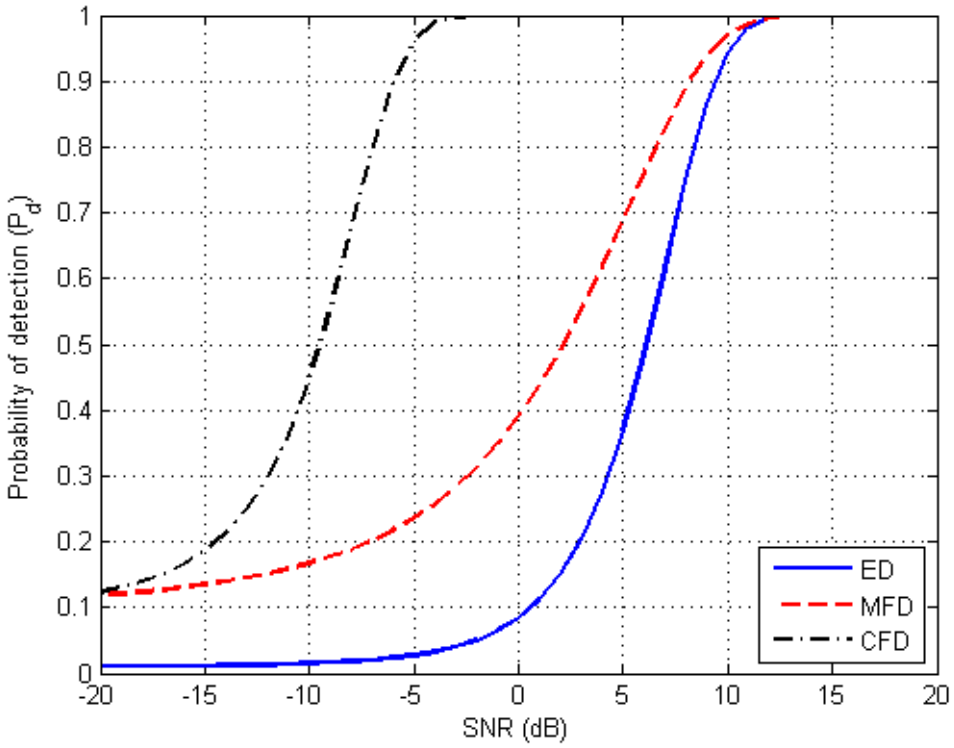

Figure 2.10: Detection performance comparison between ED, MFD and CFD spectrum sensing techniques.

Figure 2.11 illustrates the sample complexity (minimum number of samples to achieve $P_d = 0.9$ and $P_{fa} = 0.1$) of the ED, MFD and CFD-based spectrum sensing as a function of SNR. It can be seen that at high SNR regions, ED-based spectrum sensing requires less number of samples than MFD-based spectrum sensing since it uses the total signal power for detection, whereas the MFD uses only a fraction of the total signal power. Indicatively, for an SNR of 0 dB, ED-based spectrum sensing requires 14 samples while MFD requires 66. As expected, CFD-based spectrum sensing is the most complex sensing technique in terms of the number of samples with 326 samples being required to achieve a the target detection performance at 0 dB.

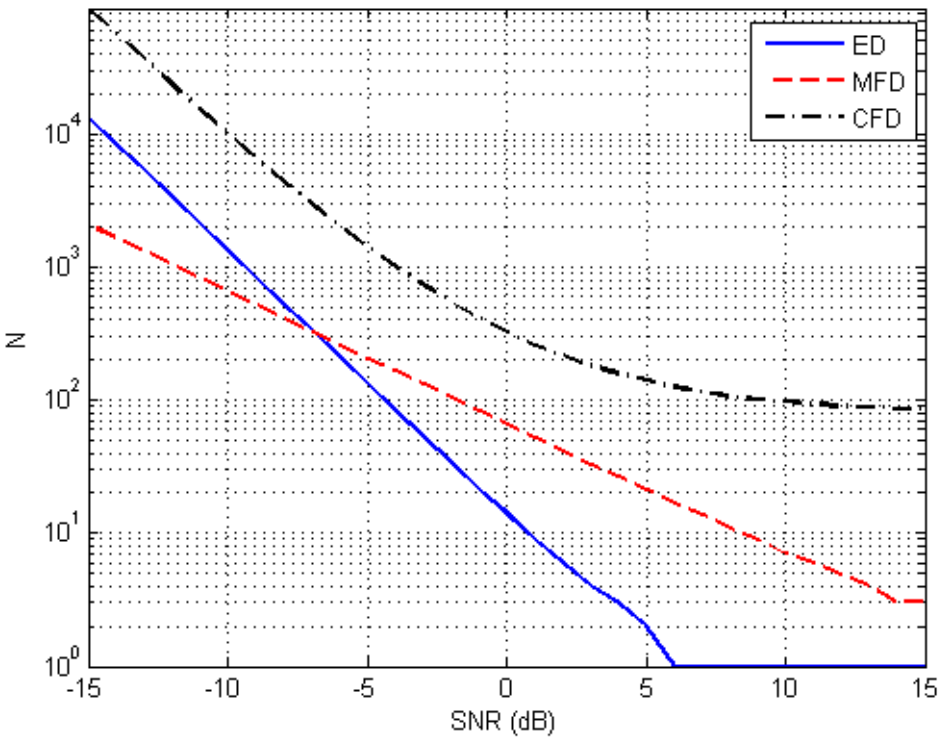

Figure 2.11: Sample complexity for ED, MFD and CFD spectrum sensing techniques.

2.4.5 Other Detection Methods

Several spectrum sensing techniques that are less commonly used than those described in the previous subsections have also been developed. Covariance-based spectrum sensing techniques exploit known properties of the sample covariance matrix of the primary signals [45]. Such properties exist in the covariance matrix of received signals by multiple antennas and encoded signals with Orthogonal Space-time Block Codes (OSTBC) [46]. In [47] the difference in the covariance matrix between received signals and AWGN is used to detect Digital TV (DTV) signals. More specifically, the proposed spectrum sensing technique is based on the fact that, under hypothesis H_0, the non-diagonal elements of the covariance matrix are equal to zero and the diagonal elements represent the noise variance, while under hypothesis H_1 the non-diagonal elements have non-zero values. Based on known properties of the covariance matrix, semi-blind spectrum sensing techniques that require no knowledge on the noise variance can be developed. However such methods require that the primary signals are correlated.

Eigenvalue-based spectrum sensing methods rely on the idea that the eigenvalues of the covariance matrix behave differently under H_0 and H_1 if the signal is correlated, even if the exact structure of the signal is not known. Given the sample covariance matrix, the corresponding eigenvalues are computed and are used to determine the detection threshold as described in [48]. Similar to the covariance-based method eigenvalue-based spectrum sensing is only based on the assumption that the primary signal is correlated. Thus, as they do not require any knowledge on the signal structure and the noise variance, eigenvalue-based methods are considered as fully blind.

Wavelet transforms may be used for detecting irregularities or singularities in the Power Spectral Density (PSD) of a signal. In the CR context, wavelet-based spectrum sensing is used for detecting varying power levels over a wide portion of the spectrum and has been found to be particularly suitable for ultra-wideband CR systems as a means of detecting narrowband incumbent PUs in a wide portion of a spectrum [49]. Although this technique alleviates

the requirements of complex bandpass filtering it requires high sampling rate which in turn increases its computational complexity and energy requirements.

A multitaper spectrum sensing is proposed in [50]. This method uses discrete prolate spheroidal wave functions also known as Slepian sequences. The two main characteristis of Slepian sequences are: 1) they have maximal energy in the main lobe; and 2) they are orthogonal. The orthogonality assures that the filter outputs are uncorrelated. Therefore, after estimating the spectrum of the band of interest, spectrum sensing can be performed with ED.

Filterbank-based spectrum sensing is a particularly useful spectrum sensing technique in the case that the primary signal is not known and has no useful features that can be efficiently exploited for signal detection. In this context, a set of bandpass filters with low side-lobes that are used to estimate the signal spectra [51]. Filterbank detection is traditionally used for spectral estimation and has also been proposed for CR spectrum sensing. Although this method is significantly complex due to the large number of the required bandpass filters it can be conveniently applied on filterbank multicarrier CR systems without any additional requirements.

CR systems may require to detect available channels over a wide frequency range (hundreds of MHz to several GHz) in order to achieve higher throughput. However, wide-band spectrum sensing requires high sampling rate and hence, high power consumption by the Analogue to Digital Converter (ADC). Compressive spectrum sensing has been proposed as a solution to this problem based on the fact that a signal can be sampled below the Nyquist rate through a special linear sampling process given that the signal is sparse in a given dimension (frequency or time) [52].

All the aforementioned sensing methods have different advantages and disadvantages and can be effectively used for a number of CR applications. However, their applicability in CR-based M2M systems may be limited due to their high complexity requirements driven by different factors such as: the high sampling rate requirements of the wavelet transform based method; the implementation complexity of the filterbank-based method; and the computational complexity of the spectrum reconstruction algorithms for compressive sensing. In addition, the fact that both covariance and eignenvalue-based methods require correlated primary signals can make them ineffective for scenarios in which the nodes operate in multipath environments where multiple uncorrelated primary signals are most likely to exist.

2.5 Energy Efficient Spectrum Sensing

Over the last years, the proliferation of mobile devices, such as smart phones and tablets, has spurred an increasing growth of high data-rate wireless services. In turn, such diverse and demanding wireless services, have led in increased energy consumption of battery-powered mobile devices. Unfortunately, the relatively slow advances on battery technology has so far eliminated the possibility of high-capacity batteries as a solution. Therefore, in order to alleviate the energy consumption of mobile devices and improve the end-user's experience, the design of energy efficient wireless communication systems has been a major focus of industry and academia [53]. With the penetration of CR technology in wireless communication systems, energy efficiency has become even more critical as additional cognitive functions are introduced to CR-enabled wireless terminals.

As discussed in the previous sections, by increasing the sensing time, robust and accurate sensing is achieved, which in turn ensures efficient spectrum utilisation. However, similar to the transmission process, spectrum sensing consumes non-negligible amounts of energy since the CR transceiver is required to be in active state [54]. As a result, increasing the sensing time results in in-

creased overall energy consumption. Additionally, in the case of fixed sensing/ transmission time slots the remaining amount of time left for transmission is limited. Therefore, careful design of CR systems that take into account the trade-off between energy efficiency and sensing accuracy is required. To this end, different techniques that improve the energy efficiency of spectrum sensing have been proposed in the literature which include sequential detection, censoring, sleeping, and clustering.

The basic idea behind sequential detection is to reduce the sensing energy by minimising the average time subject to given constraints relating to the probabilities of missed detection and false alarm, i.e. $P_{fa} \leq a$ and $P_{md} \leq b$, with $a, b \in (0, 1)$. In [55], sequential detection is proposed as a means of reducing the sensing time of a distributed spectrum sensing scheme by sensing the radio environment as long as the Likelihood Ratio (LLR), Λ, satisfies $\eta_1 \leq \Lambda < \eta_2$, with $\eta_1 = b/(1-a)$ and $\eta_2 = (1-b/a)$. In [56], all sensing nodes send their most current LLRs to a fusion centre, where an LLR test is carried out, until a positive test result is obtained and the sensing nodes can stop sensing. On the other hand, in [40] if the LLR test is negative, only one node that did not participate in the fusion gathers new information and sends its LLR to the fusion center.

Another energy efficient spectrum sensing mechanism is referred to as "censoring". This mechanism suggests that each CR node sends only informative sensing results, whereas uninformative results are censored. In [57], optimal censoring is performed in terms of the global detection error probability. As a result, the CR nodes send only their sensing outputs that can minimise the difference between the interference and the spectral efficiency of the overall system.

Sleeping or on/off spectrum sensing is another energy aware spectrum sensing mechanism where CR sensing nodes randomly stop the sensing procedure with a given probability, known as sleeping rate. The main advantage of sleeping is that the CR nodes that are asleep do not consume any power for sensing, whereas in censoring all the CR nodes have to continuously perform spectrum

sensing. However, sleeping is generally applied in combination with censoring [58], [59]. For example, in [58] the global detection error probability is optimised with respect to the sleeping rate, while in [59] the main objective of the sensing scheme is to maximise the mutual information between the occupancy and the decision state of the fusion center.

All of the aforementioned sensing mechanisms focus on the MAC-layer and are used to improve the energy efficiency at a network level through scheduling, without taking into account the energy consumption of CR sensing nodes individually. In addition, static scenarios are assumed without considering spatio-temporal changes of the PU occupancy. Therefore, adaptive sensing and learning for autonomous CR nodes is required for enhanced sensing efficiency of CR systems [60]. In this context, predictive spectrum sensing has been proposed as a means of improving the spectrum sensing of autonomous CR nodes [61]. The proposed scheme enables the CR nodes to avoid sensing channels that are predicted to be occupied in future time instants, and thus aim to improve the sensing efficiency in terms of sensing time and energy. To this end, a review of state-of-the-art prediction methods for spectrum occupancy is presented in the following section.

2.6 Spectrum Occupancy Prediction

Spectrum occupancy prediction refers to the process of estimating the future occupancy of a given frequency band based on historical data. In order to perform any prediction, a history of past observations is required as input to the prediction model. In the context of CR, the SU obtains a history of occupancy data through spectrum sensing. This history of past sensing outputs is then used for learning and inferring the spectrum occupancy at future time instants.

In this section, different spectrum occupancy prediction methods and their applicability in CR systems are presented. These methods can be broadly divided into two categories: 1) binary; and 2) non-binary time-series methods.

Binary time-series models quantise data by applying a detection threshold in the received signal power [62], whereas non-binary time series models use the received signal power values for prediction [63]. For the first category, Markov family predictors and neural networks may be applied, whereas for the second category regression models can be used.

2.6.1 Markov Family Models

The k^{th}-order Markov prediction schemes assume that a future state can be predicted based on the sequence of k most recent historical data. Such a model is mathematically described by a Markov chain of S possible states [64]. A Markov chain is a stochastic process that describes the sequence of S states and the probabilities associated with the state changes as the process evolves over time. Having a k-length binary sequence of past spectrum samples, the Markov predictor calculates the times that the k-length sequence was followed by a "0" and by a "1". By comparing these two values, the predictor estimates the channel occupancy in the next time instant. In this model, the process output is directly observable which, in the context of CR, means that such a prediction scheme assumes error-free spectrum sensing. However, in real-world communication scenarios, spectrum sensing is affected by noise and other channel impairments such as fading and multipath. In other words, the actual PU channel occupancy is hidden from the SU. Therefore, HMMs can describe more efficiently the spectrum sensing problem.

The HMM is a Markov family extension with an underlying Markov process that is not observable (hidden states) and can be observed via another stochastic process known as the observation sequence. HMMs have been widely used in machine learning applications such as DNA sequence analysis, handwritten character recognition etc. An HMM is described by the tuple $(\pi, \mathbf{A}, \mathbf{B})$, where π is the initial state distribution, $\mathbf{A}$ is the transition matrix that describes the probabilities of changing from one state to another, and $\mathbf{B}$ is the emission matrix that describes the relationship between observed and the hidden states [65].

In the context of CR, a PU transmission regime, channel occupancy can be described by a 2-state Markov process with states "0" and "1" for an idle or a busy channel, respectively. The spectrum sensing output that corresponds to the observation process can be defined by a 2-state emission space, with states "0" and "1" for a channel being sensed as unoccupied or occupied, respectively. A detailed description of the mathematical model for HMM for spectrum sensing and prediction for CR is presented in Chapters 4 and 5, respectively.

2.6.2 Artificial Neural Networks

Artificial Neural Networks (ANNs) are nonlinear parametric models that create a mapping function between the input and output data. ANNs have been used in various applications, such as system identification and time series prediction. Multi-layer Perception (MLP) network is an example of ANN and it is a structure that consists of an input layer, an output layer, and at least one hidden layer [66]. Each layer contains a number of computing units, known as neurons, which are connected to each other with a certain weight. Each neuron, with the ones in the input layer excluded, calculates a weighted sum of the input and performs a nonlinear transformation using the hyperbolic tangent function.

The MLP-based predictor parameters are updated through the training process using the batch Back-propagation algorithm (BP) [67]. More specifically, for each observation in the MLPs input layer, the outputs of each neuron from the hidden layer to the output layer are calculated. The outputs in the MLP output layer are considered as an estimate to the corresponding desired value. The difference between the estimated and the desired values is calculated as the output error. The objective of the training algorithm is to adjust the connection weights by minimising the output error. Once the training process is completed the predicted value is obtained by the latest observation in the input layer of the MLP. In the context of CR, an MLP-based spectrum hole predictor is proposed in [68]. The proposed scheme is proposed as a means of

reducing the sensing error and hence, improving spectrum utilisation.

2.6.3 Regression Models

Regression models are used for understanding and identifying the underlying context of time series, i.e. a sequence of observations sampled at uniform time intervals. An autoregressive model of order p, i.e. AR(p), represents a random time varying process where its output is linearly dependent on its previous p values [69]. An AR(p) based predictor estimates the future values based on the prediction rule: $X_t = \sum_{i=1}^{p} \phi_i X_{t-1} + \epsilon_t$, where, X_t, is the predicted value at time instant t, X_{t-1} is the time series under consideration, p is the model's order, ϕ_i is the AR coefficient and ϵ_t is Gaussian white noise. A moving average prediction model of order q, i.e. MA(q), estimates the future value of a time series as the average of the last q observations [69]. An autoregressive moving average model ARMA(p,q) combines an AR(p) and a MA(q) model. A generalisation of the ARMA(p, q) model is the autoregressive integrated moving average model ARIMA(p, d, q) with a differencing step, d, which is applied to time series that exhibit non-stationarity.

In order to determine the model in which the time series of interest belongs to, its AR and MA signatures of the autocorrelation and Partial Autoccoreation Function (PACF) plots have to be investigated. If the PACF of the differenced series displays a sharp cut-off and/or the lag 1 is positive an AR model is considered. The lag at which the PACF cuts off indicates the number of AR terms. If the ACF of the differenced series displays a sharp cut-off and/or the lag 1 autocorrelation is negative an MA model is considered [70]. The lag at which the ACF cuts off indicates the number of MA terms. After determining the model that describes the given time series, the model's parameters are estimated using either the Yule-Walker equations or the maximum likelihood estimation. When this process is completed, by using a sequence of past observation as input and the corresponding prediction rule, the future sates of the system are predicted.

In the context of CR systems, a sequence of received signal power measured

over equal time intervals can be considered as a time series and therefore analysed and predicted using time series models. The use of appropriate time series models for spectrum occupancy of cellular bands has been investigated in [71] and [72]. Furthermore, in [73], an MA-based predictor is used to improve the spectrum sensing performance of an ED-based spectrum sensing scheme in terms of energy efficiency. The CR uses a history of received power readings and predicts the future channel occupancy based on the most recent observations by assigning exponentially decreasing weights to the older ones. An AR spectrum hole prediction model for CR is proposed in [63] that could also be used for improving the energy efficiency of CR.

2.6.4 Comparison of Spectrum Occupancy Prediction Methods

The previous subsections described state-of-the-art spectrum occupancy prediction methods that can be applied in CR applications. Such predictive schemes require prediction accuracy, adaptability to the channel occupancy statistics, and low computational complexity. Prediction accuracy and adaptability are essential in order to ensure efficient spectrum utilisation. To this end, a prediction accuracy of at least 90 % that corresponds to a $P_d = 0.9$ as indicated by the IEEE 802.22 CR standard is required whereas the predictor has to adapt to channel occupancy changes in less than one sensing cycle. On the other hand, the predictor's complexity should be kept as low as possible in order to facilitate its implementation in energy-constrained CR terminals.

More specifically, k^{th}-order Markov predictors can perform fast online, i.e. real-time, predictions with low complexity. However, they have been found to be unable to quickly adapt to channel occupancy variations as there is no training included. On the other hand, the principle of HMMs allows the predictor to adjust its parameters according to a target spectrum sensing performance, whereas online training facilitates the adaptation to the channel's occupancy status. Although ANN-based predictors have similar behaviour to the HMM-

based ones, they cannot perform online predictions and require comparative long observation time which poses extra complexity. These characteristics make them ideal candidates for large scale and long term offline predictions. Regression models are linear prediction filters; therefore, they could be used to predict the spectrum occupancy of wireless systems with deterministic occupancy statistics such as broadcast TV, in which the transmission patterns are fixed. A quantitative comparison of different state-of-the-art spectrum occupancy methods is presented in Table 2.2.

Table 2.2: Overview of spectrum occupancy prediction methods.

Method	Advantages	Disadvantages
Markov chain	Online prediction No training required Low complexity	Sensitive to occupancy changes Assumes perfect sensing
HMM	Online prediction Robust to occupancy changes	Complexity
MLP	Robust to occupancy changes	Offline prediction Long observation history
Regression models	Long term predictions Trend prediction	Model fitting Offline prediction Long observation history

With reference to Table 2.2, the characteristics of HMMs, i.e. robustness to channel occupancy statistics and online parameter training and estimation, make them ideal candidates for spectrum occupancy prediction within dynamic CR scenarios with varying PU occupancy statistics. Therefore, this thesis focuses on HMM for implementing spectrum occupancy prediction as a part of a predictive spectrum sensing scheme for CR. Further details on how HMMs can be employed for modelling spectrum sensing and prediction are presented in the following chapters (Chapter 4 and 5).

2.7 Summary

This chapter has described the operation of CR and presented current and future applications of CR technology. The opportunities and challenges of CR technology for future wireless cognitive M2M communication systems have also been introduced. Being the focus of this thesis, an in depth review and analysis of state-of-the-art spectrum sensing techniques has been performed including classical as well as recently developed spectrum sensing approaches. With energy efficiency being a key feature of future CR systems, the need for energy efficient spectrum sensing and the current energy efficient sensing methods have been discussed. The concept of predictive spectrum sensing as a means of energy efficient spectrum sensing has been introduced followed by an overview of state-of-the-art spectrum occupancy prediction methods.

Chapter 3

Spectrum Sensing over Two-wave with Diffuse Power Fading Channels

3.1 Introduction

This chapter analyses the performance of ED-based spectrum sensing over TWDP fading channels. The related work in the area of spectrum sensing over fading channels is presented in Section 3.2. The fading statistics of TWDP fading and the fundamentals of ED-based spectrum sensing are presented in Section 3.3. A closed-form expression for the average detection probability of ED-based spectrum sensing over TWDP fading channels is derived in Section 3.4. This expression is then extended to account for cooperative spectrum sensing and diversity reception. Furthermore, an optimised threshold ED-based spectrum sensing method is proposed as a means of improving the detection performance under severe fading conditions. Based on the derived expressions the behaviour of ED-based spectrum sensing is studied for a variety of fading conditions including Rayleigh, Rician, and "hyper-Rayleigh" channels. These fading channels present a reliable behavioural model of M2M cognitive nodes operating in confined structures such as in-vehicular environments. The obtained results enable the design of energy efficient CR systems in the context of M2M wireless networks, and facilitate the analysis of diversity and cooperative sensing methods as a means of improving the sensing performance over worse than Rayleigh fading conditions.

3.2 Related Work

In ED-based spectrum sensing the presence or absence of a PU is determined by comparing the received signal's energy with a predetermined detection threshold at the SU end. As a result, the detection performance of ED-based spectrum sensing is significantly affected by the large-scale and small-scale fading characteristics of the wireless channel between the SU and PU nodes [74]. In this context, the effects of channel fading on ED-based spectrum sensing have been demonstrated in several studies that focused on analysing the performance of ED within different communication scenarios and fading environments.

More specifically, closed form expressions for the average probability of detection over Rayleigh, Rician and Nakagami fading channels, are applicable for CR systems that operate in land-mobile and indoor multipath propagation environments were derived in [75]. In [76], the ED performance in the case of Nakagami-m fading has been evaluated. The Nakagami-m model is a more generic fading model that can also describe Rayleigh and Rician fading as special cases. However, the arbitrary values of the fading severity index, m, lack physical interpretation. Likewise, the detection of unknown signals in low SNR regions over K-distributed and generalised K-distributed channels has been analysed in [77]. This fading model is a simplified approximation of the Rayleigh-lognormal distribution and is used to describe the performance of wireless communication links with both multipath and shadowing. The performance of ED-based spectrum sensing over κ-μ and κ-μ *extreme* fading channels has been recently investigated in [78].

All of the aforementioned studies focus on spectrum sensing for traditional indoor and outdoor fading scenarios. Yet, as technology evolves, CR is introduced in new wireless systems as a means of improving the energy and spectral efficiency for emerging application spaces such as M2M communications and Wireless Sensor Networks (WSNs) [79], [23]. These application spaces are demonstrating fading conditions that are not adequately charac-

terised by the existing fading models. Indicatively, WSNs deployed in cavity environments (e.g. aircraft, public transportation vehicles [80]), Vehicle-to-Vehicle (V2V) communications [81], Radio Frequency Identification (RFID) systems [82], and inside computer cabinets [83] have been found to exhibit frequency-dependent and spatially-dependent fading whose severity exceeds those predicted by the Rayleigh fading model, which is traditionally considered as the worst-case fading scenario for wireless systems [84]. Such small-scale fading scenarios, termed as "hyper-Rayleigh", were experimentally verified to be adequately characterised by the TWDP model [85].

3.3 System and Channel Model

A mathematical description of the system and channel model is provided in this section. The physical interpretation and the theoretical underpinnings of the TWDP fading model are introduced. Moreover, the channel statistics including the fading envelope and the SNR PDFs are provided. Furthermore, the mathematical model of ED which forms the basis for deriving the novel expressions for determining the detection performance of ED-based spectrum sensing over TWDP fading channels is described.

3.3.1 TWDP Fading Channel Model

For channels with a large number of multipath components, each of random amplitude and phase, their summation creates a complex envelope in which, by virtue of the CLT, the real and imaginary components tend to a Gaussian distribution [86]. As such, the magnitude of the envelope has been found to be Rayleigh distributed and the phase component to be uniformly distributed. On the other hand, in environments where a strong Line of Sight (LOS) component exists in addition to weaker, numerous, yet random, multipath components, the fading statistics will follow a Rician distribution. Therefore, the existence of a large number of uncorrelated multipath components results in a Rayleigh fading channel. However, if the number of multipath components reduces,

the CLT criterion is no longer met and as a result the real and imaginary components will no longer follow a Gaussian distribution. Hence, the envelope resulting amplitude statistics will no longer be described as Rayleigh. Such a scenario has been found to be adequately described by the two-wave model in [85].

This fading model is a special case of the generic multi-wave analytic TWDP fading model that is presented in [87]. Durgin et. al derived a new family of PDFs that approximates the TWDP PDF and can describe a wide range of fading scenarios. This parametric family of PDFs mathematically describes small-scale fading in the presence of two strong multipath components. It can characterise a variety of fading scenarios including those experienced by narrow-band receivers, the use of directional antennas, and wide-band signals. In addition, the TWDP fading model has been found to be particularly flexible since it can be reduced to the well-known Rician and Rayleigh distributions.

The TWDP PDF is described by two parameters related to the wireless channel. First, the ratio between the average specular power and the diffused power given by,

$$K = \frac{Average\ specular\ power}{Diffuse\ power} = \frac{(V_1^2 + V_2^2)}{2\sigma^2}. \tag{3.1}$$

The relative strength of the two specular waves is expressed as,

$$\Delta = \frac{Peak\ specular\ power}{Average\ specular\ power} - 1 = \frac{2V_1V_2}{(V_1^2 + V_2^2)}, \tag{3.2}$$

where V_1 and V_2 denote the voltage magnitudes of the two specular waves, and σ^2 indicates the average power of the diffused waves.

Given a fading channel with TWDP statistics and a transmitted signal $x(t)$ with symbol energy E_s, the received signal can be expressed as,

$$y(t) = re^{j\phi}x(t) + w(t), \tag{3.3}$$

where $x(t)$ is AWGN, random variable ϕ is the instantaneous phase, and random variable r is the the TWDP distributed fading envelope.

The approximate PDF of the fading envelope, r, is given as [87],

$$f_r(r) = \frac{r}{\sigma^2} exp\Big(- \frac{r^2}{2\sigma^2} - K \Big) \sum_{i=1}^{M} a_i D\Big(\frac{r}{\sigma}; K; a_i\Big), \tag{3.4}$$

where

$$\begin{aligned} D(x; K; a) =& \frac{1}{2} exp(aK) I_0\Big(x\sqrt{2K(1-a)}\Big) \\ &+ \frac{1}{2} exp(-aK) I_0\Big(x\sqrt{2K(1+a)}\Big), \end{aligned} \tag{3.5}$$

with $a = \Delta \cos(\pi(i-1)/2M-1)$, $I_0(.)$ denoting the zero-order modified Bessel function of the first kind, and M representing the order of approximation of the TWDP PDF. The minimum required order, M, is determined by the product of the parameters K and Δ as,

$$M_{min} \geq \left\lceil \frac{1}{2} K\Delta \right\rceil, \tag{3.6}$$

where $\lceil . \rceil$ is the ceiling function.

As the product of K and Δ increases, a higher value of M is required for a mathematically exact PDF. For the case of $K > 10$ and $\Delta = 1$ the approximate PDF will deviate from the exact PDF. However, it still gives a good approximation over the upper and lower PDF tails providing adequate modelling for wireless communication systems [88]. The exact values of the coefficients a_i for the corresponding order M are given in [87, Table II] for the first five approximation orders covering the most useful range of K and Δ.

In two special cases, the TWDP PDF is reduced to the Rician PDF when $K \neq 0$ and $\Delta = 0$, and to the Rayleigh PDF when $K = 0$. As previously described, Rayleigh fading arises from the summation of a large number of uncorrelated multipath components. However, if the number of multipath components reduces, the envelope fading statistics will no longer be Rayleigh. This extreme fading scenario of two summed multipath components with equal weights has been experimentally validated as a new worst-case fading scenario [85] and is also included as a special case of the TWDP model for $K \to \infty$

and $\Delta = 1$. Therefore, the TWDP PDFs can mathematically represent a family of PDFs for different values of K and Δ [87]. The special cases that are characterised by the TWDP model through K and Δ are shown in Table 3.1.

Table 3.1: TWDP PDF Special Cases.

Parameter		Fading
$K = 0$	–	Rayleigh
$K > 0$	$\Delta = 0$	Rician
$K \to \infty$	$\Delta = 0$	One-Wave
$K \to \infty$	$\Delta = 1$	Two-Wave

3.3.2 TWDP Fading Statistics

Given the received signal from (3.3), the instantaneous SNR, γ, per symbol is given as [86],

$$f_{\gamma}(\gamma) = \frac{E_s}{N_0} f_{r^2}(r^2), \tag{3.7}$$

where E_s is the symbol energy and N_0 is the noise power spectral density.

In order to estimate the energy of the received signal, a square transformation of RV is applied in (3.4), and hence $f_{r^2}(r^2)$ is expressed as,

$$f_{r^2}(r^2) = \frac{1}{2\sigma^2} exp\bigg(- K - \frac{r}{2\sigma^2}\bigg) \sum_{i=1}^{M} a_i D\bigg(\frac{\sqrt{r}}{\sigma}; K; a\bigg). \tag{3.8}$$

According to [87], the energy per symbol to the noise power spectral density, E_s/N_0, can be expressed as $E_s/N_0 = \bar{\gamma}/2\sigma^2(K+1)$ where $\bar{\gamma}$ is the average SNR. Hence, the instantaneous SNR, γ, can be determined in terms of the average SNR and the channel fading parameters. Thus, by substituting (3.8) into (3.7), the PDF of the SNR over TWDP fading, which is derived in [89], can

be rewritten as,

$$f_\gamma(\gamma) = \frac{K+1}{2\bar{\gamma}} exp(-K) \sum_{i=1}^{M} a_i \Bigg[exp(a_i K) exp\bigg(- \frac{(K+1)\gamma}{\bar{\gamma}} \bigg) A + exp(-a_i K) exp\bigg(- \frac{(K+1)\gamma}{\bar{\gamma}} \bigg) B \Bigg], \tag{3.9}$$

where

$$A = I_0 \left(2 \sqrt{\frac{K(K+1)(1-a_i)\gamma}{\bar{\gamma}}} \right) \tag{3.10}$$

$$B = I_0 \left(2 \sqrt{\frac{K(K+1)(1+a_i)\gamma}{\bar{\gamma}}} \right). \tag{3.11}$$

3.3.3 Energy Detection Fundamentals

In the context of a communication link, the received signal, $y(t)$, can be mathematically described as,

$$y(t) = gx(t) + w(t), \tag{3.12}$$

where $x(t)$ is the unknown transmitted signal, g denotes the channel gain, $w(t)$ is AWGN and t is the time index.

For ED, the received signal is filtered within a predefined bandwidth W, squared, and integrated over an observation interval T. The output of the integrator is the received signal's energy which is then used as a test statistic [26]. By comparing the received signals energy with a predefined detection threshold, λ, the detector has to distinguish between the following hypotheses,

$$y(t) = \begin{cases} w(t) & ,H_0 \\ hx(t) + w(t) & ,H_1, \end{cases} \tag{3.13}$$

where H_0 and H_1 denote the hypothesis of the signal to be absent or present, respectively. Given the time-bandwidth product, $u = TW$, the test statistic follows a central chi-square distribution with $2u$ degrees of freedom under hypothesis H_0 and a non central chi-square distribution with $2u$ degrees of

freedom under hypothesis H_1 [26]. As a result, the corresponding PDF is given by [75],

$$f_y(y) = \begin{cases} \frac{1}{2^u\Gamma(u)} y^{u-1} e^{-\frac{y}{2}} & ,H_0 \\ \frac{1}{2}\frac{y}{2\gamma}^{\frac{u-1}{2}} e^{-\frac{y+2\gamma}{2}} I_{u-1}(\sqrt{2y\gamma}) & ,H_1, \end{cases} \tag{3.14}$$

where γ is the instantaneous SNR, $\Gamma(a) = \int_0^\infty t^{a-1}e^{-t}dt$ is the gamma function and $I_n(x) = (1/\pi)\int_0^\pi cos(n\theta)e^{xcos(\theta)}d\theta$ is the modified Bessel function of the first kind [90].

By integrating (3.14) over the limits of zero to infinity, the mathematical expressions of the probabilities of false alarm and detection are obtained as [75],

$$P_{fa} = \frac{\Gamma(u, \lambda/2)}{\Gamma(u)} \tag{3.15}$$

$$P_d = Q_u(\sqrt{2\gamma}, \sqrt{\lambda}), \tag{3.16}$$

where $\Gamma(a, x) = \int_x^\infty t^{(a-t)}e^{-t}dt$ denotes the incomplete gamma function and $Q_m(a, b) = (1/a^{(m-1)})\int_b^\infty x^m e^{-(x^2+a^2)/2} I_{(m-1)}(ax)dx$ denotes the generalised Marcum Q-function [90], [91].

3.4 Energy Detection Over TWDP Fading Channels

In this section a novel closed-form expression for the average probability of detection over TWDP fading channels is derived for single user detection. The expression is then extended to account for cooperative detection and a SLS diversity reception spectrum sensing scheme. Additionally, a method for anatically obtaining the optimal detection threshold for ED-based spectrum sensing over TWDP is proposed. These methods are then analysed as a means of mitigating TWDP channel fades and improving the detection performance of ED-based spectrum sensing.

3.4.1 Single User Spectrum Sensing

The probability of false alarm and detection for single user spectrum sensing over AWGN are given by (3.15) and (3.16), respectively. The probability of detection over a fading channel can be obtained by averaging (3.16) over the corresponding SNR fading statistics [86],

$$\bar{P}_d = \int_0^\infty Q_u(\sqrt{2\gamma}, \sqrt{\lambda}) f_\gamma(\gamma)\, d\gamma \ . \tag{3.17}$$

Thus, the probability of detection over TWDP fading is obtained by substituting (3.9) into (3.16) and averaging as,

$$\begin{aligned}\bar{P}_{d_{TWDP}} = \int_0^\infty Q_u(\sqrt{2\gamma}, \sqrt{\lambda}) \frac{K+1}{2\bar{\gamma}} exp(-K) \sum_{i=1}^{M} \Bigg[exp(a_i K) \\ exp\bigg(- \frac{(K+1)\gamma}{\bar{\gamma}} \bigg) A + exp(-a_i K) exp\bigg(- \frac{(K+1)\gamma}{\bar{\gamma}} \bigg) B \Bigg] d\gamma \ .\end{aligned} \tag{3.18}$$

By substituting x for $\sqrt{2\gamma}$ and using [92, eq. (45)] the following Lemma yields.

Lemma 1: The average detection probability over TWDP fading channels is expressed by a closed-form representation as,

$$\begin{aligned}\bar{P}_{d_{TWDP}} = \sum_{i=1}^{M} \frac{1}{2} a_i \Bigg[Q\bigg(\sqrt{\frac{2K\bar{\gamma}(1-a_i)}{K+\bar{\gamma}+1}}, \sqrt{\frac{\lambda(K+1)}{K+\bar{\gamma}+1}} \bigg) \\ + Q\bigg(\sqrt{\frac{2K\bar{\gamma}(1+a_i)}{K+\bar{\gamma}+1}}, \sqrt{\frac{\lambda(K+1)}{K+\bar{\gamma}+1}} \bigg) \Bigg].\end{aligned} \tag{3.19}$$

A detailed proof of Lemma 1 is shown in appendix A. Note that the probability of false alarm remains the same under any fading channel since it corresponds to the noise-only case and hence, it is independent of the SNR statistics [75].

3.4.2 Cooperative Spectrum Sensing

The detection performance of ED-based spectrum sensing may be affected by destructive channel conditions since the CR terminals are unable to distinguish between an unoccupied channel and one that is attenuated by deep fading. Therefore, cooperative detection that exploits spatial diversity among SUs has been proposed as an effective means of improving the detection performance by alleviating the effects of shadowing and multipath [93], [94].

In such a cooperative scheme every CR node, i, performs spectrum sensing independently and makes a binary decision $D_i \in 0, 1 \forall i = 1, ...K$ where K is the total number of cooperative users. All 1-bit decisions are forwarded into a common receiver through an error-free channel where they are combined in order for the fusion centre to decide whether a PU signal is present or absent within the band of interest. This operation can be mathematically represented as [95],

$$\zeta = \sum_{i=1}^{K} D_i \begin{cases} < n & ,H_0 \\ \geq n & ,H_1, \end{cases} \tag{3.20}$$

where H_0 and H_1 denote the inferred hypothesis by the fusion centre that a PU signal is absent or present, respectively.

After the fusion rule the resulting probabilities of false alarm, (Q_{fa}), and detection (Q_d) for cooperative spectrum sensing are obtained as [96],

$$Q_{fa} = \sum_{l=n}^{K} \binom{K}{l} P_{fa}^{l} (1 - P_{fa}^{l})^{K-l} \tag{3.21}$$

$$Q_d = \sum_{l=n}^{K} \binom{K}{l} P_{d}^{l} (1 - P_{d}^{l})^{K-l}, \tag{3.22}$$

where n is an integer that represents the threshold for the number of cooperative users for the "n-out-of-K" voting rule. For the case of $n = 1$ the voting rule results in the OR-voting fusion rule whereas for $n = K$ results in the AND-voting fusion rule.

For a cooperative scheme with m CR collaborative SUs, the probabilities of false alarm and detection for the case of the OR-voting fusion rule are expressed as [96],

$$Q_{fa} = 1 - (1 - P_{fa})^m \tag{3.23}$$

$$Q_d = 1 - (1 - P_d)^m. \tag{3.24}$$

Similarly, for the case of the AND-voting fusion rule the corresponding probability of false alarm and detection are given as [96],

$$Q_{fa} = P_{fa}^m \tag{3.25}$$

$$Q_d = P_d^m. \tag{3.26}$$

Closed-form expressions for the average probability of detection of cooperative spectrum sensing over TWDP channels can be derived by substituting (3.19) into (3.24) and (3.26) for the case of OR-voting and AND-voting fusion rules, respectively. Hence, the following Lemmas yield.

Lemma 2: The average probability of detection of m cooperative SUs with OR-voting fusion rule operating over TWDP fading channels is expressed by a closed-form representation as,

$$\begin{aligned}\bar{Q}_{d_{TWDP}} =& 1 - \left[1 - \sum_{i=1}^{M} \frac{1}{2} a_i \left[Q\left(\sqrt{\frac{2K\bar{\gamma}(1-a_i)}{K+\bar{\gamma}+1}}, \sqrt{\frac{\lambda(K+1)}{K+\bar{\gamma}+1}} \right) \right.\right. \\ & \left.\left. + Q\left(\sqrt{\frac{2K\bar{\gamma}(1+a_i)}{K+\bar{\gamma}+1}}, \sqrt{\frac{\lambda(K+1)}{K+\bar{\gamma}+1}} \right) \right] \right]^m.\end{aligned} \tag{3.27}$$

As previously stated, the probability of false alarm is independent of the fading statistics and hence it can be evaluated as,

$$\bar{Q}_{fa} = 1 - \left[1 - \frac{\Gamma(u - \lambda/2)}{\Gamma(u)}\right]^m. \tag{3.28}$$

Lemma 3: The average probability of detection of m cooperative SUs with AND-voting fusion rule operating over TWDP fading channels is expressed by a closed-form representation as,

$$\bar{Q}_{d_{TWDP}} = \left[\sum_{i=1}^{M} \frac{1}{2} a_i \left[Q\left(\sqrt{\frac{2K\bar{\gamma}(1-a_i)}{K+\bar{\gamma}+1}}, \sqrt{\frac{\lambda(K+1)}{K+\bar{\gamma}+1}} \right) + Q\left(\sqrt{\frac{2K\bar{\gamma}(1+a_i)}{K+\bar{\gamma}+1}}, \sqrt{\frac{\lambda(K+1)}{K+\bar{\gamma}+1}} \right) \right] \right]^m . \tag{3.29}$$

Similarly, the probability of false alarm is independent of the fading statistics and hence it can be evaluated as,

$$\bar{Q}_{fa} = \left[\frac{\Gamma(u, \lambda/2)}{\Gamma(u)} \right]^m . \tag{3.30}$$

3.4.3 Spectrum Sensing with Diversity Reception

Although cooperation has been found to improve the detection performance of ED-based spectrum sensing its achievable cooperation gain can be limited by several factors. For example, the overall sensing performance can be degraded by correlated observations of CR users blocked by the same obstacle or by cooperation signaling overhead resulting in extra sensing time, delay and energy consumption. As a result, single user detection with diversity reception has been proposed as an alternative solution to improve the sensing performance over fading channels [97].

Diversity is a well known technique used to compensate for signal fades in wireless communication channels. SLS is an efficient diversity reception scheme that is highly regarded due to its simplicity. Its principle is based on selecting the branch with the maximum decision statistic [98],

$$y_{SLS} = max[y_1, y_2, ...y_L]. \tag{3.31}$$

In the case of i.i.d branch statistics P_{faSLS} can be expressed as the following conditional probability,

$$P[y_{sls} > \lambda|H_0] = 1 - \prod_{j=1}^{L} P(y_j > \lambda|H_0). \tag{3.32}$$

Since H_0 depends only on the noise statistics and thus is independent of the fading its closed-form expression is given as follows [75, eq. (14)],

$$\bar{P}_{fa_{TWDP}}^{SLS} = 1 - \prod_{j=1}^{L} \left[1 - \frac{\Gamma(u, \lambda/2)}{\Gamma(u)}\right]. \tag{3.33}$$

Following the same principle, the P_d^{SLS} can be written by the following conditional probability,

$$P[y_{sls} > \lambda|H_1] = 1 - \prod_{j=1}^{L} P(y_j > \lambda|H_1). \tag{3.34}$$

Since H_1 depends on the signal statistics and hence, on the channel fading its closed-form expression can be obtained by averaging (3.34). This can be represented as,

$$\bar{P}_d^{SLS} = 1 - \prod_{j=1}^{L} \int_0^{\infty} [1 - Q_u(\sqrt{2\gamma_i}, \sqrt{\lambda})] f_{\gamma_i}(\gamma_i) d\gamma_i. \tag{3.35}$$

By expanding (3.35) yields,

$$\bar{P}_{d_{TWDP}}^{SLS} = 1 - \prod_{j=1}^{L} \int_0^{\infty} f_{\gamma_j}(\gamma_j)\, d\gamma_j \; - \int_0^{\infty} Q_u(\sqrt{2\gamma_j}, \sqrt{\lambda}) f_{\gamma_j}(\gamma_j) d\gamma_j. \tag{3.36}$$

Taking into account that $\int_0^{\infty} f_{\gamma_j}(\gamma_j) d\gamma_j = 1$, the integral under evaluation in (3.36) is the same as the integral in (3.19). Hence, the average probability of detection for SLS over TWDP fading can be obtained by averaging 3.35 over independent TWDP branches. Therefore, by substituting (3.19) into (3.36), the following lemma yields.

Lemma 4: The closed form expression of the average probability of detection over TWDP fading channels with SLS diversity reception is deduced as,

$$\begin{aligned}\bar{P}_{d_{TWDP}}^{SLS} =& 1-\prod_{j=1}^{L}\left[1-\sum_{i=1}^{M}\frac{1}{2}a_i\left[Q\left(\sqrt{\frac{2K\bar{\gamma}_j(1-a_i)}{K+\bar{\gamma}_j+1}},\sqrt{\frac{\lambda(K+1)}{K+\bar{\gamma}_j+1}}\right)\right.\right.\\ &\left.\left.+Q\left(\sqrt{\frac{2K\bar{\gamma}_j(1+a_i)}{K+\bar{\gamma}_j+1}},\sqrt{\frac{\lambda(K+1)}{K+\bar{\gamma}_j+1}}\right)\right]\right].\end{aligned} \tag{3.37}$$

3.4.4 Threshold Optimisation

As discussed in Chapter 2, the selection of the detection threshold selection is a critical task as it determines the trade-offs between the probabilities of false alarm and detection or missed detection and, hence, affects the spectrum sensing performance. Probability of false alarm and miss detection are the two error metrics for spectrum sensing. In traditional Constant False Alarm Rate (CFAR) spectrum sensing, the detection threshold is selected subject to a given P_{fa} constraint.

The threshold selection mechanism for CFAR ED-based spectrum sensing is described in Figure 3.1. Let $f(H_0)$ and $f(H_1)$ correspond to the noise and signal power distribution. By setting a detection threshold λ_{CFAR}, the area of the $f(H_0)$ that exceeds the λ_{CFAR} expresses the P_{fa} whereas the area of $f(H_1)$ below λ_{CFAR} expresses P_{md}. However, with reference to Figure 3.2, which describes a scenario with higher SNR, it can be seen that by using the CFAR approach the probability of false alarm remains the same whereas the probability of missed detection is reduced. Therefore, taking into account both P_{fa} and P_{md} the sensing performance can be improved in terms of SNR requirements. In addition taking into account both sensing error metrics, optimal sensing performance can be achieved by improving the spectrum efficiency and minimising the interference to the primary system at the same time.

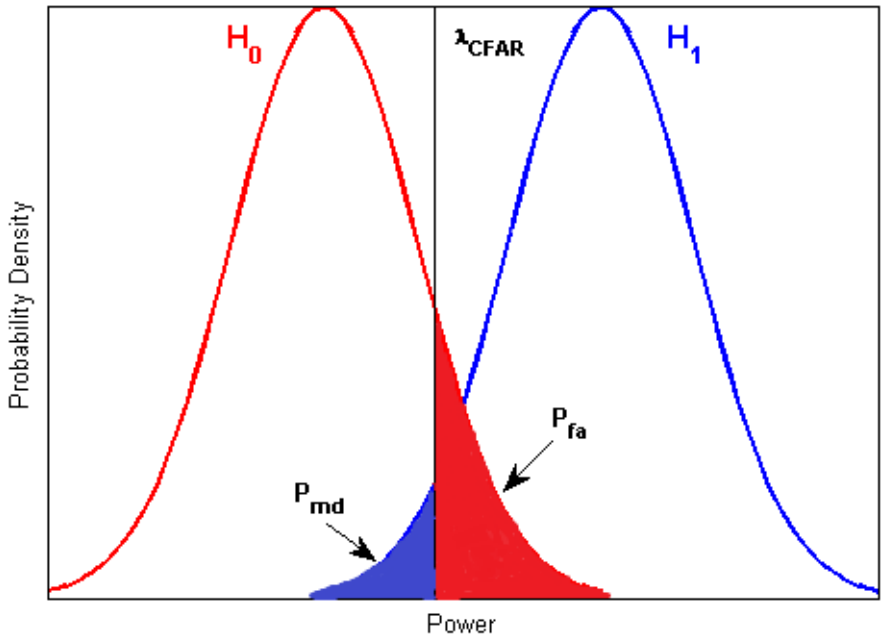

Figure 3.1: Threshold selection in CFAR ED-based spectrum sensing.

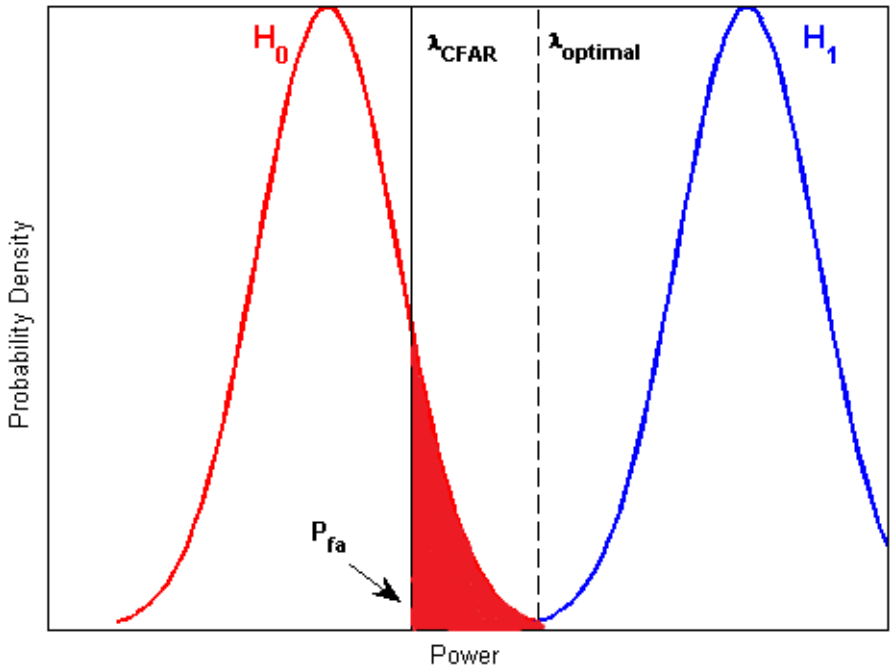

Figure 3.2: Adaptive threshold selection for ED-based spectrum sensing.

To this end, a dynamic detection threshold mechanism is proposed where contrary to CFAR ED-based spectrum sensing the detection threshold is determined with respect to the minimal detection error probability, P_e [99]. Based on the fact that false alarms and missed detections occur under hypotheses H_0 and H_1 the detection error probability can be expressed as a linear combination of P_{fa} and P_{md} with the corresponding PU occupancy statistics as weights [100]. Hence,

$$P_e = P(H_0)P_{fa} + P(H_1)P_{md}, \tag{3.38}$$

where $P(H_0)$ and $P(H_1)$ denote the probability of PU presence and absence, respectively, with $P(H_0) + P(H_1) = 1$. Note that for $P(H_0) = P(H_1) = 0.5$ (3.38) expresses the total sensing error.

The optimal detection threshold, λ_{opt}, that minimises the detection error probability, P_e, can be obtained by,

$$\lambda_{opt} = argmin(P(H_0)P_{fa} + P(H_1)P_{md}). \tag{3.39}$$

This can be achieved when,

$$P(H_0)\frac{\partial P_{fa}}{\partial \lambda} + P(H_1)\frac{\partial P_{md}}{\partial \lambda} = 0. \tag{3.40}$$

Therefore, the derivative terms $\frac{\partial P_{fa}}{\partial \lambda}$ and $\frac{\partial P_{md}}{\partial \lambda}$ need to be evaluated. As P_{fa} does not depend on the fading statistics of the channel, $\frac{\partial P_{fa}}{\partial \lambda}$ for AWGN is derived in [99] as,

$$\frac{\partial P_{fa}}{\partial \lambda} = -\frac{1}{(u-1)!}\frac{\lambda^{u-1}}{2u}e^{-\frac{1}{2}}. \tag{3.41}$$

Given the probability of detection over TWDP fading, (3.19) and based on the chain rule, $\frac{\partial P_d}{\partial \lambda}$ is obtained as,

$$\frac{\partial P_d}{\partial \lambda} = -\frac{(K+1)}{2\left(\frac{\lambda(K+1)}{K+\bar{\gamma}+1}\right)^{\frac{1}{2}}(K+\bar{\gamma}+1)} \sum_{i=1}^{M} \frac{1}{2} a_i \left[exp\left(-\frac{2K\bar{\gamma}(1-a_i)+\lambda(K+1)}{2(K+\bar{\gamma}+1)} \right) I_0\left(\frac{2K\bar{\gamma}\lambda(K+1)(1-a_i)}{(K+\bar{\gamma}+1)^2} \right) + exp\left(-\frac{2K\bar{\gamma}(1+a_i)+\lambda(K+1)}{2(K+\bar{\gamma}+1)} \right) I_0\left(\frac{2K\bar{\gamma}\lambda(K+1)(1+a_i)}{(K+\bar{\gamma}+1)^2} \right) \right]. \tag{3.42}$$

A detailed derivation of (3.42) is presented in appendix A.

Taking into account that $P_{md} = 1 - P_d$ yields $\frac{\partial P_{md}}{\partial \lambda} = -\frac{\partial P_d}{\partial \lambda}$. Hence, using (3.41) and (3.42) the solution to $P(H_0)\frac{\partial P_{fa}}{\partial \lambda} + P(H_1)\frac{\partial P_{md}}{\partial \lambda} = 0$ provides the optimal detection threshold for different occupancy statistics $P(H_0)$ and $P(H_0)$ over TWDP fading channels.

3.5 Numerical Results

This section presents numerical results on the performance of ED-based spectrum sensing for different operating scenarios and fading conditions. Different spectrum sensing schemes are considered, including single user spectrum sensing, diversity reception and cooperative spectrum sensing. The performance of ED-based spectrum sensing with optimised threshold over hyper-Rayleigh fading conditions is also analysed. Additionally, a numerical analysis of the effect of the TWDP fading parameters on the detection performance is provided. The detection performance is evaluated through the ROC (P_d vs. P_{fa}) and complementary ROC (P_{md} vs. P_{fa}) curves as well as in terms of the detection accuracy with respect to the SNR requirements.

3.5.1 Fading Scenarios

The selected fading scenarios are considered as representatives for describing the behaviour of ED-based spectrum sensing under moderate, severe and worse than Rayleigh fading conditions within realistic operational environments as per Table 3.2. Scenario 1 describes typical Rayleigh fading, while Scenario 2 represents Rician fading with a K-factor of 5 dB. These scenarios are adequent representatives of cognitive M2M wireless deployments operating in both indoor and outdoor environments. On the other hand, Scenarios 3-5 are chosen to describe the operation of cognitive M2M deployments in confined structures under extreme fading conditions.

All the aforementioned scenarios are based on the experimental work in [80] and can model the behaviour of static nodes that operate within in-vehicular environments in the 2.4 GHz Industrial Scientific and Medical (ISM) band. Three different in-vehicular environments are considered including a single-deck bus and two different types of airframe, an MD-90 and a 747-400. Due to the enclosed, metallic structure of such environments, the SU is expected to experience rapid fluctuations and deep fades in the received signal over distances of the order of a wavelength because of reflections which result in severe small-scale fading conditions [101]. Furthermore, due to the rich in multipath environment, which may lead in increased spread figures, severe frequency selective behaviour is also expected. In this context, Rician and Rayleigh fading are used to describe moderate and severe fading conditions, respectively, whereas the hyper-Rayleigh channel model is used to desrcibe extreme fading conditions.

Table 3.2: Fading scenarios.

Scenario	Environment	K	Δ	Fading
Scenario 1	Indoor/ outdoor	0 dB	-	Rayleigh
Scenario 2	Indoor/ outdoor	5 dB	$\Delta = 0$	Rician
Scenario 3	747-400 airframe	10 dB	$\Delta = 1$	hyper-Rayleigh
Scenario 4	MD-90 airframe	20 dB	$\Delta = 1$	hyper-Rayleigh
Scenario 5	Single-deck bus	30 dB	$\Delta = 1$	hyper-Rayleigh

The severity of different fading channels is presented in Figure 3.3, which describes the frequency selective fading behaviour of Rician, Rayleigh, and hyper-Rayleigh channels in the 2.4 GHz ISM band. It can be seen that all traces exhibit similar large-scale behaviour with a median received power of -45 dB (Rician), -46 dB (Rayleigh), and -48 dB (hyper-Rayleigh). However, their small-scale fading statistics are significantly different. More specifically, the Rician trace fluctuates smoothly whereas the Rayleigh and hyper-Rayleigh exhibit higher than 20 dB and 30 dB fades, respectively, which in turn result in severe and extreme fading conditions.

3.5.2 Simulation Model

The derived analytical expressions are substantiated through both numerical evaluations and simulations. The simulation model for the wireless fading channel is built as shown in Figure 3.4. This simulation model generates the received signal, $y(t)$, at the detector front-end based on the signal's structure given by expression (3.12). The required fading channel coefficients, g, for the fading channel are generated on a case by case basis. For each scenario the corresponding channel coefficients are obtained through the TWDP PDF given by expression (3.4). Noise is modelled as AWGN with variance $\sigma_w = 1$ and as such, the corresponding noise samples are drawn from a Gaussian random process $(0, 1)$.

The received SNR γ is defined as $\frac{g^2 E_b}{N_0}$. Hence, the average SNR, $\bar{\gamma} = E\big(\frac{g^2 E_b}{N_0}\big)$ where $E(.)$ denotes the mathematical expectation. According to [26],

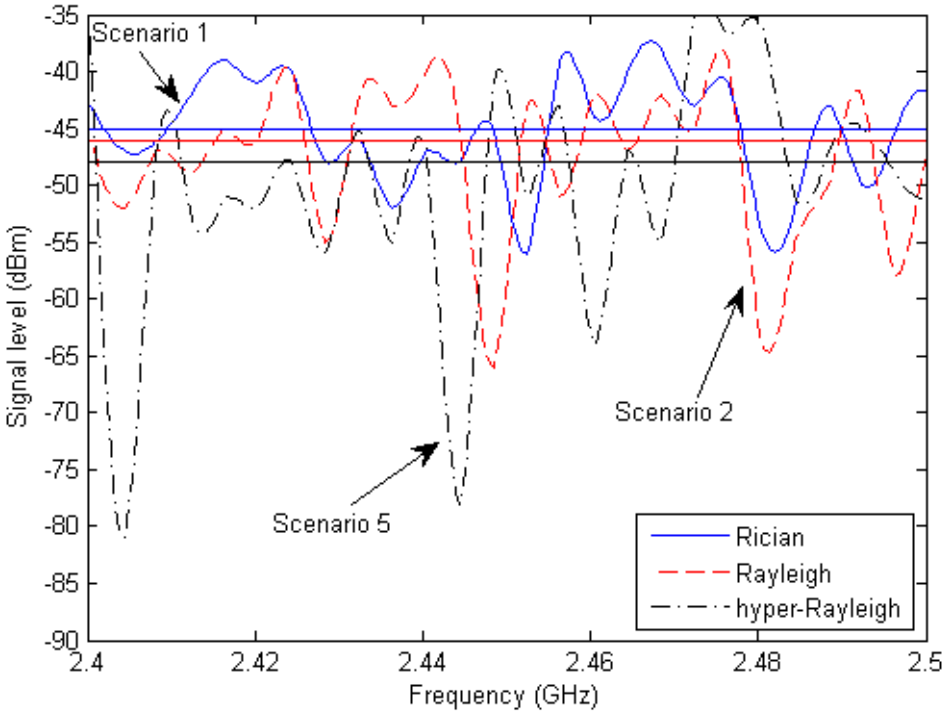

Figure 3.3: TWDP fades.

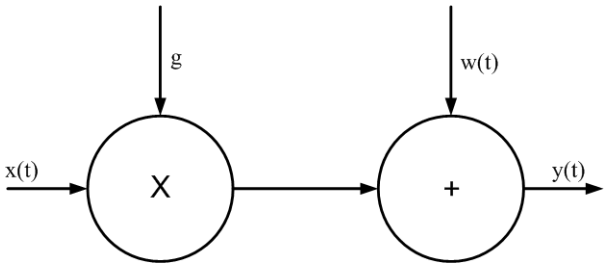

Figure 3.4: Simulation model of ED-based spectrum sensing over a fading channel.

for ED-based spectrum sensing the received signal's energy is obtained within an observation interval T as,

$$E_x = \int_0^T x^2(t)dt = \frac{1}{2TW}\sum_{i=1}^{2u} x_i^2 \tag{3.43}$$

Assuming that the energy E_y of $y(t)$ is observed within $2u$ samples,

$$x_i^2 = \frac{TWE_x}{u} \tag{3.44}$$

Therefore, based on the simulation model in [102], for a time-bandwidth

product $u = TW = 1$ and a given $\bar{\gamma}$, a minimum of $2u$ samples of $y(t)$ are required to calculate the signal's energy, E_y. Then, the $2u$ samples are multiplied with the corresponding fading channel coefficient. In the case of H_1, the samples of $y(t)$ are constructed by adding the noise samples from a Gaussian random process $(0, 1)$ to the corresponding samples of $x(t)$. In the case of H_0, no PU signal is present and thus, all x_i samples are of zero energy.

The test statistic, T_y, is generated from equally likely hypothesis (probability that event H_0 and H_1 occur is 0.5), unless otherwise stated. By comparing T_y with the detection threshold, λ, the presence or absence of a PU signal is determined. The value of λ is calculated subject to a P_{fa} constraint as discussed in the previous chapter. After 10^5 iterations, the average P_{fa} and P_d are obtained as,

$$P_{fa} = \frac{N_{fd}}{N_{H_0}} \tag{3.45}$$

$$P_d = \frac{N_{cd}}{N_{H_1}}, \tag{3.46}$$

where N_{fd} and N_{cd} denote the total number of false and correct detections, respectively whereas N_{H_0} and N_{H_1} denote the total number of times the PU signal is under hypothesis H_0 and H_1, respectively.

3.5.3 Results and Discussion

Figure 3.5 shows the complementary ROC curve for ED-based spectrum sensing over TWDP fading obtained using expressions (3.15) and (3.19) for the range of K and Δ values specified in Table 3.2. The SNR is fixed to 15 dB as it has been found to provide adequate detection performance over AWGN channels [103]. The complementary ROC curves for Rician and Rayleigh fading channels are shown in the same figure for comparison between the derived expression and the relevant expressions from [75]. Notice that these two curves closely match the curves obtained using our derived expression for the special cases of Rayleigh (K=0 dB) and Rician ($K = 5$ dB, $\Delta = 0$). The good match

between these curves and between the simulation and analysis results suggests that the proposed physical model is valid as well as that the derived expression for the average probability of detection over TWDP fading channels presents an effective approximation of realistic fading scenarios.

With reference to Figure 3.5, it can be seen that as the value of K increases, the ROC curve moves within the hyper-Rayleigh region towards the upper bound of two-ray fading ($K = \infty$, $\Delta = 1$). These results suggest that inferior detection performance is achieved when compared to the Rayleigh fading as a result of cancellation of two anti-phase specular waves and the low power of diffused components. Indicatively, for a $P_{md} = 0.1$, i.e, $P_d = 0.9$ the corresponding P_{fa} reaches 0.01 and 0.03 under Rician and Rayleigh whereas for hyper-Rayleigh fading varies from 0.27 to 0.7. Therefore, under "hyper-Rayleigh" fading conditions the required criterion $P_{fa} \leq 0.1$ is not met. It is worth noting that such high false alarm values would prevent any unused spectrum from being accessed by the CR nodes, leading to low spectral utilisation.

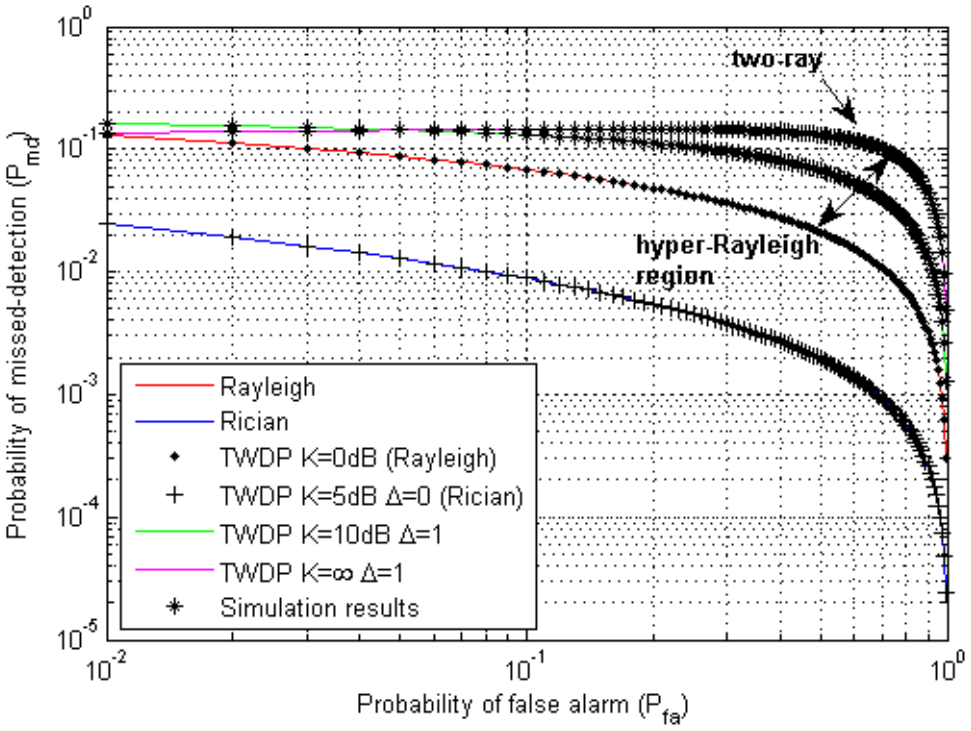

Figure 3.5: Complementary ROC curve for ED-based spectrum sensing over TWDP fading with different K and Δ values for $\bar{\gamma} = 15$ dB.

Figures 3.6, 3.7 and 3.8 present the detection performance of ED-based spectrum sensing with respect to the required average SNR, $\bar{\gamma}$, for different fading scenarios. The results are obtained by plotting (3.19) for different SNR values in the range of 0 dB-30 dB. Figure 3.6 shows the detection performance over a TWDP fading channel for the same range of K values as in Durgin's analysis in [87] and $\Delta = 1$. When $\Delta = 1$, both specular waves are out of phase and of equal strength, while the specular power is K times larger than the power of the diffuse component. This results in a poorer detection performance than for Rayleigh fading channels.

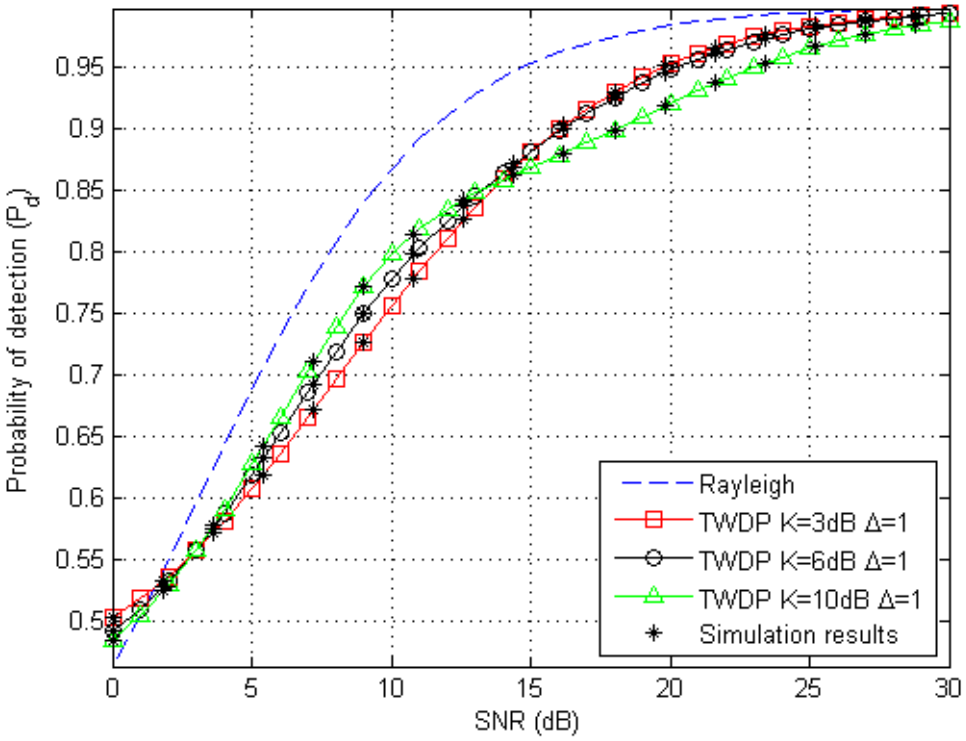

Figure 3.6: $\bar{P}_{d_{TWDP}}$ versus SNR for ED-based spectrum sensing over TWDP fading for a target $P_{fa} = 0.1$ with different values of K.

Figure 3.7 depicts the performance of ED-based spectrum sensing for $K =$ 10 dB and different values of Δ from 0 to 1. It can be seen that the detection performance deteriorates when Δ approaches to 1, i.e. moves from Rician to a two-wave scenario and the two specular components start cancelling each other out.

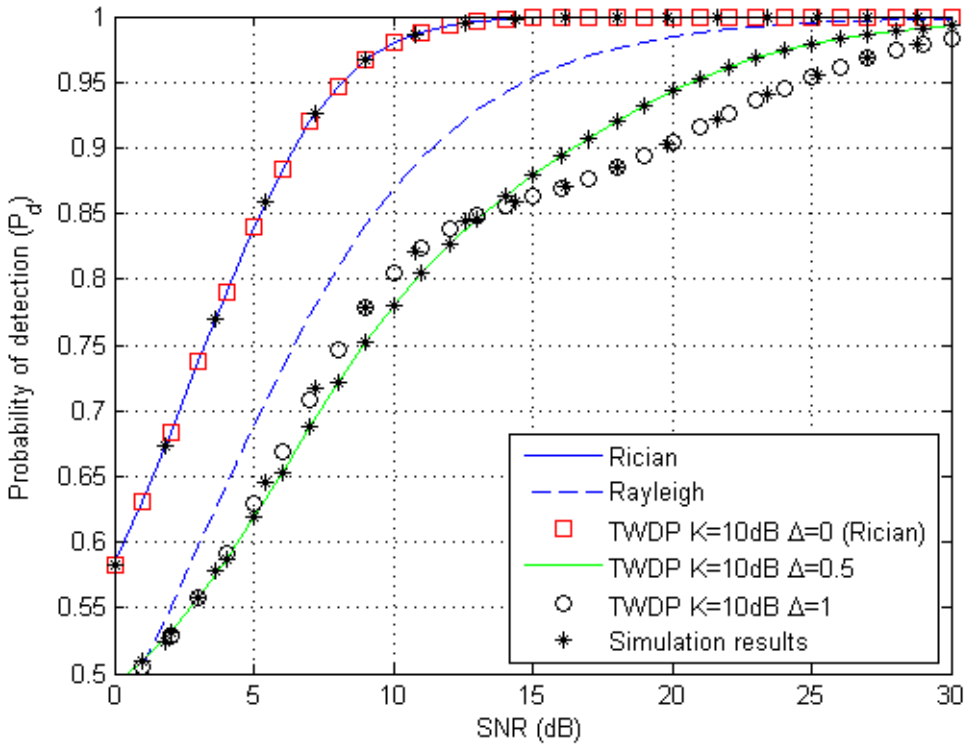

Figure 3.7: $\bar{P}_{d_{TWDP}}$ versus SNR for ED-based spectrum sensing over TWDP fading for a target $P_{fa} = 0.1$ with different values of Δ.

Similarly, Figure 3.8 describes the sensing performance within a severe fading scenario, i.e. $K \geq 10$ dB and $\Delta = 1$, in which the diffuse components are of equal power whereas the total power of the specular waves is at least ten times that of the diffuse component. Under such fading conditions, as the value K increases, the product of K and Δ becomes large and the TWDP PDF becomes bimodal, thus exhibiting two maxima [87]. This in turn results in the order change that is observed in the $\bar{\gamma}$ versus $\bar{P}_{d_{TWDP}}$ curves at an SNR of 15 dB. The curve for the case of two-ray fading channel is also provided as the upper-bound of hyper-Rayleigh fading.

The obtained results suggest that the average detection performance deteriorates as K increases, (the PDF moves from Rician to the two-wave fading scenario) as the two specular components cancel each other out and the power difference between the multipath components and the corresponding diffuse components increases. More specifically, for $\Delta = 1$, $K = 10$ dB, a minimum SNR of 18 dB is required to achieve a $P_d = 0.9$, while for $\Delta = 1$, $K = 20$ dB and $\Delta = 1$, $K = 30$ dB a minimum SNR of 21 dB and 23 dB is required, respectively. On the other hand, ED-based spectrum sensing over Rayleigh requires and SNR of 13 dB. According to these SNR figures, it is deduced that the SNR requirements for $P_d = 0.9$ are increased up to 77% which would significantly affect the energy efficiency of energy-constrained CR nodes.

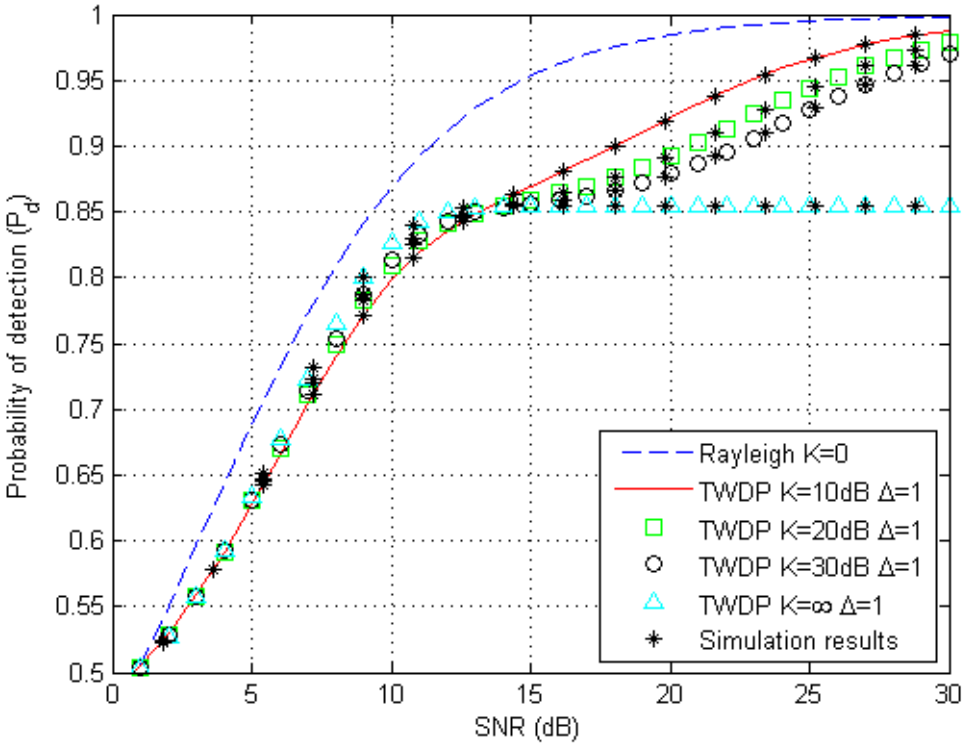

Figure 3.8: $\bar{P}_{d_{TWDP}}$ versus $\bar{\gamma}$ for ED-based spectrum sensing over TWDP fading for a target $P_{fa} = 0.1$ with different values of $K \geq 10dB$ and $\Delta = 1$.

Figure 3.9 describes how the detection performance of ED-based spectrum sensing in terms of P_d is affected as K increases, for the extreme case of the two-wave fading channel, i.e. $\Delta = 1$. The behaviour of ED-based spectrum sensing is studied for three scenarios with a target $P_{fa} = 0.1$ and SNR values of 3 dB, 6 dB and 10 dB. It is observed that although the detection performance is not very sensitive to the variations of K, for such fading conditions, ED is unable to achieve a probability of detection of P_d, that ensures efficient spectrum sensing in terms of interference to the PUs as indicated by the IEEE 802.22 standard in [13].

Similarly, Figure 3.10 presents the effect of the fading parameter Δ on the detection performance in terms of the corresponding for a fading scenario with $K = 10$ dB. It can be seen that the detection performance degrades significantly as Δ increases from 0 (Rician) to 1 (two-wave) since the channel exhibits worse fading than Rayleigh due to deep fades.

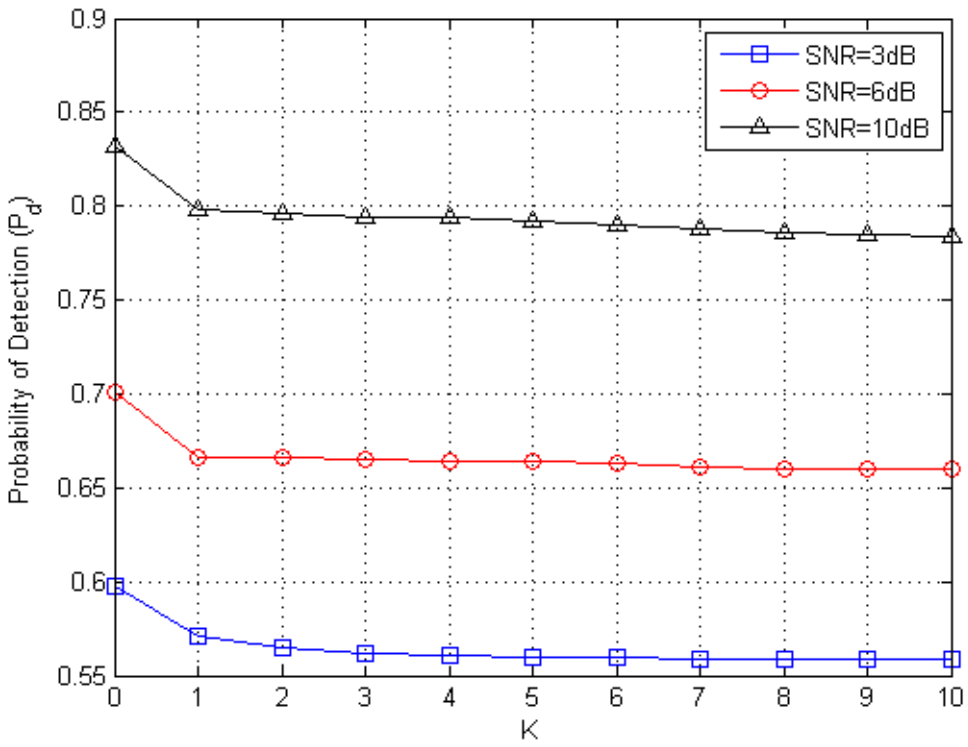

Figure 3.9: $\bar{P}_{d_{TWDP}}$ versus K for ED-based spectrum sensing over TWDP fading for a target $P_{fa} = 0.1$ with different values of $\bar{\gamma}$.

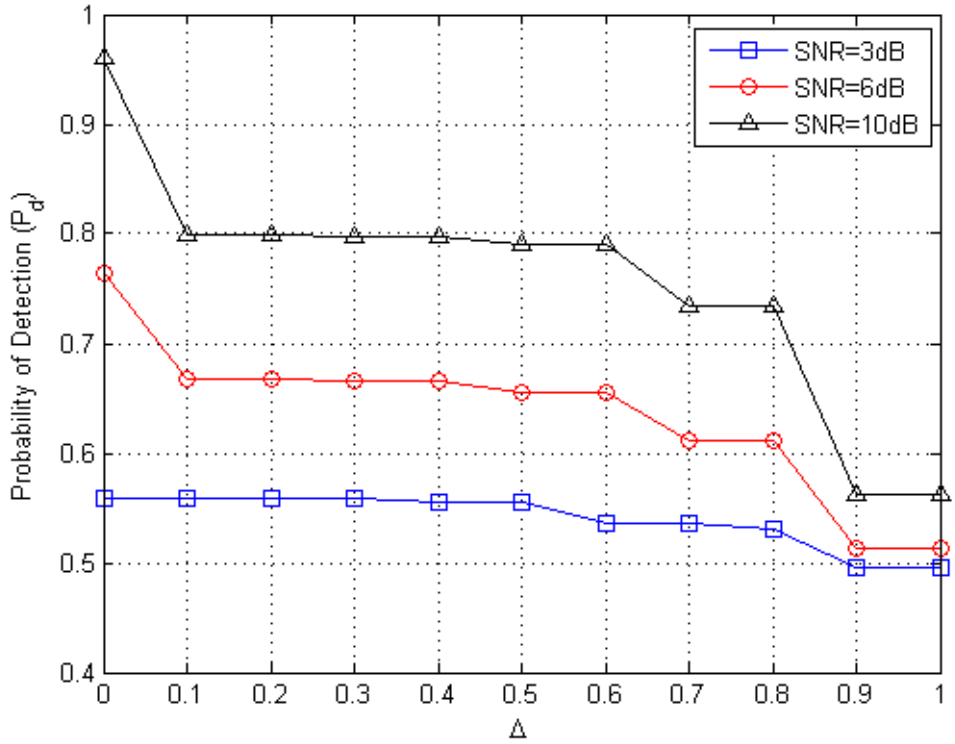

Figure 3.10: $\bar{P}_{d_{TWDP}}$ versus Δ for ED-based spectrum sensing over TWDP fading for a target $P_{fa} = 0.1$ with different values of $\bar{\gamma}$.

These results indicate that the overall detection performance is affected by the fading parameters, particularly in high SNR regions. More specifically for a fading scenario of an in-vehicular network, with $K = 10$ dB and $\Delta = 1$, SNR of more than 19 dB is required in order to achieve a detection performance of $P_d = 0.9$ and $P_{fa} = 0.1$, while for Rayleigh and Rician fading an SNR of 13 dB and 8 dB is required, respectively. Such SNR requirements could significantly affect the energy efficiency of energy-constrained terminals in such WSN deployments. Although, such deep fades could be avoided by simply moving the receiver a fraction of a wavelength, this is not always possible, as in the case of a static node deployment that is often used in WSNs and M2M deployments. Therefore, cooperation and diversity reception are proposed as a means of mitigating the effect of TWDP fades in the spectrum sensing performance.

In this context, by plotting expressions (3.27) and (3.28), Figure 3.11 illustrates the ROC curve for ED-based spectrum sensing with up to six cooperative CR users over a TWDP fading channel with $K = 10$ dB and $\Delta = 1$. For this scenario the OR-voting fusion rule with an average SNR of $\bar{\gamma} = 10$ dB is considered. It can be seen that the detection performance of the ED-based scheme improves substantially as the number of cooperative CR users increases. The Rayleigh curve for single-user detection is also provided for comparison. For this fading scenario, for a target probability of false alarm $P_{fa} = 0.1$, the probability of detection for six cooperative users is approximately 45% larger than for single user spectrum sensing.

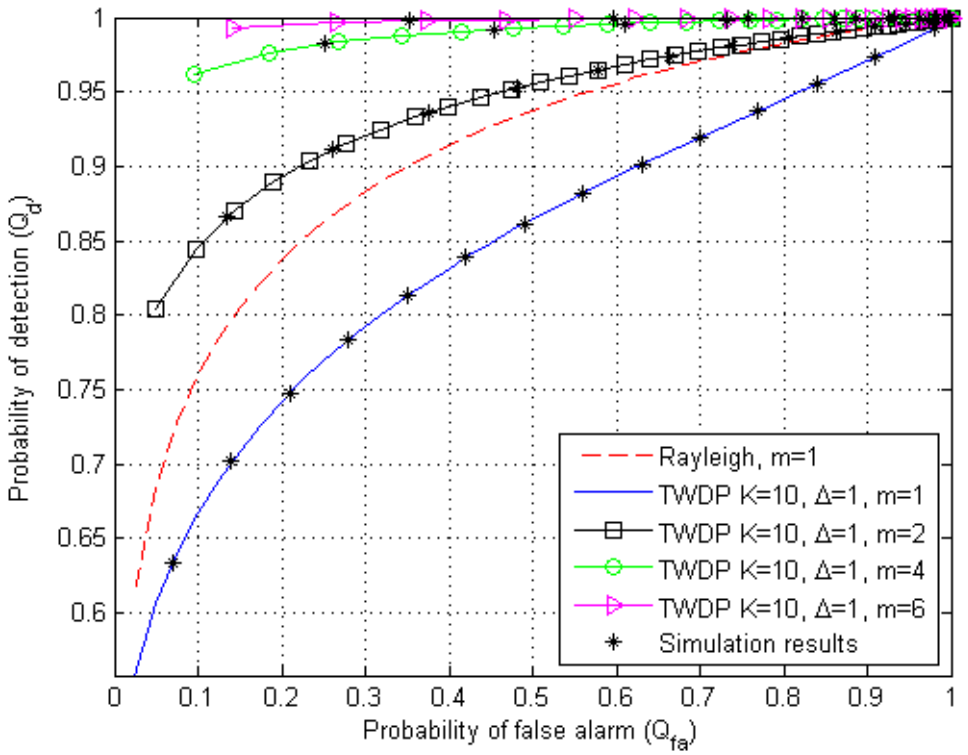

Figure 3.11: ROC curves for ED-based spectrum sensing with OR-voting fusion rule based cooperation with n SUs for $\bar{\gamma} = 5$ dB, $K = 10$ dB and $\Delta = 1$.

Figure 3.12 shows the ROC curve for ED-based spectrum sensing over the same operational scenario and fading conditions. However, for this case an AND-voting fusion rule is considered. As it can be seen, cooperative spectrum sensing with AND-voting fusion rule cannot improve the detection performance over TWDP fading channels as it requires from all the cooperative sensing users to have the same sensing result in order to determine whether a PU is present or absent. Hence, over such severe fading conditions the probability of all cooperative SUs to have same sensing results decreases exponentially (Figure 3.13) which in turn results in overall detection performance degradation.

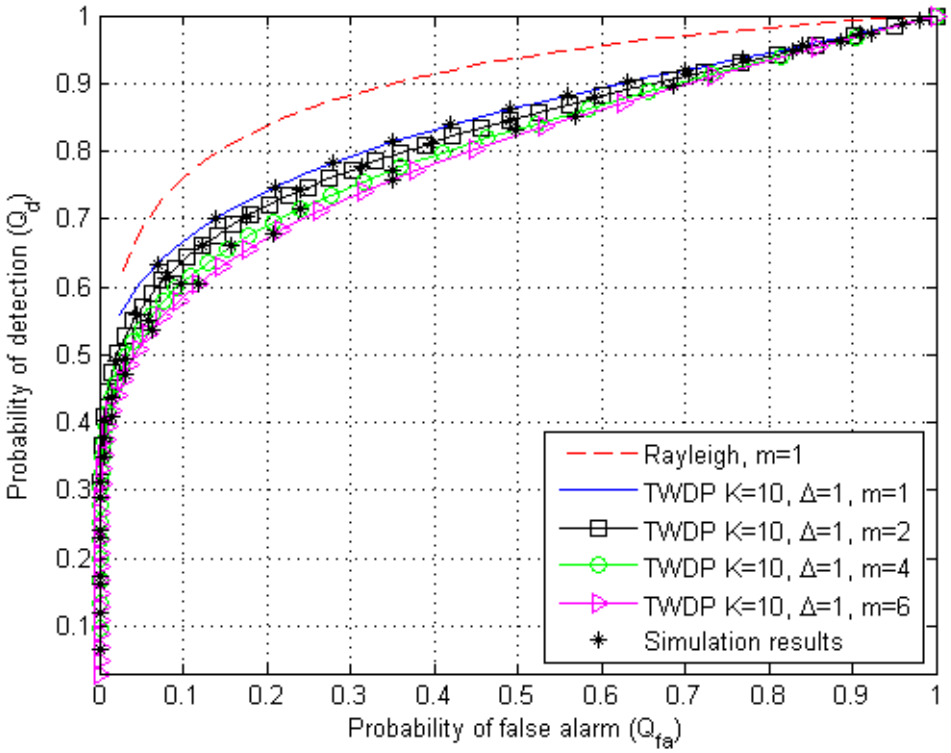

Figure 3.12: ROC curves for ED-based spectrum sensing with AND-voting fusion rule based cooperation with n SUs with $\bar{\gamma} = 5$ dB, $K = 10$ dB and $\Delta = 1$.

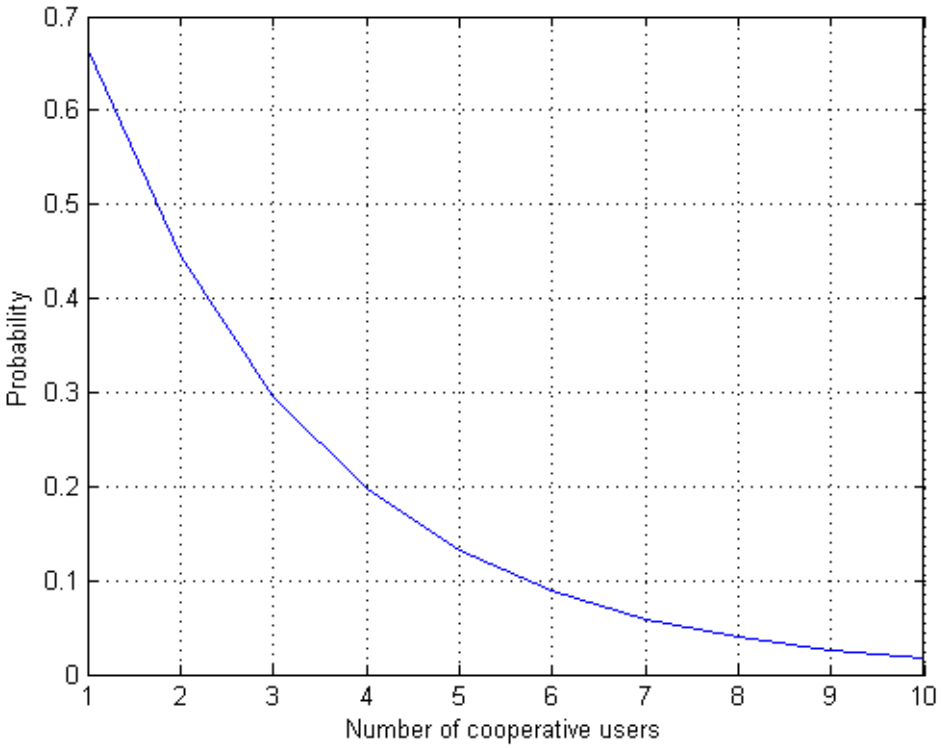

Figure 3.13: Probability of detection versus the number of cooperative users for AND-voting fusion rule.

Based on the obtained results, OR-voting fusion rule has been found to be a more effective cooperative spectrum sensing scheme compared to AND-voting fusion rule. In this context, Figure 3.14 describes the performance of the OR-voting fusion rule cooperative scheme over TWDP fading with respect to the SNR requirements. The highest cooperation gain is observed from the single-user to the two cooperative users case. Indicatively, for a target $P_d = 0.9$ an SNR value of 18 dB is required for single-user spectrum sensing whereas for the case of two cooperative sensing users the same performance is achieved for an SNR of 6.5 dB resulting in a cooperation gain of 11.5 dB.

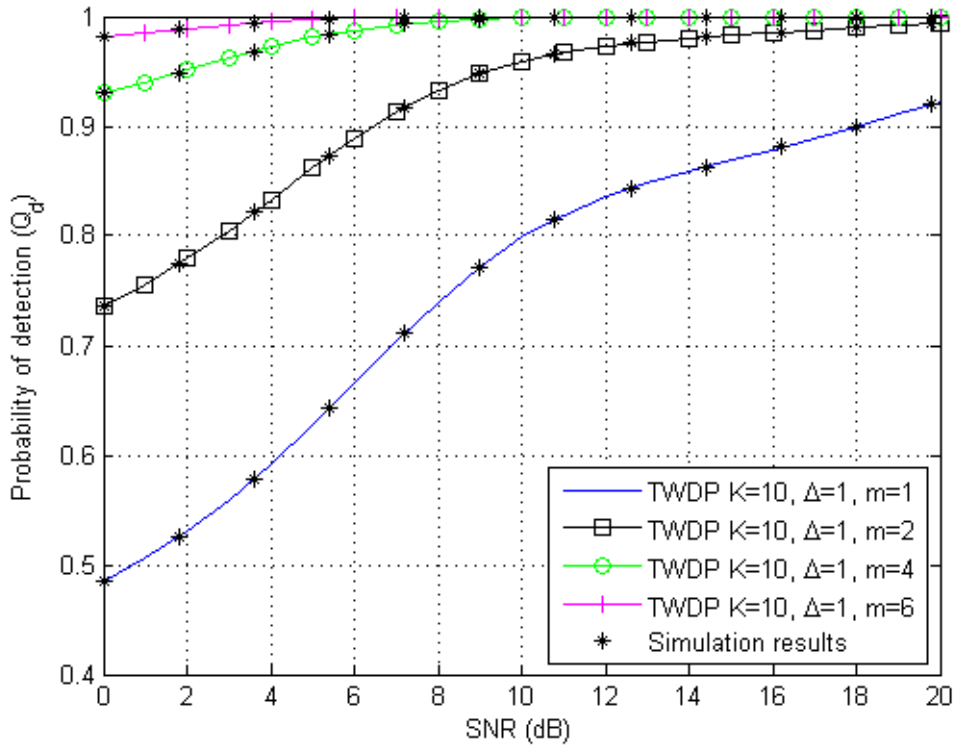

Figure 3.14: Probability of n cooperative users to have the same sensing output of a TWDP fading channels with $K = 10$ dB and $\Delta = 1$.

Although cooperation achieves significant gains and can improve the sensing performance over TWDP fading channels it requires dedicated channels for exchanging sensing results between the cooperative nodes. In addition, as the number of cooperative nodes increases the communication overhead increases which may result in sensing delays and low spectrum utilisation. Thus, SLS diversity reception can be employed to mitigate the fading effects with reduced complexity and infrastructure requirements. More specifically, Figure 3.15, obtained by plotting expressions (3.33) and (3.37), describes the detection performance for and SLS diversity scheme with up to five branches. The average SNR for each branch is set to $\bar{\gamma}_1 = 5$ dB, $\bar{\gamma}_2 = 1$ dB, $\bar{\gamma}_3 = 2$ dB, $\bar{\gamma}_4 = 3$ dB and $\bar{\gamma}_5 = 4$ dB.

With reference to Figure 3.15 it can be seen that as the number of diversity branches increases the detection performance improves as the average probability of detection increases by up to 38% for $L = 5$. More specifically, for a target probability of false alarm $P_{fa} = 0.1$, the probability of detection for $L = 5$ is 95% larger than the corresponding value for $L = 1$. Additionally, the highest diversity gain is observed from the no diversity case to the dual branch ($L = 2$) scheme.

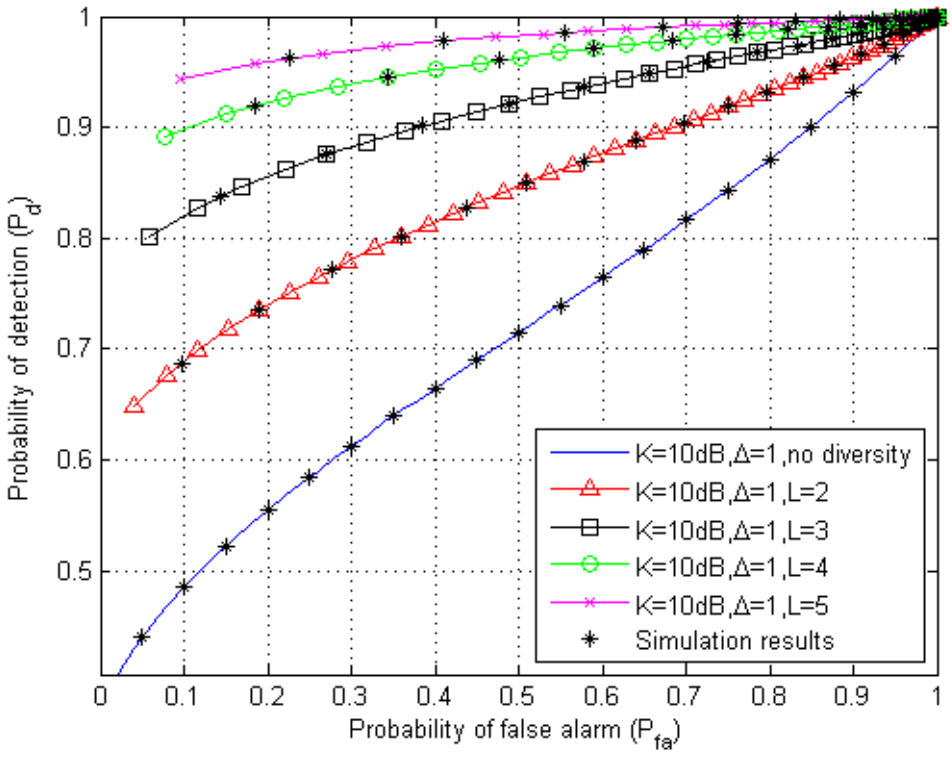

Figure 3.15: ROC curves for ED-based spectrum sensing with SLS diversity reception over TWDP fading with $K = 10$ dB, $\Delta = 1$ and $\bar{\gamma}_1 = 0$ dB, $\bar{\gamma}_2 = 1$ dB, $\bar{\gamma}_3 = 2$ dB, $\bar{\gamma}_4 = 4$ dB.

In all previous cases, CFAR ED-based spectrum sensing with the detection threshold being determined subject to a $P_{fa} = 0.1$ constraint is considered. By analysing the detection performance, in terms of the detection error probability, P_e, as discussed in Subsection 3.4.4, with respect to the required SNR it can be seen that the resulting curves have a global minimum for any fading scenario as shown in Figure 3.16. This implies that there is an exact value of λ, which minimises P_e which can analytically be obtained as shown in Subsection 3.4.4. As expected, the best detection performance is achieved over AWGN with $P_{e_{min}} = 0.05$, whereas $P_{e_{min}} = 0.3$ over TWDP with $K = 10$ dB and $\Delta = 1$.

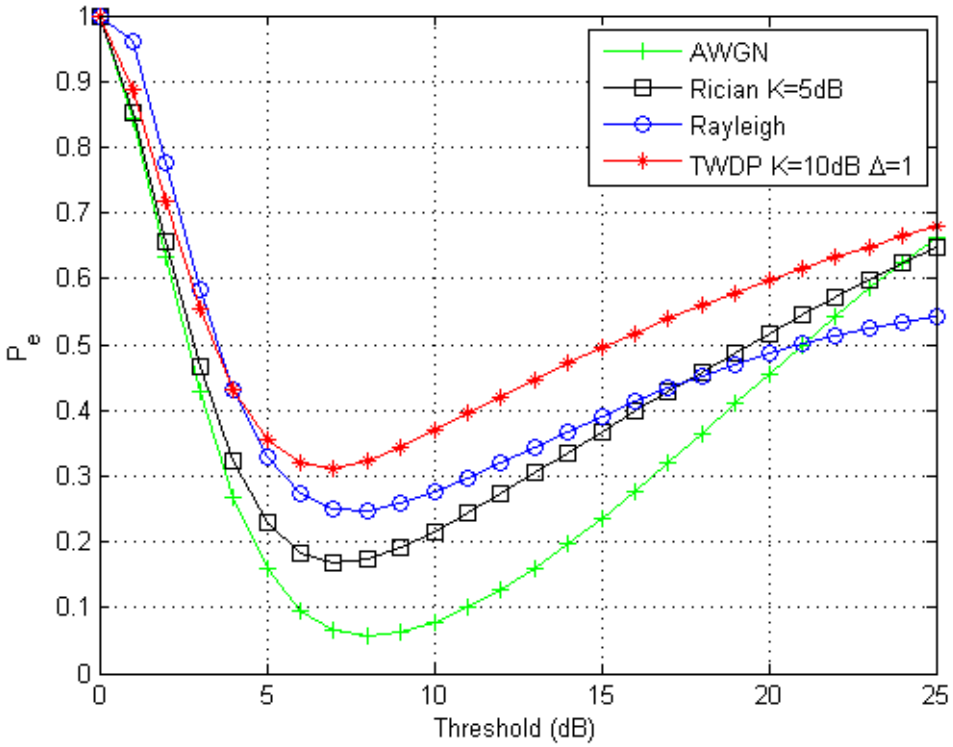

Figure 3.16: Detection error probability of ED-based spectrum sensing over different fading channels for $\bar{\gamma} = 10$ dB

The CFAR performance curves are obtained by evaluating (3.19) with respect to the required SNR for a detection threshold $\lambda = 4.6$ dB that corresponds to a target $P_{fa} = 0.1$. On the other hand, the performance curves of the optimal threshold approach are obtained by evaluating (3.19). The detection performance is analysed for the operational scenarios and fading conditions as per Table 3.2. The extreme case of two-ray fading with $K = \infty$ and $\Delta = 1$ is also considered as the upper bound of hyper-Rayleigh fading.

In Figure 3.17 the performance of CFAR and optimal threshold ED-based spectrum sensing is compared for a range of fading scenarios. Rayleigh fading (highlighted curves) is considered as a performance benchmark whereas the two-ray fading scenario is considered as the upper bound of "hyper-Rayleigh" fading. It is observed that the optimal threshold sensing approach outperforms the CFAR one. Indicatively, the average P_e is improved by approximately up to 50% for every fading scenario. In addition, it is shown that using optimal detection threshold the SNR requirements are significantly reduced. More specifically, for Scenario 1, CFAR achieves a minimum $P_e = 0.22$ at 25 dB whereas the same P_e is achieved for an SNR of 13 dB when optimal threshold is applied. Similarly, for Scenario 2 the minimum P_e of 0.24 is achieved for an SNR of 25 dB whereas the optimised method requires an SNR of 12 dB to achieve the same performance. For Scenario 3, an SNR of 25 dB is required for a P_e of 0.26. On the other hand, under same fading conditions, an SNR of 11 dB is required when optimal threshold is applied. Those results suggest that the use of the optimal threshold can achieve SNR gains of up to 13 dB in terms of detection error probability P_e.

These results suggest that the use of the optimal threshold can achieve SNR gains of up to 13 dB in terms of detection error probability P_e. Such gains are achieved due to the fact that the threshold is selected based on the SNR and the signal fading statistics as explained in Subsection 3.4.4. To this end, the performance of the optimal detection ED-based spectrum sensing in terms of false alarm and detection probabilities independently is analysed in Figure 3.18. It can be seen that although the proposed approach achieves similar P_d

to the CFAR ED-based spectrum sensing it significantly reduces the P_{fa}. This in turn explains the high SNR gains in the detection performance in terms of P_e.

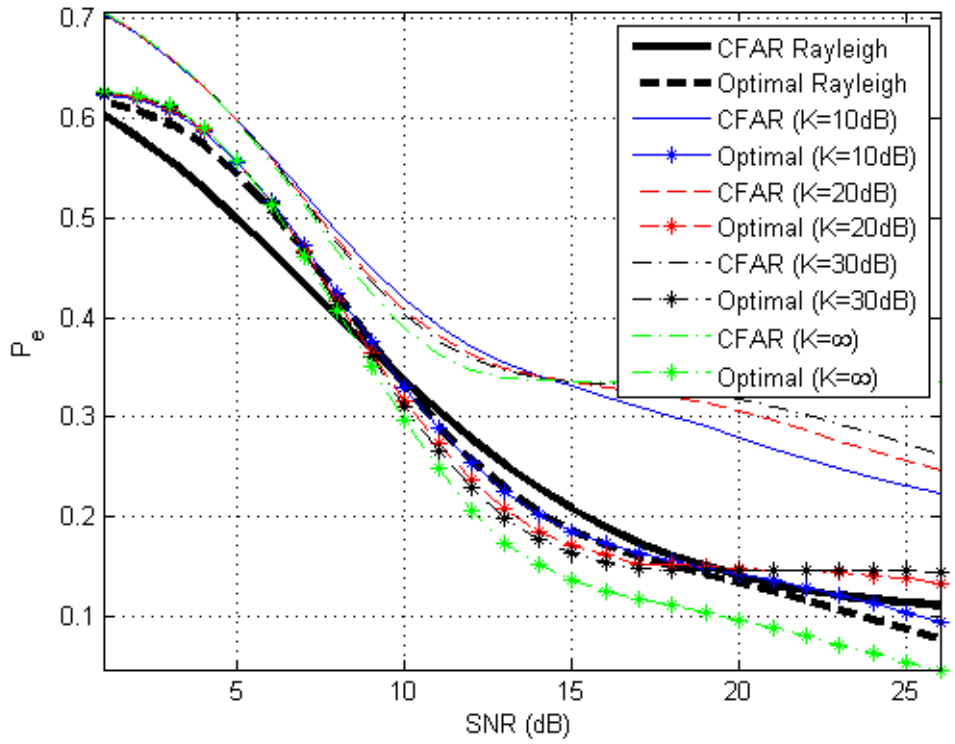

Figure 3.17: Detection error probability, P_e, for CFAR and optimal threshold ED-based spectrum sensing over different fading channels.

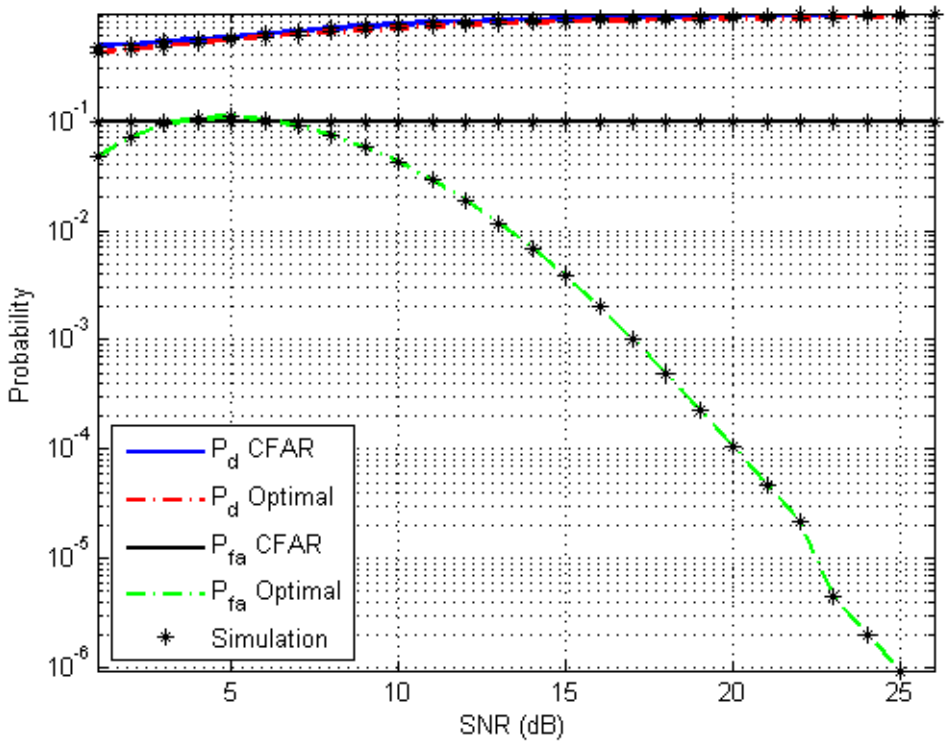

Figure 3.18: Probability of detection and false alarm for CFAR and optimised ED-based spectrum sensing over different TWDP fading with $K = 10$ dB and $\Delta = 1$.

In all previous cases, equal occupancy probabilities $P(H_0) = P(H_1) = 0.5$ are considered. However, as it can be seen from (3.40) the optimal detection threshold depends on the spectrum occupancy statistics. In this context, Figure 3.19 analyses the performance of the optimal threshold approach in terms of P_e with respect to the received signal's SNR and the spectrum occupancy statistics $P(H_0)$. Note that, $P(H_0)$ denotes the spectrum availability and thus, spectrum occupancy $P(H_1)$ is given as $1 - P(H_0)$.

With reference to Figure 3.19 it is shown that highly occupied channels ($0 \leq P(H_0) \leq 0.2$) result in high P_e within the range of 0.6-1 as the probability of a TWDP fade with $K = 10$ dB and $\Delta = 1$ to occur is in the range between 80%-100%. As a result the sensing performance is affected with such P_e figures resulting in degraded spectrum utilisation and increased interference to the PUs.

On the other hand, for low (0% - 19%) and moderate (20% - 80%) and spectrum utilisation, the detection performance is improved with P_e values ranging between 0.6 and 0.1 based on the received signal's SNR as discussed previously in this subsection. Based on these results, optimal detection performance can be achieved for SNR values higher than 13 dB and spectrum availability higher than 20%.

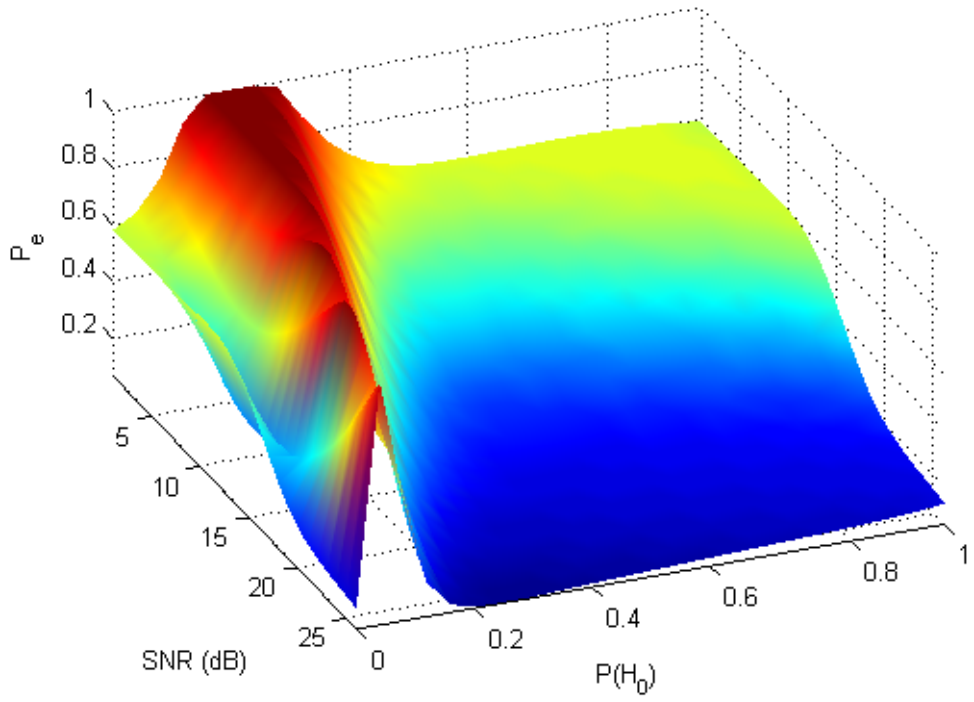

Figure 3.19: Evolution of P_e with respect to SNR and channel availability $P(H_0)$.

3.6 Summary

The performance of ED-based spectrum sensing under moderate and severe fading conditions as described by the TWDP fading channel model has been analysed in this chapter. An analytic expression for the average probability of detection over TWDP fading channels is derived, which also encompasses Rayleigh and Rician fading as special cases. This expression has been extended to the case of SLS diversity reception scheme as well as to the case of cooperative spectrum sensing. These derivations allowed us to quantify the effects of fading in the performance of ED-based spectrum sensing for CR enabled applications that could not be adequately characterised by traditional fading models. The obtained results demonstrate that under such fading conditions, 46% and 137% higher SNR is required to achieve the same detection performance as in Rayleigh and Rician fading respectively. To this end, diversity reception and cooperative detection are proposed and investigated as a means of improving the detection performance and reduce the requirements in terms of SNR by up to 18 dB. Additionally, the performance of an ED-based spectrum sensing scheme with optimal detection threshold selection is proposed. Different from traditional CFAR spectrum sensing, the proposed scheme selects a threshold dynamically subject to a minimum detection error probability which in turn results in an up to 13 dB SNR gain. The presented results, provide a comprehensive performance analysis of ED-based spectrum sensing for cognitive radio systems in worse than Rayleigh fading scenarios which can lead to the design of improved CR receivers that enhance the overall performance of CR communication systems operating in confined structures such as in-vehicular wireless M2M environments.

Chapter 4

A Hidden Markov Model for Spectrum Occupancy Prediction

4.1 Introduction

With reference to the analysis on state-of-the-art prediction methods, as presented in Chapter 2, HMM-based spectrum occupancy prediction is considered the most appropriate scheme for real-time channel occupancy state prediction owing to its statistical properties and characteristics. To this end, this chapter describes how the spectrum sensing problem can be formulated as an HMM and how HMMs can be further used to model and predict spectrum occupancy. More specifically, in Section 4.2 the related work on spectrum occupancy modelling and estimation using Markov and Hidden Markov processes (HMPs) is reviewed, whereas in Section 4.3 the theoretical background of HMMs is described. The spectrum occupancy model in the context of CR including the PU activity model, the channel model and the spectrum sensing model are described in Section 4.4. Based on this model, the framework for modelling the perceived spectrum occupancy as an HMM is presented in terms of the model's structure and parameters. In Section 4.5 the algorithms for HMM state estimation and prediction are presented. These algorithms include the forward-backward algorithm, the Viterbi algorithm, the Baum-Welch Algorithm (BWA) and the state prediction algorithm. Note that in the literature, HMPs are more commonly referred to as HMMs, as the term HMP emphasises the process itself rather than its use as a model. Therefore, the term HMM will be used throughout this thesis.

4.2 Related Work

The existence of a Markovian pattern in spectrum occupancy has been experimentally validated in [104], through spectrum activity measurements in the 928-948 MHz paging band. The main objective of that work was to estimate the hidden sequence of channel occupancy base on the observation sequence of past spectrum sensing results with the use of the Viterbi algorithm. However, this approach is restricted only to parameter estimation for a narrow spectrum of 20 MHz. Furthermore, its applicability to real-world scenarios is significantly limited as perfect spectrum sensing has been assumed.

An HMM-based dynamic spectrum allocation algorithm for CR has been proposed in [105]. The proposed algorithm is based on a Markov chain with a finite-state observable process, whose parameters are estimated online using the Baum-Welch training algorithm. The CR accesses the spectrum based on the estimated parameters and the PU activity is inferred based on the joint probability of the observation sequence and the hidden state. However, the proposed access method has only been based on the occupancy state estimation rather than spectrum occupancy prediction. This approach has been found to outperform the traditional Carrier Sense Multiple Access (CSMA) method in terms of SNR. However, due to the assumption of error-free spectrum sensing the applicability of the proposed algorithm is limited only to high SNR scenarios.

In [106], an HMM-based channel status predictor has been proposed as a means of minimising the negative impact of response delays caused by SDR platforms. The model's parameters are estimated by a simple statistical process over a training sequence of spectrum sensing outputs instead of using a training process. As a result, the model's parameters cannot be optimised, which in turn may have degraded its overall prediction performance. The prediction performance of the proposed model has been evaluated using Wi-Fi signals with periodic patterns in an indoor measurement environment. However, the use of periodic patterns diminishes the advantages of HMMs. Addition-

ally, although the proposed model has been clearly described, its prediction performance has not been compared with other prediction methods.

In [107] a discrete-time Markov chain has been used to model the spectrum sensing problem in the time domain. By using the Viterbi algorithm, a sequence detection algorithm is proposed to decode the PU state given the observation sequence. Unlike the previous studies, spectrum sensing errors have been considered in terms of the probabilities of missed detection and false alarm. More specifically, the proposed algorithm has been based on the assumption that spectrum sensing can be described by an HMM and has exploited the forward-backward algorithm to estimate the actual channel state through a noisy channel to improve the sensing accuracy of ED-based spectrum sensing in terms of P_{fa} and P_{md}. The proposed sequence detection algorithm improves the overall sensing performance with up to 10 dB SNR gains compared to classical ED. However, the Baum-Welch algorithm has not been used to estimate the model's parameters and the problem of predicting future PU occupancy states has not been considered.

Existing research has shown that HMMs can effectively describe temporal spectrum occupancy. However, the majority of literature is focused on estimating the actual occupancy state for a current time instant rather than predicting it in future time instants. Furthermore, the majority of the aforementioned studies applied HMMs for decision-theoretic access protocols at the MAC layer. In this work, HMM is used to model the PHY-layer spectrum sensing for CR by integrating the PU occupancy statistics as a means of improving spectrum sensing efficiency. Given that HMM provides a simple yet effective framework for modelling PHY-layer spectrum sensing this approach results in reduced complexity compared to MAC-layer approaches that require more sophisticated statistical tools such as queuing theory models or Partial Observable Markov Decision Processes (POMDP). In addition, the HMM-based PHY-layer approach can be further exploited for cross-layer implementation of efficient spectrum sensing and access mechanisms.

In this context, this work focuses on modelling PHY-layer spectrum sensing

using an HMM as a means of improving the sensing efficiency of autonomous SUs in terms of energy and time consumption. On-line training of the HMM-based prediction model is considered to facilitate real-time parameter estimation, and thus, prediction. In addition, spectrum sensing errors are considered in the model formulation to account for realistic CR scenarios.

4.3 Hidden Markov Model Fundamentals

A random process can be characterised as a Markov process if the Markovian property is satisfied, i.e. given a present event, future and past events are independent [108]. The output of a Markov process is assumed to be directly observable. However, in some cases the observable output depends on the outputs of an underlying process. In this context, an HMM is described as a doubly stohastic process that incorporates an observable process with an underlying one. The underlying process is a Markov chain that is observed through a memoryless, discrete-time invariant channel and is referred to as the hidden process, whereas the observable process is a sequence of conditionally independent random variables [109]. The hidden process can be either a discrete-time or a continuous-time finite-state homogenous Markov chain, whereas the output of the observable process can either have a finite or a general alphabet.

4.3.1 Mathematical Formulation

Given a hidden process, $\{X_t\}$, and an observable process, $\{Y_t\}$, an HMM can be described as a doubly embedded process $\{X_t, Y_t\}$, $t = 0, 1, ...T$ as shown in Figure 4.1. The hidden process $\{X_t\}$ consists of N number of hidden states within the state space S of $\{S_1, ...S_N\}$ and satisfies the Markovian property. Formally,

$$P(x_t = S_i | x_{t-1} = S_j, x_{t-2} = S_N, ...) = P(x_t = S_i | x_{t-1} = S_j), \tag{4.1}$$

where x_t denotes the hidden state at time instant t.

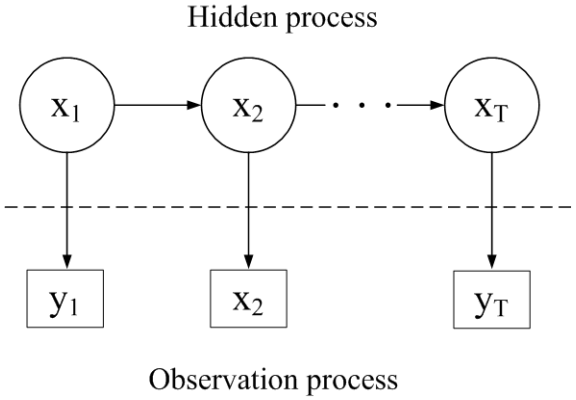

Figure 4.1: Hidden Markov model.

As a Markov process, X_t is characterised by the transition probabilities a_{ij}, and the initial state distribution π_i. The transition probabilities describe the relation between the current and past states of the process, whereas the initial state distribution expresses the probabilities that the process starts from a given state. Formally,

$$a_{ij} = P(x_t = S_i | x_{t-1} = S_j), \quad 1 \leq i, j \leq N \tag{4.2}$$

$$\pi_i = P(x_1 = S_i), \quad 1 \leq i \leq N, \tag{4.3}$$

with $a_{ij} \geq 0$ and $\sum_{j=1}^{N} a_{ij} = 1$.

In addition to the transition probabilities and initial state distribution, another critical element to characterise an HMM is the set of the emission probabilities $b_j(v_k)$. Given the observable discrete output Y_t, the emission probabilities express the probability of observing a particular output for a given state. Formally,

$$b_j(v_k) = P(y_t = V_k | x_t = S_j), \quad 1 \leq j \leq N, 1 \leq k \leq M, \tag{4.4}$$

where M is the number of observations v_k within the emission space $V_1, ...V_M$

and y_t is the observable state at time instant t.

4.3.2 Application to real-world problems

In order to describe and apply HMMs in real-world applications the transition and emission probabilities are used in the form of a matrix. The transition probability matrix is a square $N \times N$ matrix that contains the set of a_{ij} and the emission matrix is an $N \times M$ matrix that contains the set of $b_j(v_k)$. Using all the essential parameters, an HMM is characterised by the tuple $\lambda = (\pi, \mathbf{A}, \mathbf{B})$ with π denoting the initial state distribution, and $\mathbf{A}$ and $\mathbf{B}$ denoting the transition and emission matrices, respectively. There are three problems when HMMs need to be used in real-world applications [65]:

- **Problem 1:** Given the model parameters the probability of a particular observation sequence to have been generated by the given model must be computed.

- **Problem 2:** Given the model parameters and a particular observation sequence the hidden sequence that has most likely generated the output sequence must be determined.

- **Problem 3:** The maximum likelihood estimate of the model parameters that have generated the given set of the observation sequence must be obtained.

These problems are known as the HMM canonical problems. Therefore, in order to apply HMMs in spectrum occupancy prediction, all three problems need to be solved. Problem 1 can be solved using a dynamic programming approach for calculating efficiently the likelihood that a particular observation has been generated by a given model; Problem 2 can be solved through the decoding process using the Viterbi algorithm; and Problem 3 can be solved during the learning process by applying the Baum-Welch algorithm [65]. The following sections provide the framework for modelling spectrum occupancy as

an HMM and describe how the three aforementioned problems are solved in the context of spectrum occupancy prediction.

4.4 System Model

Let X_t and Y_t denote the PU activity and sensing output at the SU, respectively. The PU activity X_t is unknown to the SU, and thus it is considered as the hidden state of an underlying process. Spectrum sensing is performed at the CR node by measuring the received signal power and comparing it to a predefined detection threshold to determine the PU occupancy status, X_t, as active or idle. By using past spectrum sensing outputs the PU occupancy state is estimated and is used for spectrum occupancy prediction without any knowledge on the current sensing output.

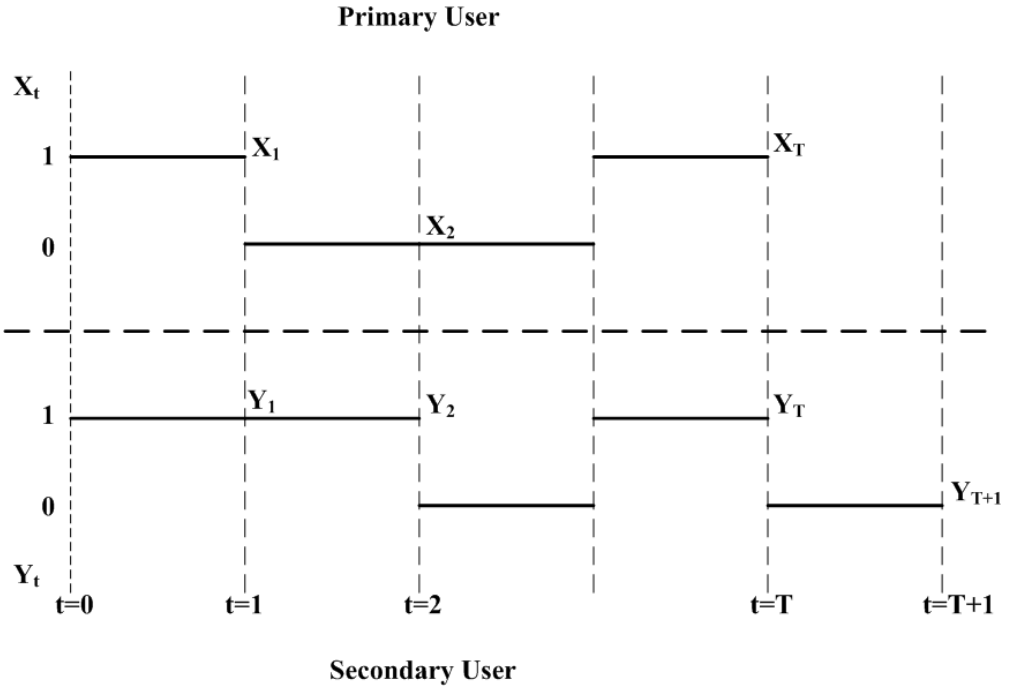

Figure 4.2: Spectrum occupancy prediction description.

As shown in Figure 4.2 spectrum occupancy describes how the PU activity is perceived by the SU subject to a noisy wireless channel. In this context, spectrum occupancy can be described by three components:

1. the PU activity model
2. the channel model between the PU and SU
3. the spectrum sensing model.

4.4.1 Primary User Activity Model

The PU activity model is used to describe the features of the primary system that can be further exploited by the SU in order to distinguish between a PU transmission and noise. In this work, PU activity is assumed to follow a first-order Markov chain. Despite the simplicity of Markov models, they have been found to provide a strong mathematical framework for modelling different stochastic processes and they are considered as the most popular tool for modelling network users' activity from the early wireless network activity models to the latest advances in CR [110]. Furthermore, the assumption of modelling PU activity as a Markov chain is experimentally verified in the following chapter. Thus, in the CR context, PU activity can be described by a two-state, discrete-time Markov chain with a state space $S\{0, 1\}$ as shown in Figure 4.3 [111].

Let the random variable $S_t \in \{0, 1\}$ describe the channel occupancy state at time instant t with $S_t = 1$ corresponding to an active state (PU is transmitting) and $S_t = 0$ corresponding to an idle state (PU is not transmitting). Since only two states are considered, the transition between idle and active states are mathematically described by a set of transition probabilities $a_{ij} = P(x_{t+1} = S_j | x_t = S_i)$, for $i, j \in \{0, 1\}$, which in turn are used to form the transition matrix as,

$$\mathbf{A} = \begin{bmatrix} a_{00} & a_{01} \\ a_{10} & a_{11} \end{bmatrix}. \tag{4.5}$$

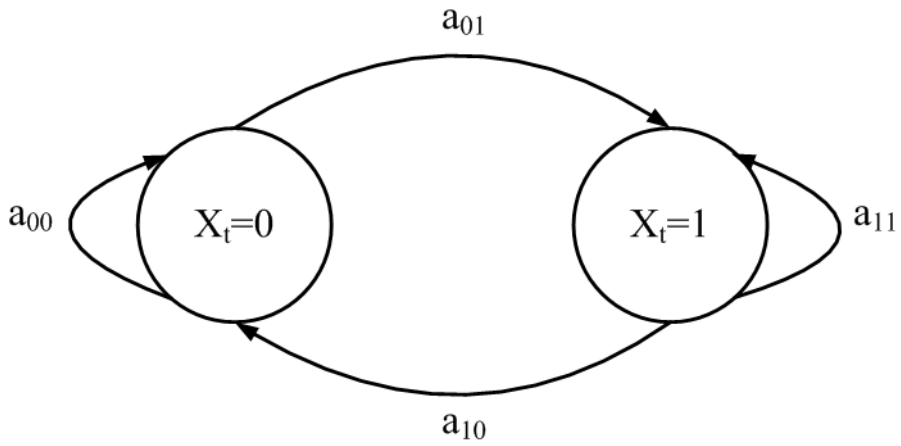

Figure 4.3: PU transmission model.

Let the random variables μ_0 and μ_1 express the time duration that the PU remains in idle and active state, respectively. Since the PU transmissions are modelled as a first-order Markov process, μ_0 and μ_1 will be geometrically distributed with parameters a_{01} and a_{10}, respectively, i.e. $E[\mu_0] = 1/a_{01}$ and $E[\mu_1] = 1/a_{10}$ with $E[.]$ denoting the expectation of a random variable. Furthermore,the initial state distribution is assumed to be in steady state and can be obtained by [112],

$$\begin{aligned} \pi =&[\pi_0, \pi_1] = [P(x_t = 0), P(x_t = 1)] \\ &= \left[\frac{a_{10}}{a_{01} + a_{10}}, \frac{a_{01}}{a_{01} + a_{10}}\right], t = 0, 1, 2, ...T. \end{aligned} \tag{4.6}$$

Note that in this work slotted PU transmission is assumed without synchronisation between the PU and the SU. Hence, throughout this thesis, the term "slot" refers to the irreducible time interval within which a sensing or a transmission event occurs.

4.4.2 Channel Model

Although a Markov chain is appropriate for modelling the PU activity the true state of the PU transmission is not known to the SU at any particular instant since the SU observes an emission of the actual PU state as it receives a noisy version of the transmitted signal. The received signal, Y_t, can be

mathematically described as,

$$Y_t = S_t X_t + W_t \tag{4.7}$$

where X_t is the primary signal, S_t is the PU state, and W_t is the noise term modelled as AWGN with zero mean and variance σ^2.

A Gaussian channel is considered for simplicity and due to the fact that it can describe several channel impairments such as fading, shadowing, multipath and interference [113]. In addition, the use of a Gaussian channel is verified by the measurement results as shown in the following chapter.

4.4.3 Spectrum Sensing Model

Spectrum sensing can be performed using different techniques as discussed in Chapter 2. In this work, ED-based spectrum sensing is considered due to its low implementation and computational complexities. As presented in detail in previous chapters, for ED-based spectrum sensing the sensing output is determined by comparing the received signal's energy with a detection threshold.

Having modelled the PU activity model as a two-state discrete-time Markov chain as described in Section 4.4.1, an SU that performs ED-based spectrum sensing has to determine the PU state at time instant t based on the following hypotheses

$$\begin{aligned} H_0 : X_t = 0 \rightarrow PU\ transmission\ absent \\ H_1 : X_t = 1 \rightarrow PU\ transmission\ present. \end{aligned} \tag{4.8}$$

However, the actual channel state is not directly observable due to errors caused by noise and other channel impairments. Hence, spectrum sensing can be modelled as an HMM with state space $S = \{0, 1\}$ and emission space $V = \{0, 1\}$ as shown in Figure 4.4.

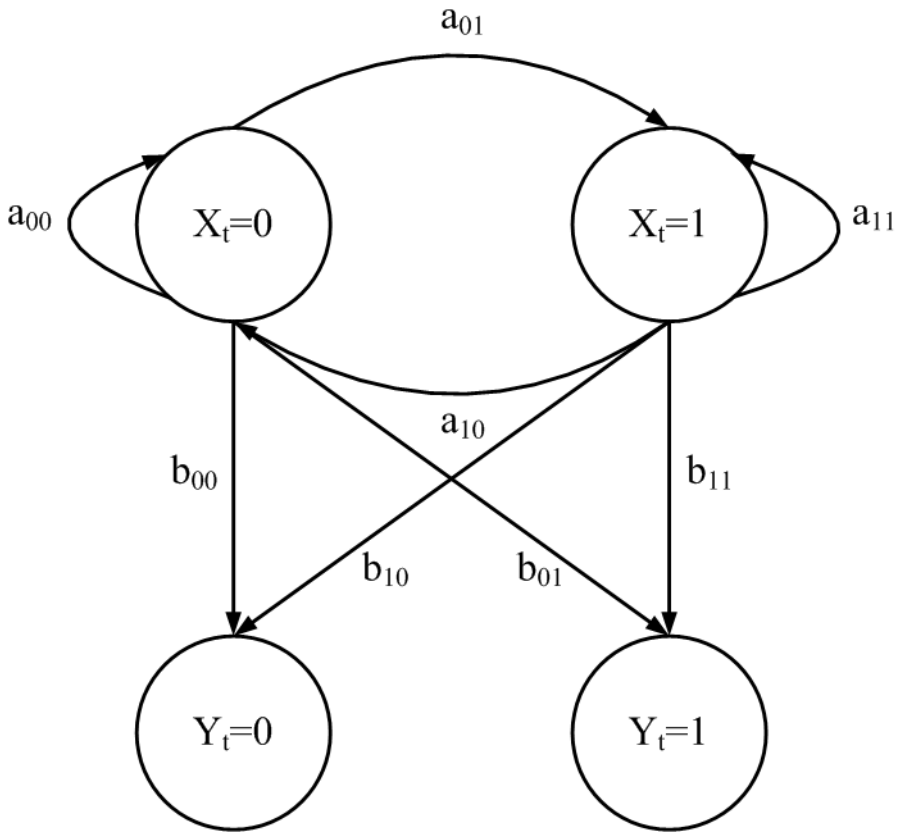

Figure 4.4: Spectrum sensing model.

Let $X_t = (x_1, x_2, ...x_T)$ denote the PU transmission state, and $Y_t = (y_1, y_2, ...y_T)$ the SUs spectrum sensing output. The conditional probability of observing y_t given state x_t at time instant t is expressed as $f_{Y|X}(y_t|x_t)$. Based on the first-order Markov assumption and the Markovian property, the observed states within the observation sequence are conditionally independent of the state sequence. Thus,

$$f_{Y_t|X_t,Y_{t-1}}(y_t|x_t, y_{t-1}) = f_{Y|X}(y_t|x_t). \tag{4.9}$$

Hence, given that, spectrum sensing is modelled as a two-state HMM, the emission probabilities can be expressed as,

$$b_{01} = P(X_t = 0|Y_t = 1) = \frac{\Gamma(u, \lambda/2)}{\Gamma(u)} \tag{4.10}$$

$$b_{00} = P(X_t = 0|Y_t = 0) = 1 - b_{01} \tag{4.11}$$

$$b_{10} = P(X_t = 1|Y_t = 0) = 1 - b_{11} \tag{4.12}$$

$$b_{11} = P(X_t = 1|Y_t = 1) = Q_u(\sqrt{2\gamma}, \sqrt{\lambda}). \tag{4.13}$$

Note that the emission probabilities b_{01} and b_{11} correspond to the probabilities of false alarm and probability of detection, respectively. Hence, for ED-based spectrum sensing they can be determined by expressions (3.15) and (3.16) as discussed in Chapter 3.

4.5 Spectrum Occupancy Estimation and Prediction

The objective of spectrum occupancy prediction is first to determine the channel occupancy states up to time instant T and then predict the occupancy state $T+d$ based on the SU' s observation sequence up to time instant T, with T and d denoting the length of spectrum sensing history and the prediction step, respectively. The following subsections provide a detailed description of the algorithms to be used for channel occupancy parameter estimation and prediction based on the considered HMM spectrum occupancy model. More specifically, the following algorithms provide solutions to each one of the canonical problems associated with HMMs (see Subsection 4.3.2) in the context of spectrum occupancy prediction.

4.5.1 Forward-Backward Recursions

In order to solve the first canonical problem, the likelihood of the observed signal, and the conditional probability of observing a state given the observation process is required. Let $O = o_1, o_2, ...o_T$ denote a history of spectrum sensing

outputs up to time instant T. The probability of observing a sequence O that has been generated by a state sequence S given an HMM λ can be described mathematically as [65],

$$P(O, S|\lambda) = P(O|S, \lambda)P(S|\lambda), \tag{4.14}$$

where

$$P(O|S, \lambda) = \prod_{t=1}^{T} P(o_t|s_{i_t}, \lambda) = b_{1_t}(o_1)b_{2_t}(o_2)...b_{i_t}(o_T) \tag{4.15}$$

and

$$P(S|\lambda) = \pi_{s_{i_1}} a_{s_{i_1} s_{i_2}} a_{s_{i_2} s_{i_3}} ... a_{s_{i(T-1)}} s_{i_T}. \tag{4.16}$$

Hence, expression (4.14) can be rewritten as,

$$P(O, S|\lambda) = (\pi_{s_{i_1}} b_{i_1}(o_1)) \prod_{t=2}^{T} a_{s_{i_{(t-1)}} s_{i_t}} b_{i_{t(o_t)}}. \tag{4.17}$$

Although expression (4.14) can compute $P(O, S|\lambda)$, in practice it is not useful because the state sequence is still unknown at this stage. Therefore, the observation sequence O may have been generated by more than one state sequences, S. Hence, $P(O, S|\lambda)$ can be calculated by determining the most probable S that has generated O. This can be achieved by computing the probability of observing O given all the possible paths within λ that could have generate it, expressed by,

$$P(O|\lambda) = \sum [P(O|S, \lambda)P(S|\lambda)] \tag{4.18}$$

However, this solution is not useful in practice because the number of possible paths grows exponentially with the length of the sequence. To this end, the forward-algorithm is used for efficient and accurate computation of $P(O|\lambda)$ [114]. The forward-backward algorithm is a dynamic programming algorithm that exploits the Markovian property of O and is used to calculate the forward variable α which represents the probability of observing sequence O_T being in state $S_i$at a time instant t, given an HMM λ. The forward variable α is defined

as [114],

$$\alpha_i(t) = P(o_1, ...o_t, S_i(t)|\lambda). \tag{4.19}$$

The forward probability α is recursively calculated using the forward-algorithm as follows [115],

1. Initialisation:

$$\alpha_i(1) = \pi_i b_i(o_1) \quad 1 \leq i \leq 2. \tag{4.20}$$

2. Recursion:

$$\alpha_j(t) = \Big[\sum_{i=1}^{2} \alpha_i(t-1)a_{ij}\Big] b_j(o_t) \quad 2 \leq t \leq T, 1 \leq j \leq 2. \tag{4.21}$$

3. Termination:

$$P(O|\lambda) = \sum_{i=1}^{2} \alpha_i(T). \tag{4.22}$$

In Step 1 the forward probabilities are initialised as the joint probability the initial state distribution and the probability of the observation for all states at time instant $t = 1$. Based on the fact that $\alpha_i(t)$ expresses the joint probability of sequence O to be observed and the last state is S_t, the product $\alpha_i(t)a_{ij}$ expresses the joint probability of the sequence to be observed and state S_j is reached at time instant $t+1$ through state S_i at time instant t. The summation of this product over all the possible states results in the probability of state S_j at time instant t with all previous observations. Since S_j is now known, $\alpha_j(t+1)$ is obtained by multiplying the summed quantity by the probability $b_j(o_{t+1})$ for the two states. Finally, Step 3 calculates $P(O|\lambda)$ as the sum of all the terminal forward variables $a_i(T)$ based on the definition of the forward variable given by expression 4.19. Using the forward-algorithm, the calculation of $\alpha_i(t)$ requires $O(2^2T)$ calculations rather than $O(2T2^T)$ as required by direct calculation using expression (4.18).

Similarly, the backward variable $\beta_t(i)$ expresses the probability of the partial observation sequence from time instant $t+1$ to the end, given a state S_i

at time instant t and the model parameters λ . Formally,

$$\beta_t(i) = P(O_{t+1}, O_{t+2}, ..., O_T | x_t = S_i, \lambda). \tag{4.23}$$

The backward variable $\beta_t(i)$ is computed recursively as follows,

1. Initialisation:

$$\beta_T(i) = 1 \quad 1 \leq i \leq 2. \tag{4.24}$$

2. Recursion:

$$\beta_t(i) = \sum_{i=1}^{2} a_{ij} b_j(o_{t+1}) \beta_{t+1}(j) \quad 1 \leq i \leq 2. \tag{4.25}$$

In Step 1 $\beta_T(i)$ is arbitrarily initialised to 1. The backward variable $\beta_t(i)$ is then computed taking into account the transition from S_i to S_j for the two states, (a_{ij}), as well as the observation o_{t+1} in state S_j and the remaining partial observation sequence o_{t+1} from state j expressed by the terms $b_j(o_{t+1})$ and $\beta_{t+1}(j)$, respectively.

Owing to the nature of CR, spectrum sensing is performed frequently within short time intervals to ensure reliable and efficient spectrum usage. As a result, the spectrum sensing history is continuously updated resulting in reduced precision of $P(O|\lambda)$. Therefore, in order to ensure the numerical stability and precision on the forward-backward recursions an embedded scaling procedure is implemented.

Hence, the scaled forward variable is obtained by [116],

$$\bar{\alpha}_i(t) = \frac{\alpha_i(1)}{\sum_{x_t} \bar{\alpha}_i(t)} \quad t = 1, ...T. \tag{4.26}$$

Similarly the scaled backward variable is obtained by [116],

$$\bar{\beta}_i(t) = \frac{\beta_i(1)}{\sum_{x_t} \bar{\beta}_i(t)} \quad t = 1, ...T. \tag{4.27}$$

Although the backward variable is not directly related to the solution of Problem 1, Problems 2 and 3 require its computation. Therefore, the backward

variable is computed at this step in order to reduce the complexity of the prediction algorithm in total.

4.5.2 Decoding Process

Problem 2 requires the inference of the optimal state sequence that has been generated by the observation O given the model's parameters λ. This problem can be treated as an optimisation and as such the Viterbi algorithm is used to find the optimal state sequence that maximises $P(S|O,\lambda)$ [117]. Let variable $\delta_t(i)$ express the highest probability within a path, at time instant t, which accounts for the first t observations and ends in state S_i. This is mathematically described as [117],

$$\delta_t(i) = \max_{x_1,...x_{t-1}} P(x_1,...x_{t-1} = i, O_1, O_2, ...O_T|\lambda). \tag{4.28}$$

By induction, this yields

$$\delta_{t+1}(i) = [\max_i \delta_t(i)a_{ij}]b_j(O_{t+1}). \tag{4.29}$$

In order to retrieve the state sequence a track of the argument that maximises (4.28) must be kept. This can be achieved by using an array $\psi_t(j)$. Based on (4.28), the optimal state sequence is inferred recursively using the Viterbi algorithm as follows [117], [118]:

1. Initialisation:

$$\delta_t(i) = \pi_i b_i(o_1) \quad 1 \leq i \leq 2 \tag{4.30}$$

$$\psi_t(1) = 0. \tag{4.31}$$

2. Recursion:

$$\delta_t(j) = \max_{1\leq j\leq 2}[\delta_i(t-1)a_{ij}|b_j o_t] \quad 2 \leq t \leq T, 1 \leq j \leq 2 \tag{4.32}$$

$$\psi_t(j) = \arg\max_{1\leq j\leq 2}[\delta_i(t-1)a_{ij}] \quad 2 \leq t \leq T, 1 \leq j \leq 2. \tag{4.33}$$

3. Termination:

$$\hat{P}_T = \max_{1\leq j\leq 2}[\delta_T(i)]. \tag{4.34}$$

$$\hat{x}_T = \arg\max_{1\leq j\leq 2}[\delta_T(i)]. \tag{4.35}$$

4. Backtracking:

$$\hat{x}_t = \psi_{t+1}(\hat{x}_{t+1}). \tag{4.36}$$

Note that the Viterbi algorithm is similar to the forward algorithm except for the backtracking step. The major difference between the Viterbi and the forward algorithm is the maximisation of previous states (4.32) which is used instead of the summation in (4.21).

4.5.3 Training Process

The Baum-Welch algorithm is an iterative expectation maximisation (EM) algorithm used to adjust the HMM parameters $\lambda = (\pi, \mathbf{A}, \mathbf{B})$ so that the probability of the observations sequence to have been generated by a given state sequence $P(O|\lambda)$ is maximised [119]. More specifically, the Baum-Welch algorithm estimates the optimal parameters $\lambda^* = (\pi, \mathbf{A}^*, \mathbf{B}^*)$ by iteratively updating the parameters until a terminating condition is satisfied [120]. This process, known as training or learning process can be described in three basic steps as follows:

- **Step 1:** Initialise the model's parameters λ_0 and compute $P(O|\lambda_0)$.
- **Step 2:** Given the observation sequence O and the model's parameters λ_{k-1} estimate λ_k, after k iterations with $k = 1, 2, ..$
- **Step 3:** If $P(O|\lambda_k) > P(O|\lambda_{k-1})$ continue from Step 2. Otherwise, terminate the procedure with λ_k being the optimal parameters λ^*.

The key step of the Baum-Welch algorithm is Step 2 where the model's parameters are re-estimated. In order to describe the re-estimation process, the probability of being in state S_i at time instant t, and in state S_j at instant $t+1$ can be defined as [119],

$$\xi_t(i,j) = P(x_t = S_i, x_{t+1} = S_j)|O, \lambda). \tag{4.37}$$

Based on the definitions of the forward (4.19) and backward (4.28) variables, $\xi_t(i,j)$ can be rewritten in terms of the forward and backward variables as,

$$\begin{aligned} \xi_t(i,j) &= \frac{\alpha_t(i)a_{ij}b_j(O_{t+1})\beta_{t+1}(j)}{P(O|\lambda)} \\ &= \frac{\alpha_t(i)a_{ij}b_j(O_{t+1})\beta_{t+1}(j)}{\sum_{i=1}^{2}\sum_{j=1}^{2}\alpha_t(i)a_{ij}b_j(O_{t+1})\beta_{t+1}(j)} \end{aligned} \tag{4.38}$$

$$\gamma_t(i) = P(x_t = S_i|O, \lambda) \tag{4.39}$$

$$\gamma_t(i) = \frac{\alpha_t(i)\beta_t(i)}{P(O|\lambda)} = \frac{\sum_{i=1}^{2}\beta_t(i)}{P(O|\lambda)}. \tag{4.40}$$

Having defined $\gamma_t(i)$ it can be related to $\xi_t(i,j)$ as follows,

$$\gamma_t(i) = \sum_{j=1}^{2}\xi_t(i,j). \tag{4.41}$$

By employing the concept of counting event occurrences and the above expressions, the optimal HMM parameters are obtained using the following expressions,

$$\pi_i^* = expected\ frequency\ in\ state\ S_j\ at\ time\ (t=1) = \gamma_1(i) \tag{4.42}$$

$$a_{ij}^{*} = \frac{expected\,number\,of\,transitions\,from\,state\,S_i\,to\,state\,S_j}{expected\,number\,of\,total\,transitions\,from\,state\,S_i} \tag{4.43}$$

$$= \frac{\sum_{t=1}^{T-1} \xi_t(i,j)}{\sum_{t=1}^{T-1} \gamma_t(i)}$$

$$b_j^{*}(k) = \frac{expected\,number\,of\,times\,in\,state\,S_j\,observing\,symbol\,v_k}{expected\,number\,of\,times\,from\,state\,S_j} \tag{4.44}$$

$$= \frac{\sum_{s,t,O_t=v_k}{}_{t=1}^{T} \gamma_t(i)}{\sum_{t=1}^{T} \gamma_t(j)}.$$

Note that during the re-estimation procedure the stochastic constraints of the HMM parameters are automatically satisfied at each iteration [120]. That is,

$$\sum_{i=1}^{2} \pi_i^{*} = 1 \tag{4.45}$$

$$\sum_{j=1}^{2} a_{ij}^{*} = 1, \quad 1 \leq i \leq 2 \tag{4.46}$$

$$\sum_{k=1}^{2} b_j^{*}(k) = 1, \quad 1 \leq j \leq 2. \tag{4.47}$$

4.5.4 State Prediction

Having obtained the optimal HMM parameters $\lambda^* = (\pi^*, \mathbf{A}^*, \mathbf{B}^*)$ after the training process, the channel occupancy status at a future time instant, $T+d$, of a prediction time span d, can be determined based on the following decision rule,

$$\hat{x}_{T+d} = \begin{cases} 0, \ P(O_{T+d}, 0|\lambda^*) \geq P(O_{T+d}, 1|\lambda^*) \\ 1, \ P(O_{T+d}, 0|\lambda^*) < P(O_{T+d}, 1|\lambda^*), \end{cases} \tag{4.48}$$

where $P(O_{T+d}, 0|\lambda^*)$ and $P(O_{T+d}, 1|\lambda^*)$ express the joint probabilities of an observation sequence O_T to be followed by an unoccupied, and by an occupied channel at a future time slot $T+d$, respectively.

Having an HMM with parameters $\lambda = (\pi, \mathbf{A}, \mathbf{B})$ and a two-state Markov process X_t, the probability of being in state x_t given an observation sequence O_T can be expressed in terms of the forward variable as,

$$P(x_t|O_T, \lambda) = \alpha(x_t, O_T), \quad t = 0, ...T. \tag{4.49}$$

Based on the forward variable definition, the joint probability $P(x_t|O_T, \lambda)$ can be computed recursively using expressions (4.20) and (4.21). Thus, the conditional d-step ahead predicted state probabilities of x_{t+d} given O_T are computed as,

$$\begin{aligned} P(x_{t+d}|O_t, \lambda) &= \sum P(x_t|O_t, \lambda^*) P(x_{t+m}|O_t, \lambda^*) \\ &= \sum \alpha(x_t, O_t) b_j(o_t) [A]^d. \end{aligned} \tag{4.50}$$

It can be seen that $P(x_{t+d}|O_t, \lambda)$ is obtained by the forward part of the forward-backward algorithm and hence, $P(x_{t+d}|O_t, \lambda)$ can be computed after $O(4T)$ multiplications.

4.6 Summary

This chapter has focused on providing a complete description of the framework for describing spectrum sensing as an HMM. The system model consists of the PU transmission model, the channel model between the PU and the SU, as well as the spectrum sensing method on the SU end. The PU activity is modelled as a two-state Markov chain, whereas ED-based spectrum sensing has been assumed. In addition, the wireless channel between the PU and the SU is described by a Gaussian model. Based on these assumptions, the HMM structure and the model parameter's have been described, followed by a detailed mathematical description of the algorithms that are used for state estimation and prediction in the context of spectrum occupancy prediction for CR applications.

Chapter 5

Predictive Spectrum Sensing

5.1 Introduction

Having described the framework for modelling spectrum occupancy as an HMM and presented the required algorithms for estimation and prediction, in this chapter a "smart" spectrum sensing method based on spectrum occupancy prediction is introduced. The HMM-based spectrum occupancy prediction model is integrated to ED-based spectrum sensing as a means of improving the sensing efficiency of CR systems. The related work on smart spectrum sensing is presented in Section 5.2, while in Section 5.3 the system model of the proposed predictive sensing scheme is described. In Section 5.4 the methodology that is followed for analysing the performance of the proposed scheme is described including an overview of a spectrum activity measurement campaign, the performance metrics and the evaluation process. The obtained results on the prediction performance of the proposed scheme are presented and compared with state-of-the-art prediction methods in Section 5.5 followed by a performance analysis on the sensing efficiency of the proposed scheme through a case study.

5.2 Related Work

Adaptive spectrum sensing also known as "smart" sensing has been proposed as a means of reducing the amount of spectrum to be sensed by the SUs. Owing to the opportunistic nature of CR, the channel availability depends on the PU transmission patterns. Therefore, the more channels that are being sensed, the higher the probability for the SU to access the primary spectrum. However, the wider the sensed bandwidth, the higher the cost for the CR nodes [121]. As a result, several adaptive sensing techniques have been proposed as a means of reducing the sensing cost in terms of sensing time and energy consumption.

A parametric adaptive sensing scheme based on historical occupancy data has been proposed in [122]. In this technique the channels to be sensed are selected based on the DC of each channel. The performance of this scheme was analysed through simulations and was found to improve the sensing efficiency for up to 80% when applied to the DTV frequency bands. A first-order Markov chain was used to determine the channels to be sensed based on the transition probabilities by selecting the channels with the minimum probability of changing from unoccupied to occupied [123]. Furthermore, in [124], the use of periodicities in the PU signals has been proposed for adaptive sensing in DSA networks.

The performance of these methods has been evaluated based on real-world measurements within the cellular frequency bands in [125]. All the proposed schemes have been found to improve sensing efficiency by exploiting long-term periodicities within 24 hours. However, such "smart" sensing schemes do not enable real-time adaptation and have large memory requirements. As a result, the practical realisation of such predictive sensing schemes, may be feasible for a sensing infrastructure but not for low-cost, energy-constrained mobile CR terminals.

Contrary to the already proposed smart sensing methods, this work proposes a predictive spectrum sensing scheme which exploits short term periodicities to perform real-time spectrum occupancy predictions based on short

sensing history. Owing to these characteristics the proposed scheme is expected to enable low-cost autonomous CR nodes to perform prediction within dynamic environments with fast changing occupancy statistics as a means of reducing the number of sensed channels and hence, the sensing time and energy expenditure.

5.3 System Model

Let a CR network with N_i, $i = 1, 2, ...N$ frequency channels shared between N_{PU} primary and N_{SU} secondary users. The SUs are assumed to monitor the PU activity using ED-based spectrum sensing. The SU senses the PU spectrum and stores the sensing outputs in its memory. The past spectrum sensing outputs are then used as inputs into the HMM-based prediction model to determine the spectrum occupancy output at future time instants. Upon the request of data transmission the SU senses only the channels that have been predicted to be unoccupied. A block diagram of an ED-based predictive spectrum sensing scheme is shown in Figure 5.1.

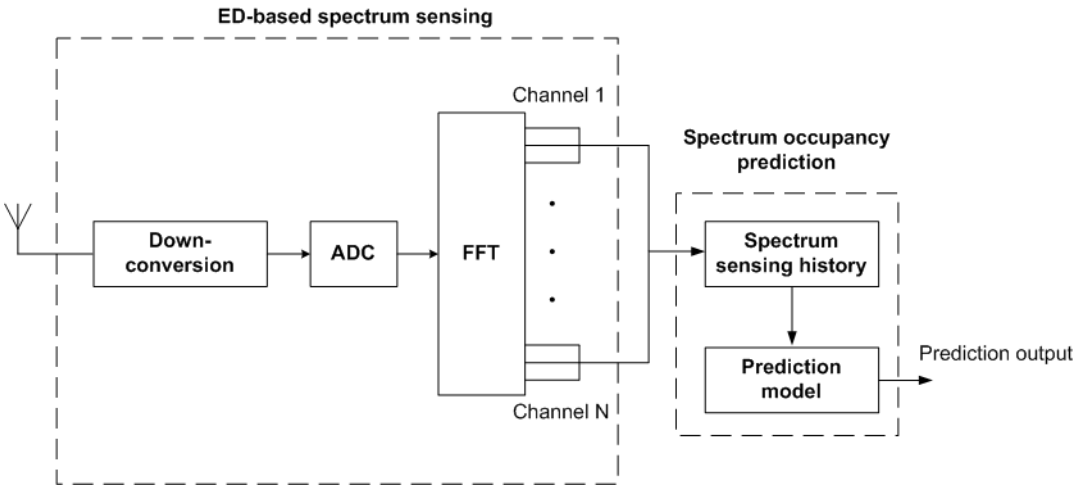

Figure 5.1: Predictive spectrum sensing scheme.

The proposed predictive spectrum sensing scheme enables the SU to determine whether a PU transmission is present in a given channel in future time instants. Therefore, in comparison with the conventional ED-based spectrum sensing, predictive spectrum sensing exploits historical knowledge on the PU behaviour to sense the channels that are predicted to be unoccupied. Such a predictive way of sensing is expected to outperform traditional spectrum sensing in terms of reduced sensing time and hence energy consumption.

Let the CR to sense a frequency spectrum $F = f_{max} - f_{min}$ with f_{max} and f_{min} denoting the upper and lower bound of the spectrum of interest. The spectrum consists of N number of frequency channels $N = F/R$ with R denoting the frequency resolution of the SU. At each sensing event the CR senses N frequency channels indexed as $i = 1, 2, ...N$. Therefore, the CR creates a history with N vectors of length T with binary occupancy data. The historical spectrum sensing outputs are stored in the CR's memory and used to develop the HMM that best represents the historical spectrum occupancy binary time series.

The pseudocode of the predictive spectrum sensing algorithm is presented below with Learning, Prediction and Sensing being the three kernel functions for the main algorithm. The Learning function is an implementation of the BWA training algorithm based on Section 4.5.3 of the previous chapter whereas the Prediction function performs prediction as per Section 4.5.4. Based on the prediction outcome, spectrum sensing is performed by the Sensing function for updated sets of f^*_{max} and f^*_{min}.

Algorithm 1 Main

Require: Spectrum sensing history O_T
Ensure: Channel state prediction $x_{i_{T+d}}$
  Algorithm starts when SU wants to transmit
  if SU senses for the first time **then**
    Initialise λ_i with random parameters
  else
    Initialise λ_i based on historical data
  end if
  $\lambda_i^* = Learning(\lambda_i, O_{i_T})$
  $x_{i_{T+d}} = Prediction(\lambda^*, O_{i_T})$
  $Sensing[x_{i_{T+d}} = 0]$

Algorithm 2 Learning

Require: λ, O_{i_T}
Ensure: λ^*
  Calculate α_i, β_i, ξ_i and γ_i using (4.26), (4.27), (4.38) and (4.39)
  Calculate $P(O|\lambda)$ using (4.22)
  repeat
    Recalculate α_i, β_i, ξ_i and γ_i using (4.26), (4.27), (4.38) and (4.39)
    Adjust π_i^*, A_i^* and B_i^* using (4.42), (4.43) and (4.44)
    Calculate $P(O|\lambda^*)$ using (4.22)
  until $log(P(O_i|\lambda_i^*)) > log(P(O_i|\lambda_i))$
  Replace π_i, A_i and B_i with π_i^*, A_i^* and B_i^*
  return $\lambda^* = (\pi_i^*, A_i^*$ and $B_i^*)$

Algorithm 3 Prediction

Require: λ_i^*, O_{i_T}
Ensure: x_{T+d}
  Determine prediction span d
  Calculate $P(x_{i_{t+d}}|O, \lambda)$ using (4.50)
  Calculate $argmaxP(x_{i_{t+d}}|O, \lambda)$
  return $x_{i_{T+d}}$

Algorithm 4 Sensing

Require: i
Ensure: Spectrum sensing output
  Adjust f_{min} and f_{max}
  Perform ED-based spectrum sensing within $F^* = f_{max}^* - f_{min}^*$
  return Spectrum sensing output

5.4 Evaluation Methodology

In this section the evaluation process for the spectrum occupancy prediction scheme is described. This process consists of data collection process, performance analysis and comparison with different prediction schemes using the obtained data. To this end, in this section the spectrum activity measurement campaign, the performance metrics and the performance evaluation process are described.

5.4.1 Spectrum Occupancy Measurements

In order to evaluate the prediction performance of the proposed spectrum occupancy prediction scheme within realistic scenarios a series of spectrum activity measurements were conducted in different frequency bands. The frequency bands under investigation include the DL and UL bands of 2G (GSM 900, GSM 1800) and 3G (Universal Mobile Telecommunications System (UMTS) 2100) cellular standards as well as the 2.4 GHz ISM band. The purpose of the measurement system is to provide insight on the PU activity as perceived by an SU that performs spectrum sensing in an indoor environment. In this context, the measurement campaign took place inside an urban building, in the third floor of a four-floor building in the central campus of University of Bedfordshire.

The measurement equipment consists of an R&S FSL6 spectrum analyser, configured as per Table 5.1. The spectrum analyser was programmed to perform automated measurements controlled by a host computer using a tailor-made software written in Labview. The sensing parameters were chosen based on the sensing requirements indicated by the IEEE 802.22 CR standard. More specifically, the resolution bandwidth was set to 100 kHz with respect to the minimum signal bandwidth within the investigated bands, i.e. GSM signal of 200 kHz, whereas the sensing time was set to 1 s (IEEE 802.22 suggests a maximum of 2 s). Due to the time varying nature of the measured signals, the detection mode was set to Root Mean Square (RMS).

Table 5.1: Measurement set-up.

Parameter	Value
Resolution bandwidth	100 kHz
Sweep time	1 s
Detector type	RMS
Reference level	-20 dBm

In order to monitor the frequency bands of interest three different types of antennas were used as shown in Table 5.2. Antennas 1 and 2 were used for measuring the spectrum activity within the cellular frequencies GSM/UMTS whereas Antenna 3 was used for the 2.4 GHz ISM band.

Table 5.2: Antenna specifications.

Antenna	Frequency (MHz)	Gain (dBi)	Polarisation	Impedance (Ω)
1	824-980 / 1710 -1990	3	Linear	50
2	1710-2120	3	Linear	50
3	2400 - 2480	3	Linear	50

Although the analysis of transmission patterns and characteristics of different wireless standards and frequency bands is beyond the scope of this work, a brief analysis is performed to provide an insight on the spectrum occupancy scenarios under investigation. The metrics that are used to describe spectrum occupancy are: duty cycle; channel occupancy; and transition rate. With reference to ED, the occupancy metrics were obtained by comparing the received power with a detection threshold which is determined based on the noise level of the spectrum band and the system's noise figure. Figure 5.2 shows the noise and signal power distribution as obtained by the measurements campaign, and the detection threshold of -95 dBm which is employed to distinguish between an occupied and an unoccupied channel.

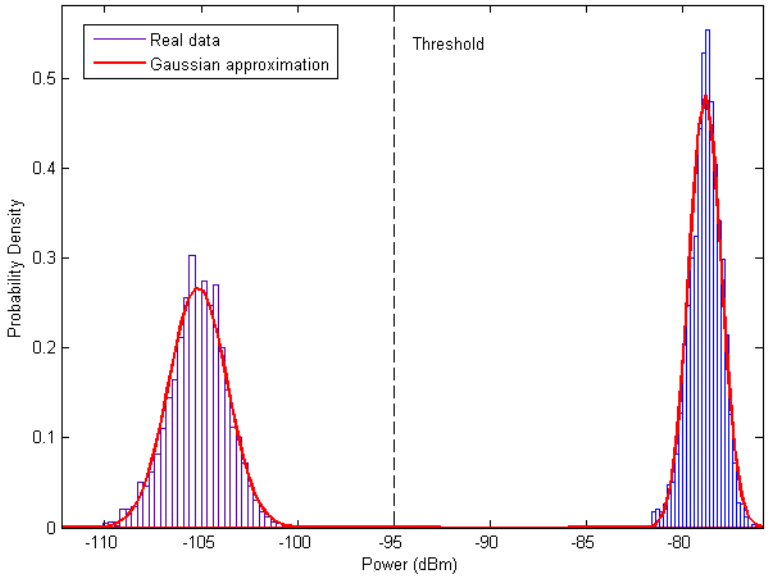

Figure 5.2: Measured noise and signal distributions.

Duty cycle, DC_f, is defined as the portion of time during which the power of a frequency channel exceeds the detection threshold and is defined as,

$$DC_f = \frac{1}{N} \sum_{1}^{T} \{X_t = 1\}, \tag{5.1}$$

where N is the number of sensing events and X_t is the channel occupancy state as described in the previous chapter.

The percentage of the channels that are occupied in a frequency band at a given time is determined by channel occupancy. A straight forward estimate of channel occupancy is given as,

$$z = \frac{N_{occupied}}{N_{total}}, \tag{5.2}$$

where $N_{occupied}$ is the number of channels that exceed the detection threshold and N_{total} is the total number of channels in the band of interest.

Having modelled the PU transmission as a Markov process as described in the previous chapter, the transition rate is defined as the probability of the channel to change from an occupied to an unoccupied state (a_{10}) and vice versa (a_{01}). This pair of transition probabilities can be used as an indication of the

temporal correlation of the channel. More specifically, the higher the probability that the channel state alternates from unoccupied to occupied or vice versa, the lower the temporal correlation is. A summary of the spectrum occupancy characteristics based on the described occupancy metrics is presented in Table 5.3.

Table 5.3: Occupancy statistics.

Band	DC (%)	Occupancy (%)	Rate (%)
GSM 900 DL	68	66	27
GSM 900 UL	10	9	18
GSM 1800 DL	63	77	40
GSM 1800 UL	26	27	39
UMTS 2100 DL	91	82	16
UMTS 2100 UL	23	24	33
ISM 2.4 GHz	66	35	44

Figures 5.3 to 5.12 describe the spectrum occupancy statistics of each band as obtained by the measurement campaign for a period of 30 minutes. The top sub-figure describes the spectrum occupancy in the frequency domain in terms of the maximum and average received power. The mean is obtained by averaging the power values of each 100 kHz frequency during the measurement period whereas, the maximum is obtained by the maximum power observed in each frequency bin during the measurement duration. These results are used to investigate the temporal behaviour of each frequency band. The difference between the average and maximum received power values suggests intermittent PU transmissions over a fading channel. The middle sub-figure shows the temporal variation of the PSD and is used to describe how the received power varies in time for a given frequency band of interest. The bottom sub-figure describes the channel occupancy in the time domain in terms of the DC of each frequency bin within each band of interest.

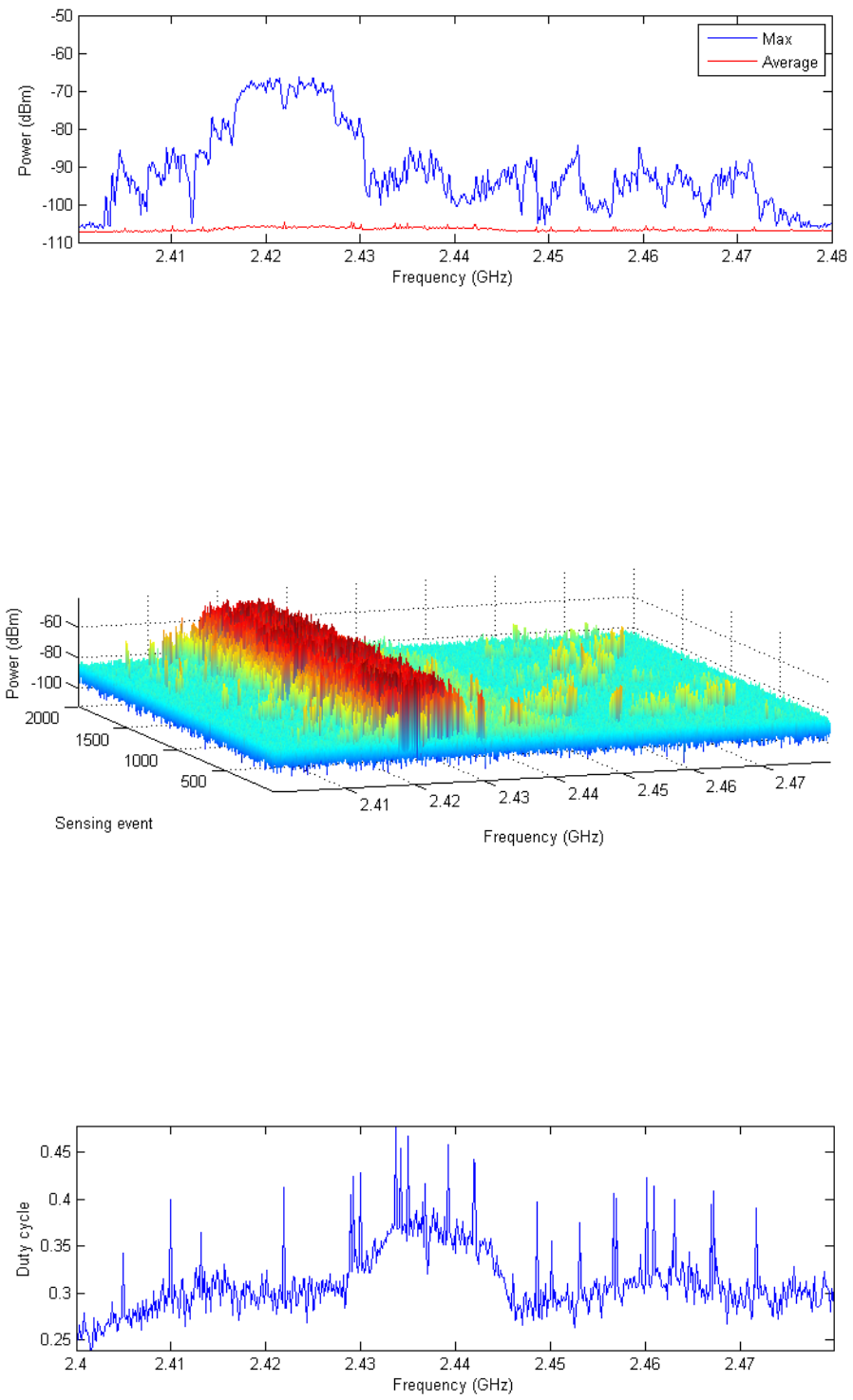

Figure 5.3: 2.4 GHz ISM band spectrum occupancy analysis.

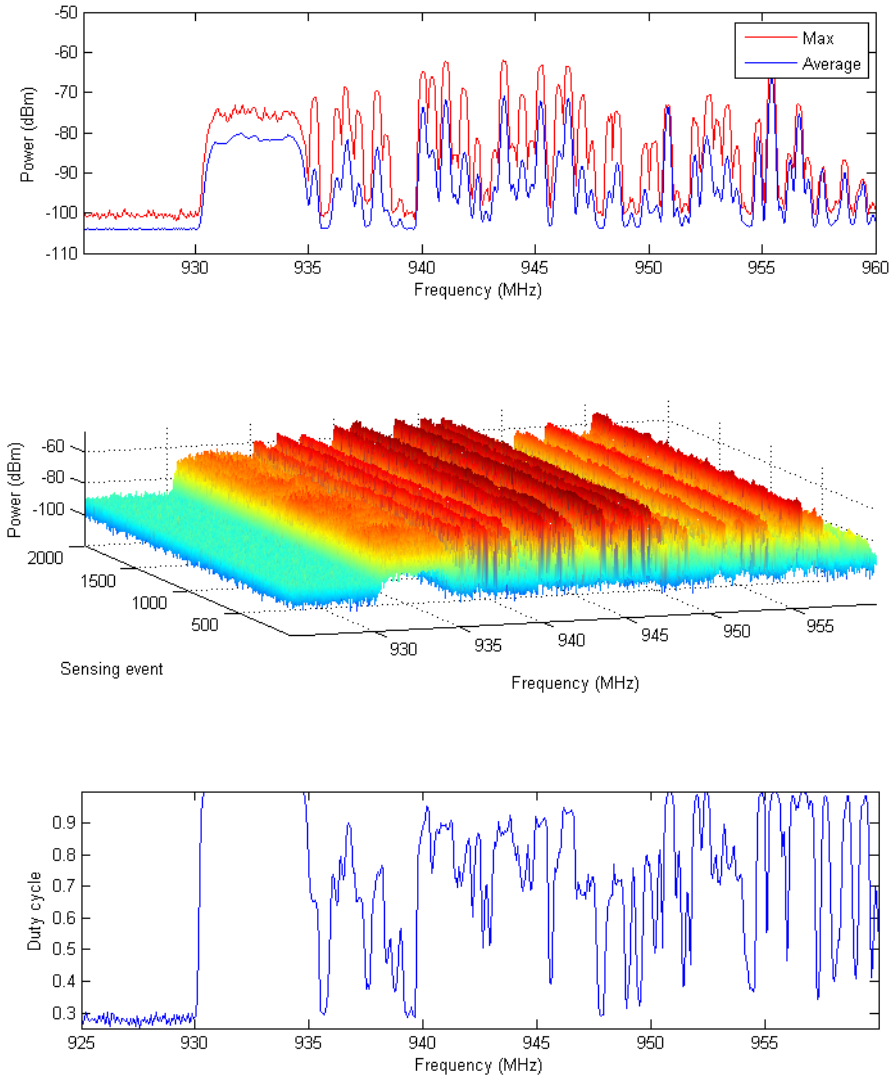

Figure 5.4: GSM 900 DL band spectrum occupancy analysis.

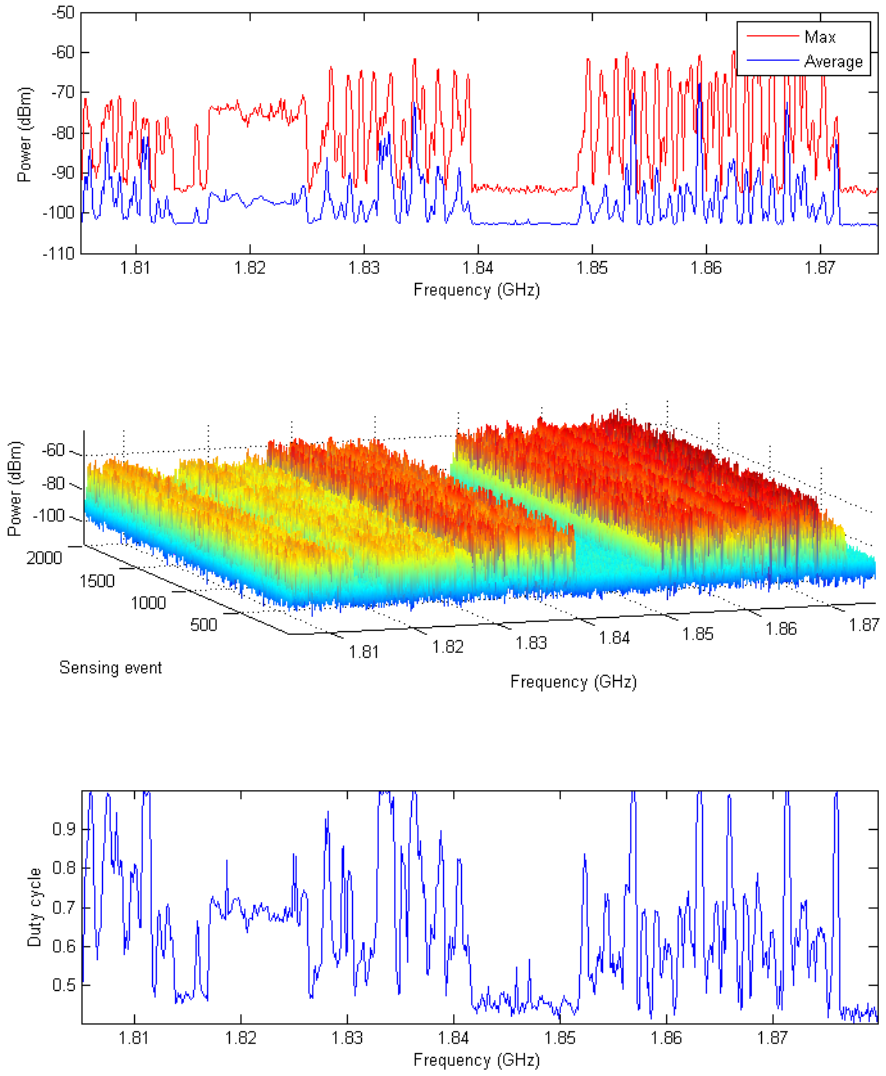

Figure 5.5: GSM 1800 DL band spectrum occupancy analysis.

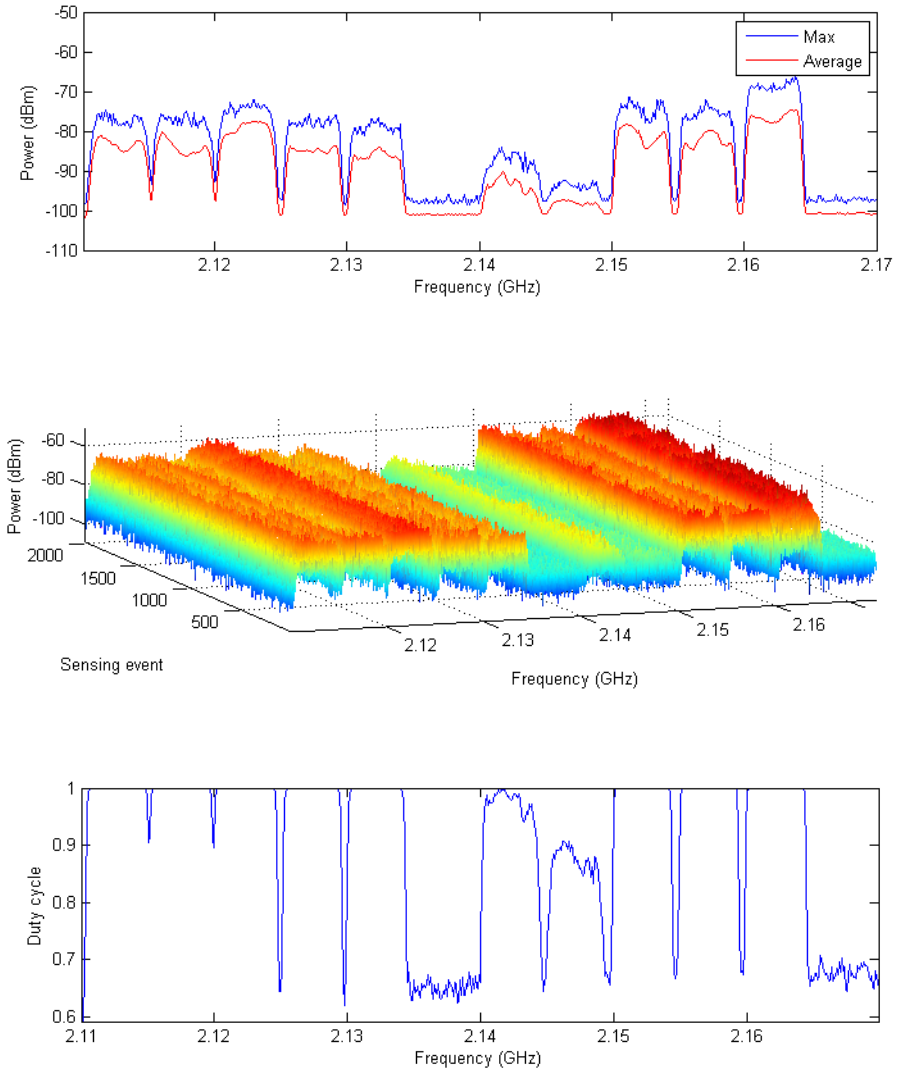

Figure 5.6: UMTS 2100 DL band spectrum occupancy analysis.

Based on the obtained spectrum activity results, the frequency bands can be categorised in terms of occupancy as: a) high; b) moderate; and c) low. An example of a highly occupied frequency band in both the frequency and time domain is the UMTS 2100 DL band (Figure 5.6) which has been found to be occupied 91% of the time with more than 80% occupied channels. On the other hand, the GSM 900 DL shows low occupancy statistics with 10% of the channels being occupied for less than 10% of the time. All the other bands in this study show mixed occupancy statistics with their duty cycle varying in the range between 20% to 80% with the cellular UL bands being up to 40% less congested than the DL bands. Furthermore, the 2.4 GHz ISM band is found to have similar occupancy statistics with the cellular up-link bands with an average duty cycle and channel occupancy of 66% and 60%, respectively. However, due to the short duration and random access intervals from Wi-Fi and Bluetooth systems the transition rate is higher than any other frequency band.

In addition to the aforementioned occupancy metrics, channel vacancy duration expresses the time period during which a frequency channel remains idle. Having modelled the channel occupancy as a binary time-series, channel vacancy duration can be obtained by observing the number of consecutive zeros in the occupancy sequence. Based on the observed data, Figure 5.10 describes the channel vacancy duration of the investigated frequency bands.

By applying the least-square regression analysis to the empirical data, channel vacancy duration in the 2.4 GHz ISM band can be approximated by an exponential distribution with a coefficient of determination $r^2 > 0.95$. The fitting parameters for the channel vacancy duration distribution are shown in Table 5.4. The geometrical distribution of the channel vacancy duration implies a memory-less process, i.e. the duration of a channel being in a given state is independent of its past states which in turn validates the selection of a Markov chain to model and predict the PU activity and hence, occupancy.

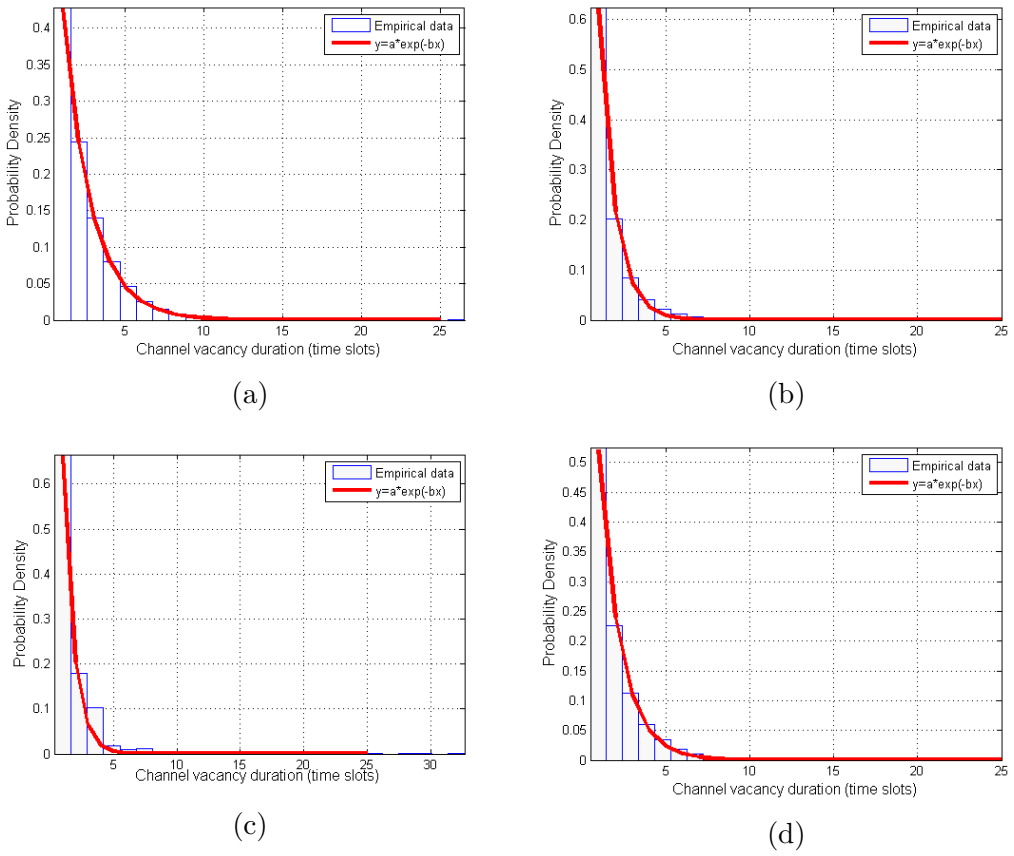

Figure 5.7: Channel vacancy duration: a) 2.4 GHz ISM band; b) GSM 900 DL; c) GSM 1800 DL; d) UMTS 2100 DL.

Table 5.4: Channel vacancy duration fitting parameters.

Frequency band	a	b	r^2
GSM 900 DL	1.78	1.054	0.992
GSM 1800 DL	2.136	1.172	0.994
UMTS 2100 DL	1.129	0.7737	0.998
ISM 2.4 GHz	0.7501	0.5605	0.997

5.4.2 Performance Metrics

In order to evaluate the prediction performance of the proposed scheme two metrics are considered. False Positive Rate (FPR) expresses the probability of predicting an unoccupied channel to be occupied, whereas True Positive Rate (TPR) expresses the probability of correctly predicting a channel to be occupied. Let $\hat{x}_{t+d} = 0$ denote the d-step ahead predicted channel occupancy state at time instant $t + d$ FPR and TPR are expressed as,

$$FPR = \frac{P(\hat{x}_{t+d} = 1 | x_{t+d} = 0)}{P(x_{t+d} = 0)} \tag{5.3}$$

$$TPR = \frac{P(\hat{x}_{t+d} = 1 | x_{t+d} = 1)}{P(x_{t+d} = 1)}. \tag{5.4}$$

Note that FPR and TPR are similarly defined as the detection metrics that are described in Chapter 2 with FPR corresponding to P_{fa} and TPR to P_d. However, the terms FPR and TPR are going to be used throughout the rest of this thesis when referring to spectrum occupancy prediction. As a binary decision problem, the prediction performance can be accessed using a confusion matrix [126]. A confusion matrix consists of two columns and two rows with each column representing the predicted instances of channel occupancy, and each row representing the actual ones (Table 5.5).

Table 5.5: Confusion matrix.

		Prediction outcome		
		0	**1**	**total**
actual value	**0**	True Negative	False Positive	N
	1	False Negative	True Positive	P
	total	$\hat{N}$	$\hat{P}$	

The confusion matrix entries can be categorised as: True Positives (TP); False Positives (FP); True Negatives (TN); and False Negatives (FN). The number instances that a channel is correctly predicted as occupied is expressed by TP, whereas the number of instances that an unoccupied channel is predicted to be occupied, is expressed by FP. On the other hand, TN corresponds to the number of correct predictions of an unoccupied channel, whereas the number of instances that an occupied channel is predicted as occupied corresponds to FN. Given the confusion matrix, FPR and TPR are obtained as,

$$FPR = \frac{FP}{P} \tag{5.5}$$

$$TPR = \frac{TP}{N}. \tag{5.6}$$

Additionally, prediction accuracy, which expresses the rate of correct predictions is obtained as,

$$Accuracy = \frac{TP + TN}{TP + TN + FP + FN}. \tag{5.7}$$

The above prediction methods are used to assess the prediction performance of the proposed scheme with respect to SNR, occupancy transition rate, history length and prediction span. By evaluating the prediction accuracy with respect to SNR and transition rate the robustness and the adaptability of the proposed scheme are assessed. In addition, the required sensing history is used to evaluate the complexity requirements of the proposed scheme to achieve a target prediction performance as the length of history determines the number of operations and the prediction time for the HMM as discussed in Chapter 4. In order to evaluate the reliability of the proposed scheme the relation between the prediction accuracy and the prediction span is analysed.

5.4.3 Evaluation Process

The occupancy status of each frequency channel is obtained by comparing the PSD data that have been obtained through the measurement campaign described in Subsection 5.3.1. with a predefined threshold based on the system's noise floor. The resulting binary occupancy sequence for each frequency index is treated as a binary time-series. Therefore, in order to evaluate the prediction performance, each binary time series that corresponds to one frequency channel is divided in two data subsets, the training and the test data-set.

The training data-set is used as input to the HMM-based spectrum occupancy prediction scheme whereas the test data-set is used to evaluate the prediction performance. The prediction performance is then evaluated by comparing predictor's output with the occupancy states of the test data-set. However, since the actual channel occupancy sequence is not directly observable from the measurement results the BWA is used to estimate the corresponding HMM parameters and then the Viterbi algorithm is used to infer the actual PU state sequences that have generated the observed data. The performance evaluation process is illustrated in Figure 5.8.

The performance of the HMM-based spectrum occupancy predictor is compared with a Markov predictor and an autoregressive model. A 1^{st} and a 2^{nd}-order Markov predictors are considered. The 2^{nd}-order Markov predictor is considered as higher order Markov chains can capture more complete temporal correlation. However, the analysis is limited to the 2^{nd}-order Markov chain as higher order results in higher complexity on the prediction algorithm. In addition, an AR(2) model is considered as proposed in [63] for spectrum hole prediction in CR systems. These methods that are used for performance comparison have already been described in Chapter 2.

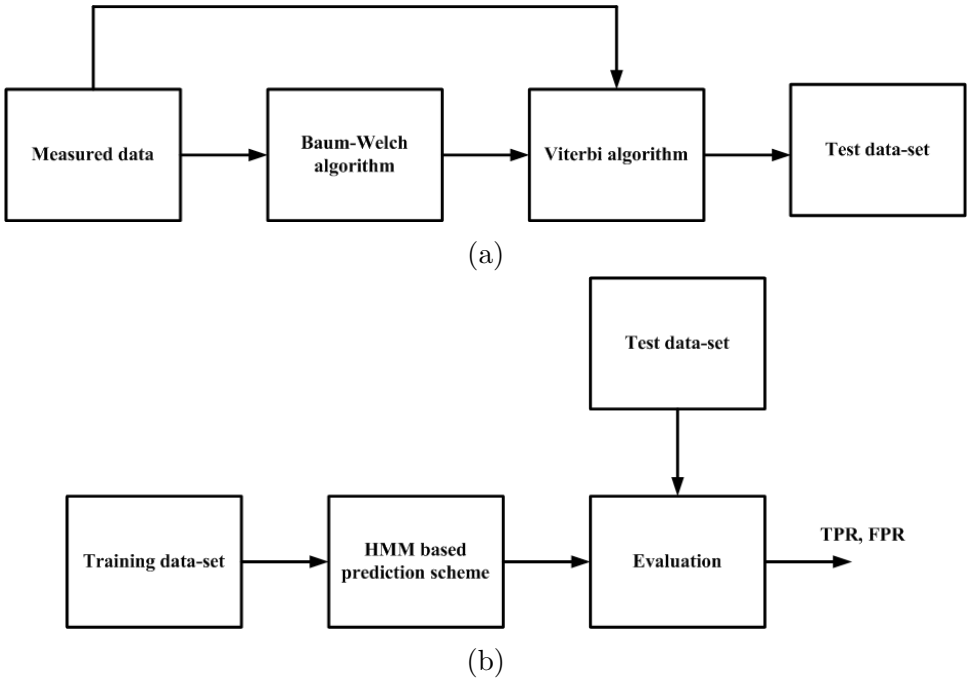

Figure 5.8: Prediction performance evaluation process: a) Test data preprocessing; b) Performance evaluation.

5.5 Numerical Results

In this section the performance of the proposed predictive spectrum sensing scheme is analysed. First, the performance of the HMM-based spectrum occupancy prediction is evaluated and compared with state-of-the-art prediction methods, with respect to the performance metrics that have been introduced in the previous subsection. In addition to the prediction performance, the efficiency of the predictive spectrum sensing scheme is analysed in terms of energy and time consumption. Based on the obtained occupancy results, most of the frequency bands under investigation could be potentially used for DSA since large portions of their spectrum have been found to remain unused for long periods of time. However, the 2.4 GHz ISM band is selected for evaluating in detail the performance of the proposed spectrum occupancy scheme because of its occupancy characteristics which pose extra challenge for occupancy prediction compared to frequency bands with determinist occupancy patterns.

5.5.1 Validation of Hidden Markov Model For Channel Occupancy Estimation

The first step to HMM-based spectrum occupancy prediction is the estimation of the optimal HMM parameters λ. To this end, as discussed in the previous chapter, the BWA training algorithm is applied to the training data-set. The algorithm is initialised with parametres $\lambda_0 = (\pi_0, A_0, B_0)$. The π_0 and A_0 values can be initialised either through statistical analysis of past sensing data or randomly. In this work, π_0 and A_0 are obtained through statistical analysis on the historical data for optimal performance. On the other hand, B_0 is initialised for a target sensing performance with $P_{fa} = 0.1$ and $P_d = 0.9$ as specified by the CR standard. Hence, the HMM emission matrix is initialised as,

$$\mathbf{B} = \begin{bmatrix} 0.9 & 0.1 \\ 0.1 & 0.9 \end{bmatrix} \tag{5.8}$$

Figure 5.9 shows the learning curve of the BWA algorithm in which the optimal HMM parameters are estimated over 40 iterations. The algorithm is terminated when the log-likelihood value is smaller than 10^{-4}. In case that the BWA algorithm does not converge, the training process finishes after 100 iterations in order to ensure that the training process finishes within the time constraint of 1 sec.

In order to test whether HMMs can model channel occupancy of real-world systems, a cross validation method is followed. First, the HMM parameters are randomly initialised and then are optimised through the training process using 1000 observations for each frequency channel in the observed frequency bands. When the training process has been completed the estimated transition matrices for each frequency channel is compared with the actual transition rate as obtained by the measured data.

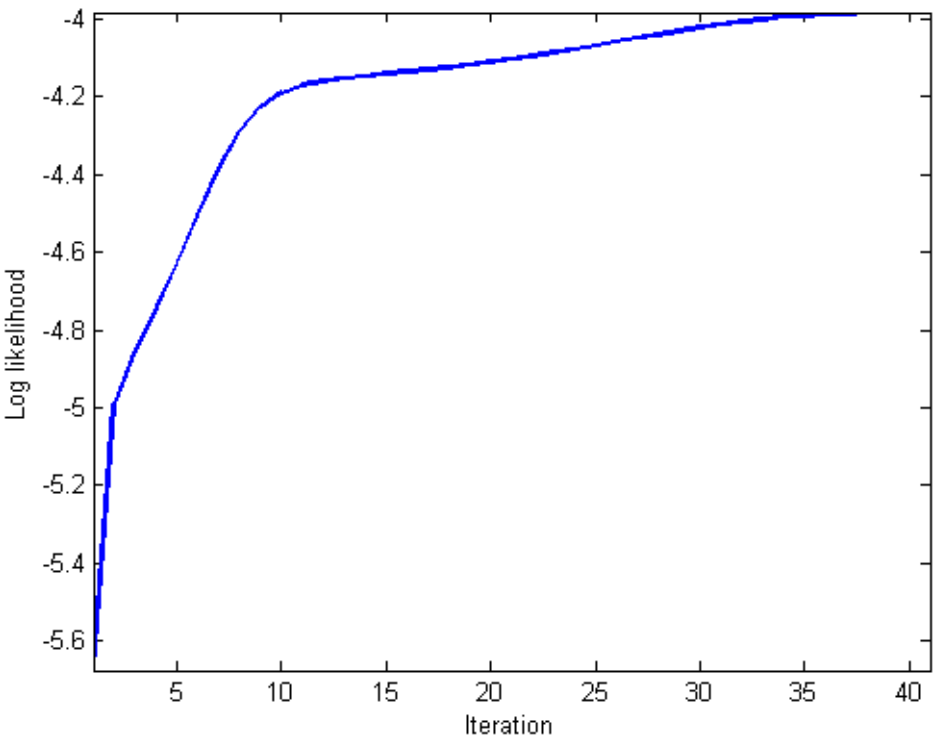

Figure 5.9: BWA learning curve.

Figures 5.10, 5.11, 5.12, and 5.13 compare the actual transition rates with the HMM estimates for the GSM 900, GSM 1800, UMTS 2100 and 2.4 GHz ISM bands, respectively. The accuracy of the HMM parameter estimation was validated in terms of the Root Mean Square Error (RMSE). A summary of the error between the estimated and actual transition rate for each frequency band is shown in Table 5.6. It is worth noting that for some cases the BWA algorithm has been found not to converge with the target value of 10^{-4} within the constraint of 100 iterations. This explains the underestimation of the transition rate as shown for example in Figure 10 for the channels between 925 MHz and 930 MHz. The estimation accuracy of the algorithm could be improved by increasing the number of training iterations. However, such an increase would result in increasing the overall duration of the prediction process beyond the time constraint of 1 sec which equals to sensing interval.

The findings in Section 5.4.1 showed that PU activity can be described by a Markov chain owing to the memoryless nature of the observed process indicated by the geometrical distribution of the channel vacancy duration. Therefore, given that PU activity can be described by a Markov process and the estimation accuracy of the BWA, channel occupancy has been verified to be adequately modelled by an HMM for a range of well-known frequency bands.

Table 5.6: HMM parameters estimation.

Frequency band	RMSE
GSM 900 DL	0.084
GSM 1800 DL	0.050
UMTS 2100 DL	0.036
ISM 2.4 GHz	0.054

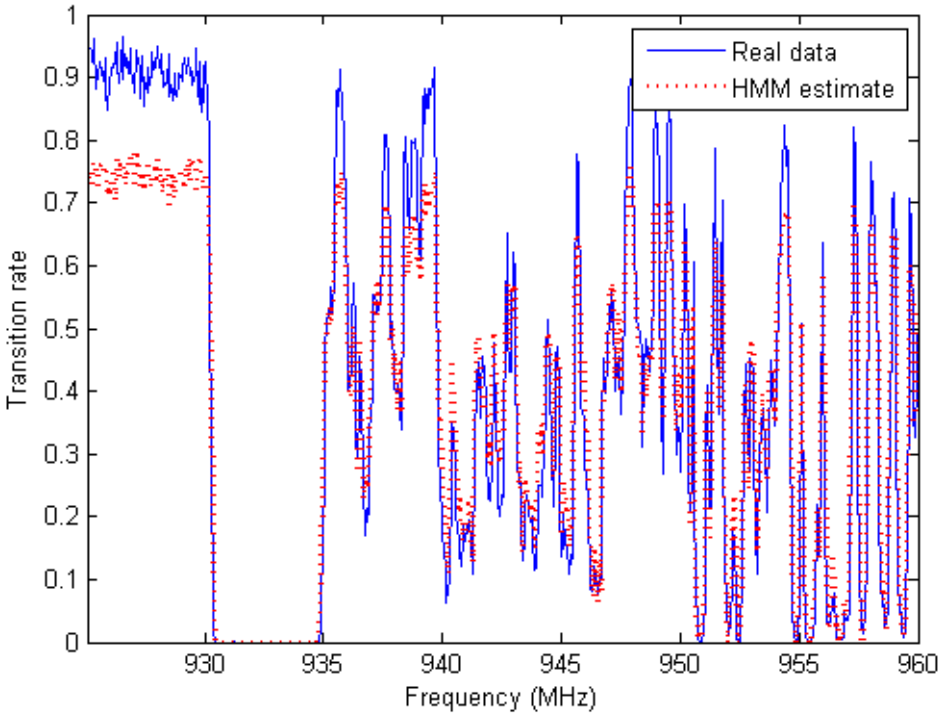

Figure 5.10: Estimation of state transition probability for the GSM 900 DL band.

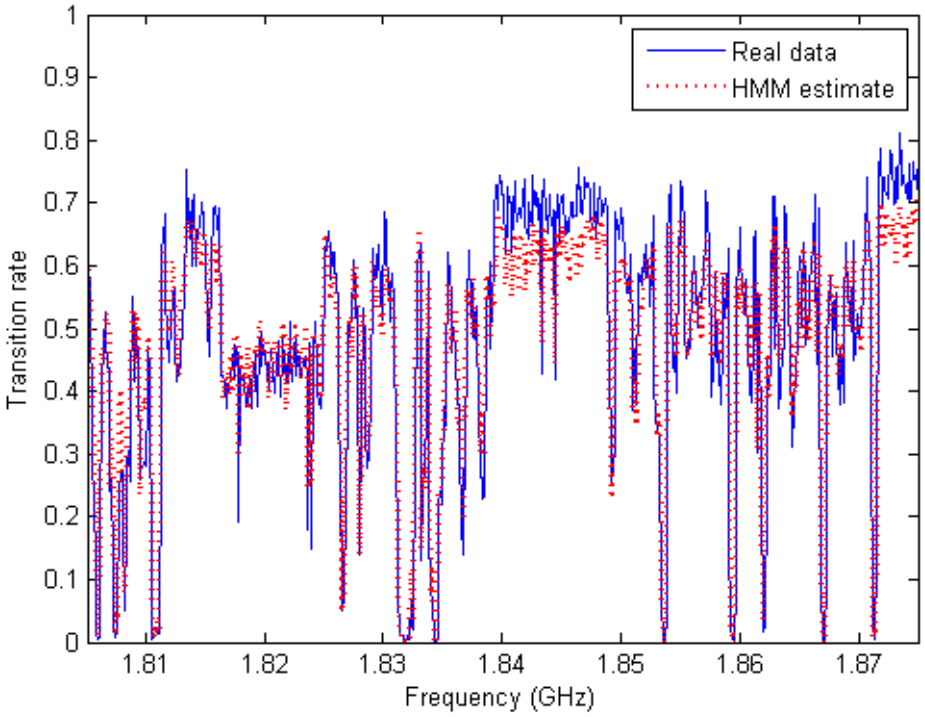

Figure 5.11: Estimation of state transition probability for the GSM 1800 DL band.

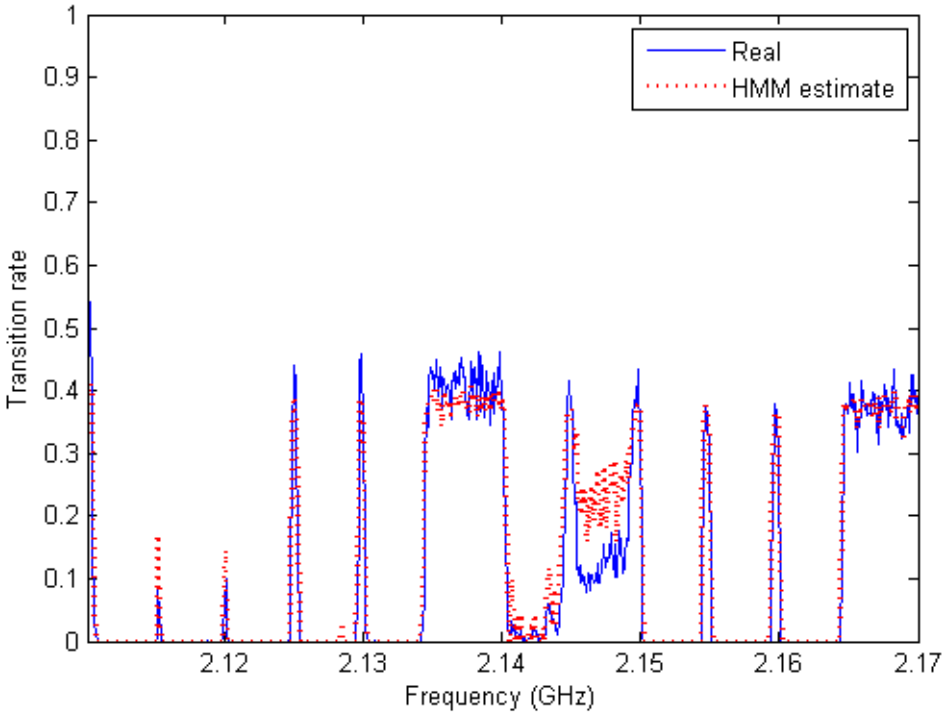

Figure 5.12: Estimation of state transition probability for the UMTS 2100 DL band.

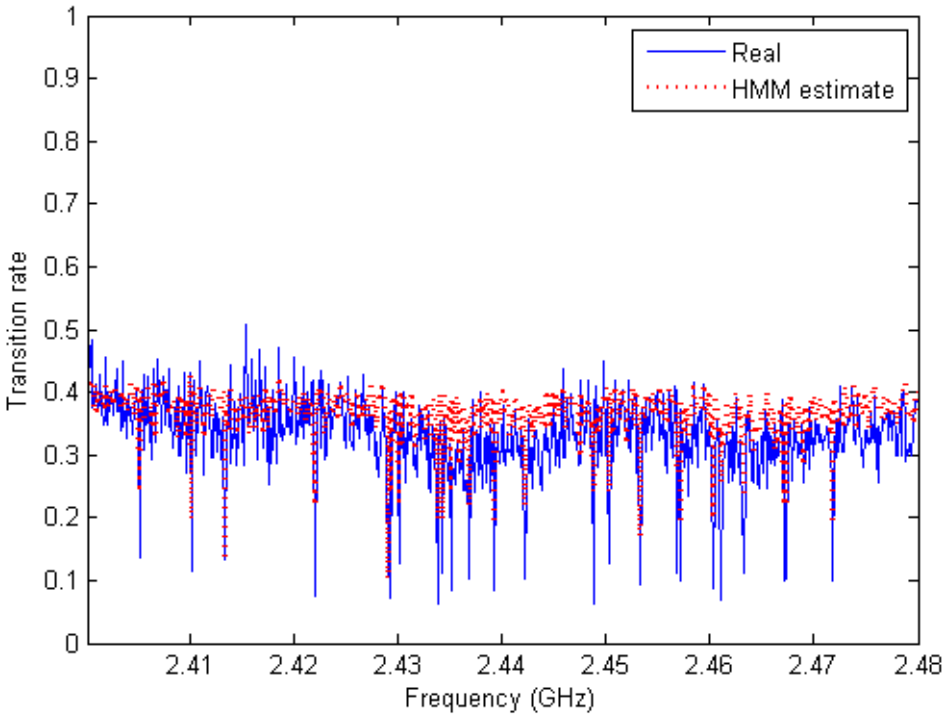

Figure 5.13: Estimation of state transition probability for the 2.4 GHz ISM band.

5.5.2 Prediction Performance

Having verified that HMM can model spectrum occupancy, the performance of the HMM-based spectrum occupancy prediction algorithm can now be evaluated. The prediction performance is first evaluated for one step-ahead predictions, i.e. predict channel occupancy at time instant $T + 1$, with a history of 200 previous observations. The performance of the HMM-based prediction scheme is compared with a 1^{st} order Markov, 2^{nd} order Markov and an AR(2) autoregressive model.

Figure 5.14a describes how TPR varies with respect to the channel occupancy transition probability. This analysis assesses the performance of the prediction schemes to correctly predict occupied channels with respect to the probability of the channel occupancy state changes within the historical data. It can be observed that the HMM-based approach outperforms all other methods by achieving a $TPR = 0.9$ until a transition rate of 0.4 is reached. The fact that the model's parameters are adjusted online via the BWA algorithm results in higher adaptability of the HMM-approach. In other words, the HMM approach learns faster than the Markov and the autoregressive approach owing to its inherent training capabilities. Moreover, with reference to Figure 5.14b it can be seen the HMM-based approach also achieves better prediction performance in terms of false predictions with up to 50% lower FPR compared to the Markov and AR methods.

In addition to the transition probability, the prediction performance is also analysed with respect to SNR, as shown in Figures 5.15a and 5.15b where it can be seen that as the SNR increases, the TPR increases as well, which in turn implies higher prediction accuracy. This is because ED-based spectrum sensing can detect the presence of a PU signal with up to 100% in the SNR regions above 11 dB. Therefore, having a history of error-free spectrum sensing results, which suggest the existence of a dominant PU signal, spectrum occupancy prediction is not very challenging.

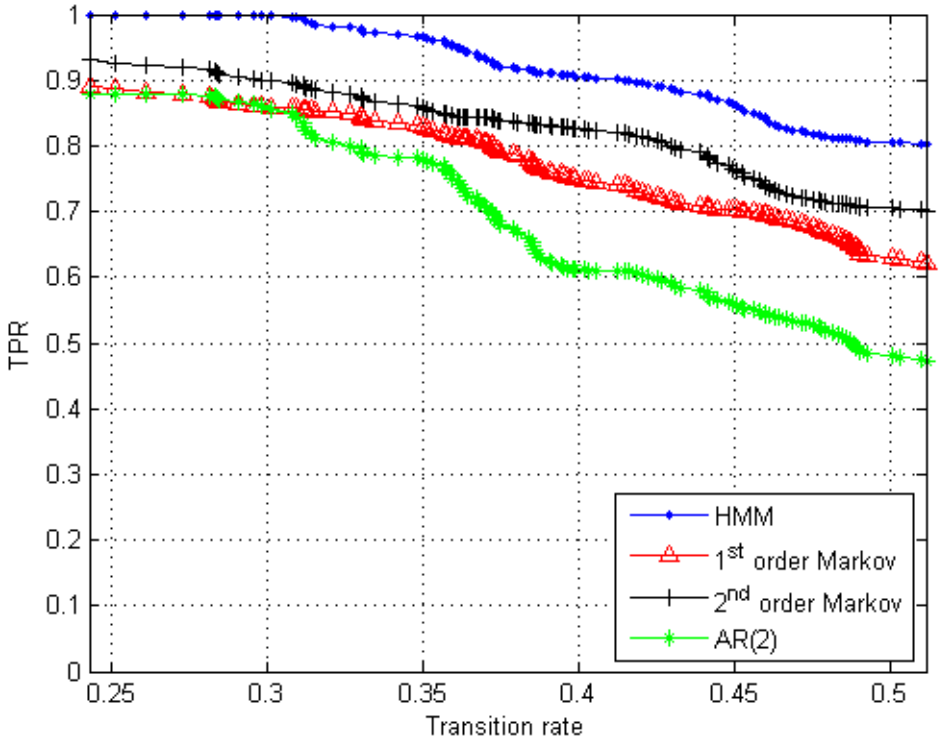

(a)

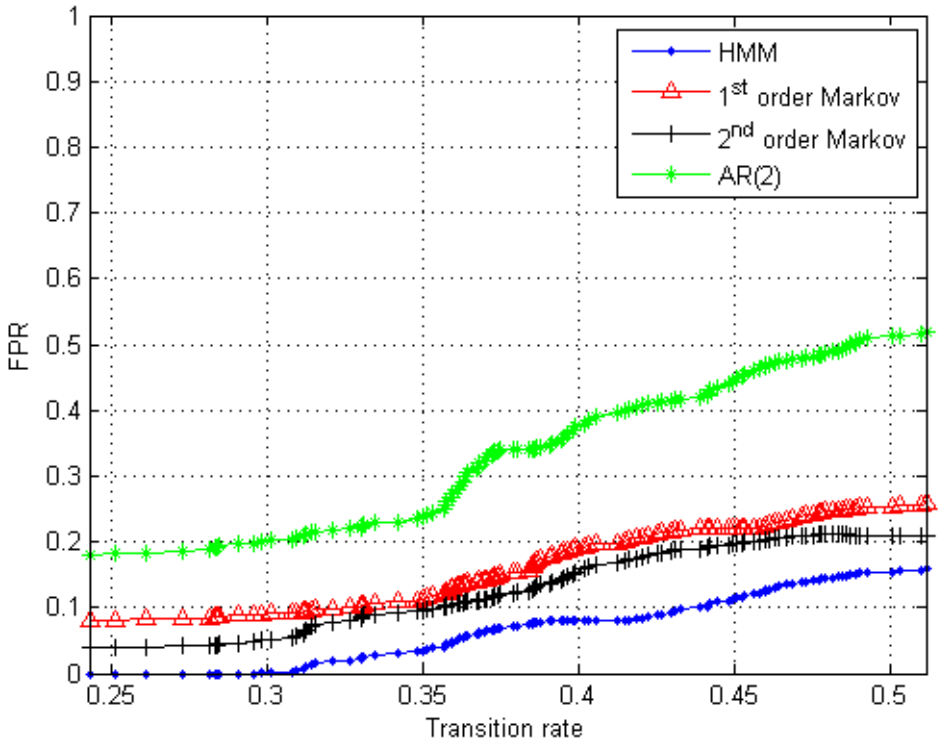

(b)

Figure 5.14: Prediction performance: a) TPR versus transition rate; b) FPR versus transition rate.

However, for SNR regions below 9 dB where ED starts failing to accurately detect the presence of PU signals, spectrum occupancy prediction becomes a very complicated task. To this end, it can be seen that the HMM-based approach significantly outperforms the other candidates with up to 90% higher prediction accuracy in the SNR regions below 10 dB. The superior prediction performance of the HMM approach can be explained by the use of the emission matrix in the HMM for modelling the sensing errors within the historical data. Therefore, through the training process the HMM parameters used for prediction are optimised based on the sensing performance of the CR system. As a result, the propagation of errors from the historical data to the predicted ones is limited compared to the other prediction methods. More specifically, as shown in Figure 5.15b, the HMM-based method achieves a TPR of 0.9 for an SNR value of 4 dB with an up to 10 dB gain compared to the AR(2) approach. Similarly, the HMM-based approach reaches an FPR of 0.1 for an SNR of 1 dB with an up to 15 dB gain.

Overall, the HMM-based method achieves 30% and 80% higher prediction accuracy in terms of TPR and FPR, respectively. Moreover, it is shown that using a higher order Markov chain results in negligible performance improvement with less than 5% higher TPR between the 2^{nd} and 1^{st} order Markov approaches. Therefore, with reference to Table 5.7, the HMM-based spectrum occupancy prediction approach outperforms the Markov and AR ones with a mean TPR and FPR of 0.93 and 0.07, respectively. Such TPR and FPR values suggest that the HMM-based meets the requirements of $P_d = 0.9$ and $P_{fa} = 0.1$ in accordance with the CR standard specifications.

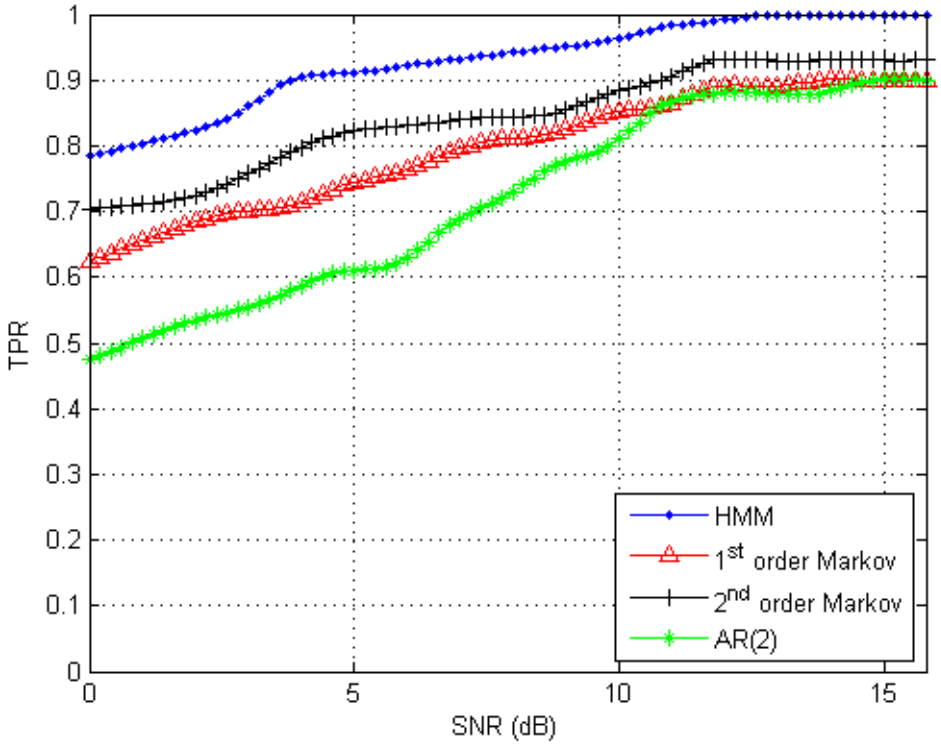

(a)

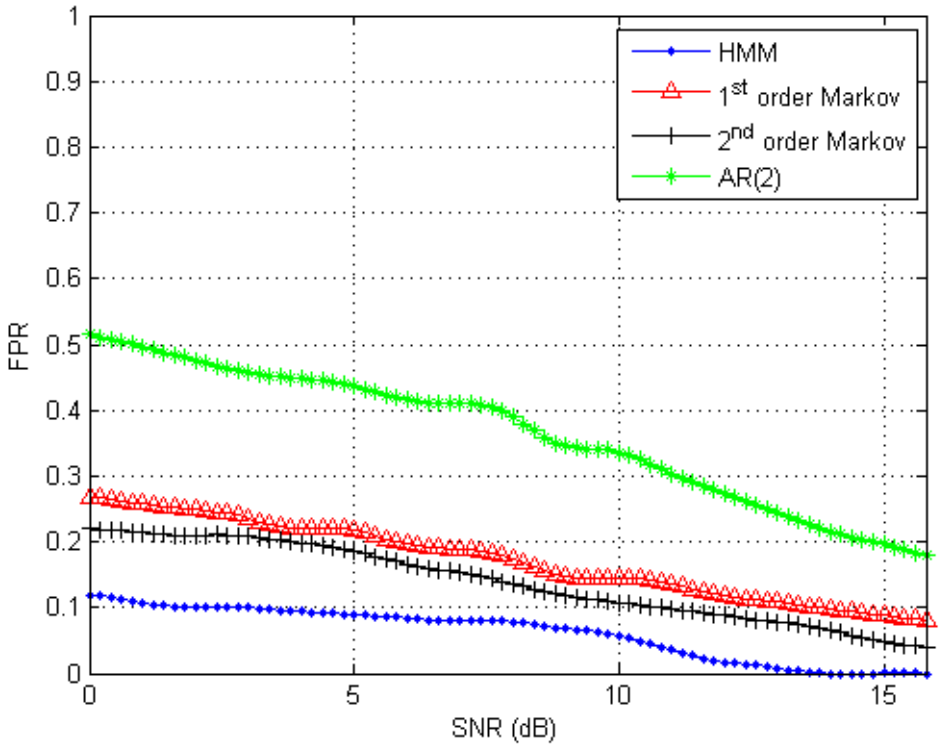

(b)

Figure 5.15: Prediction performance: a) TPR versus SNR; b) FPR versus SNR.

Table 5.7: Prediction performance.

Method	TPR	FPR	$SNR\|_{TPR=0.9}$	$Transition\,rate\|_{TPR=0.9}$
HMM	0.93	0.07	3.8 dB	0.4
1^{st} order Markov	0.79	0.18	12 dB	0.3
2^{nd} order Markov	0.82	0.15	10 dB	0.2
AR(2)	0.71	0.36	14 dB	0.2

Having analysed the performance of the HMM-based spectrum occupancy prediction method for one-step ahead predictions, multi-step ahead predictions are now considered. To this end, Figure 5.16 describes how the prediction performance varies with respect to the length of history and the prediction span. With reference to Figure 5.16 can be obserced that as the the length of history increases, the prediction performance improves. On the other hand, as the prediction span increases the prediction performance degrades. More specifically, using 190 past spectrum sensing outputs a prediction accuracy of 90% is achieved for one-step ahead predictions. Nevertheless, in order to achieve 90% prediction accuracy for a prediction span, $d = 10$, a history of 450 past sensing outputs is required. Furthermore, it is worth noting that when prediction starts without any historical information the predictor performs random guess resulting in 50% accuracy.

For real-world systems the trade-off between the length of history and the prediction span can be quantified in terms of computational complexity. As discussed in the previous chapter, the computational complexity of HMM scales to $O(4T)$ multiplications. Hence, given a target prediction accuracy of 90%, for one step-ahead predictions 760 multiplications are required, while for ten step-ahead predictions this number increases to 1800. To this end, given that the computational complexity of an FFT (key signal processing component of ED-based spectrum sensing) scales to $O(Nlog_2(N))$, for a 512 point FFT 4608 operations are required. Thus, in order to predict the ten step-ahead occupancy of a frequency channel, less than half operations are performed compared to those performed by a standard FFT process resulting in no ad-

ditional computational burden to the CR.

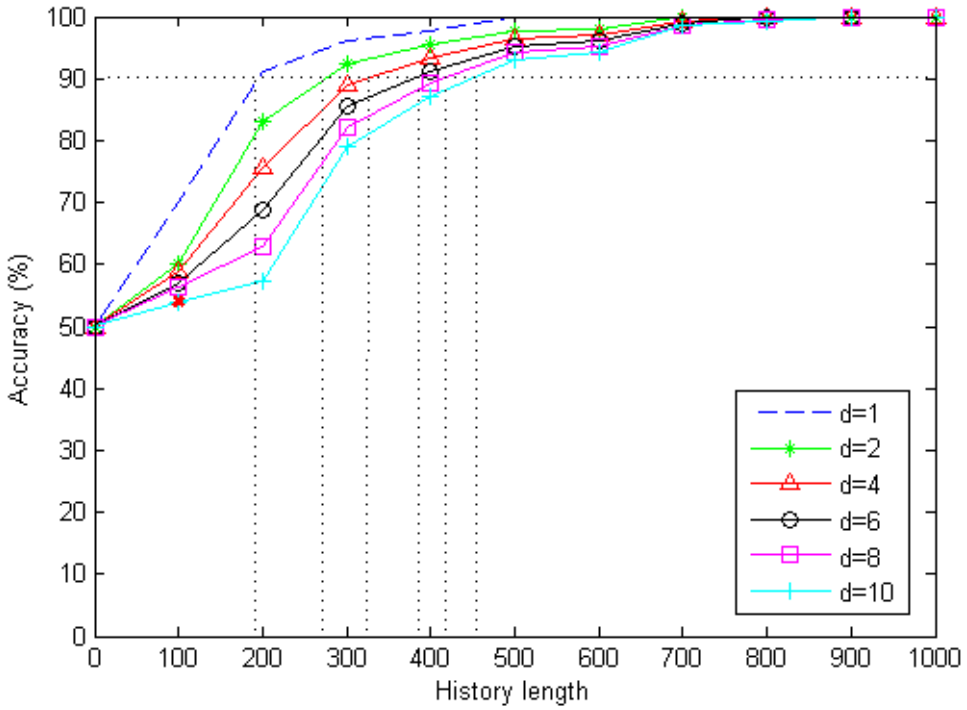

Figure 5.16: Multi-step ahead prediction performance for d=1 to d=10.

5.5.3 Case Study

In this section it is demonstrated how the integration of HMM-based spectrum occupancy prediction scheme to ED-based spectrum sensing can enhance the sensing efficiency of CR systems. Sensing efficiency expresses the total number of channels that need to be sensed in order to determine the channel availability within a given band of interest. Hence, the sensing efficiency, $\eta_{sensing}$, can be expressed as,

$$\eta_{sensing} = \frac{N_{free}}{N_{sense}}, \tag{5.9}$$

where N_{free} denotes the number of free channels and N_{sense} denotes the total number of frequency channels that have been sensed.

Assuming that in order to sense N_{sense} number of channels requires a τ_{sense} (s) time unit the total sensing time for N_{sense} channels equals to T_{sense} =

$\tau_{sense} \times N_{sense}$. As a result, given that an energy unit, e_{sense} (j/s), per time unit is required to perform spectrum sensing, the total sensing energy can be expressed as $E_{sense} = T_{sense} \times e_{sense}$. Given that sensing time and energy per channel are constant, the total sensing energy consumption can be expressed as $E_{sense} = e_{sense} \times \tau_{sense} \times N_{sense}$. Therefore, based on expression (5.9), spectrum, energy and time efficiency are directly related to the number of sensed channels.

Let a CR network with N_{total} licensed channels, with different PU occupancy statistics, shared between the PUs and SUs. Every SU performs multi-channel spectrum sensing over a constant sensing time-slot and stores a history of the past sensing outputs for every channel. In such a multi-channel scenario, a CR that performs conventional ED-based spectrum sensing would sense the entire band of interest to identify the available channels to be dynamically accessed, i.e. $N_{sense} = N_{total}$. However, when predictive spectrum sensing is employed, the CR senses only the channels that will be predicted to be unoccupied. Hence, for predictive spectrum sensing the number of sensed channels equals to the number of the predicted channels, $N_{sense} = N_{pred}$, with $N_{pred} \leq N_{total}$. Therefore, predictive spectrum sensing is expected to reduce the sensing cost in terms of the required sensing energy and time. The percentage of saved sensing cost compared to the conventional ED-spectrum sensing is obtained as,

$$C_{sensing} = \frac{N_{total} - N_{pred}}{N_{total}}. \tag{5.10}$$

The performance of the predictive spectrum sensing algorithm, as described in Subsection 5.3.1, is analysed in terms of the sensing cost over different frequency bands and PU occupancy statistics. In order to mimic realistic scenarios, the obtained data from the measurement campaign as previously described in this chapter are used to generate synthetic occupancy data for each frequency band of interest. The simulated scenario consists of one SU that performs predictive spectrum sensing and multiple PUs that transmit in the primary bands. The primary bands include the GSM 900 and GSM

1800, UMTS 2100 and 2.4 GHz ISM bands. Given the prediction performance analysis as presented in the previous section, the SU is assumed to have already created a history of 200 past sensing outputs which are subsequently used to perform one-step ahead predictions.

Figure 5.17 shows how predictive spectrum sensing can reduce the sensing cost compared with conventional ED-based spectrum sensing for different frequency bands. The performance of predictive spectrum sensing is analysed for time duration of 100 sensing slots which correspond to approximately 1.5 minutes. It can be seen that a maximum sensing cost reduction of up to 84% is achieved in the UMTS band whereas the minimum improvement is observed in the ISM band with an up to 45% reduction. It is worth noting that these results are in line with the occupancy statistics of the bands which reveals the prediction accuracy of the predictive sensing scheme. Furthermore, it is observed that the predictive sensing scheme requires approximately 20 past sensing outputs in order for the BWA algorithm to converge.

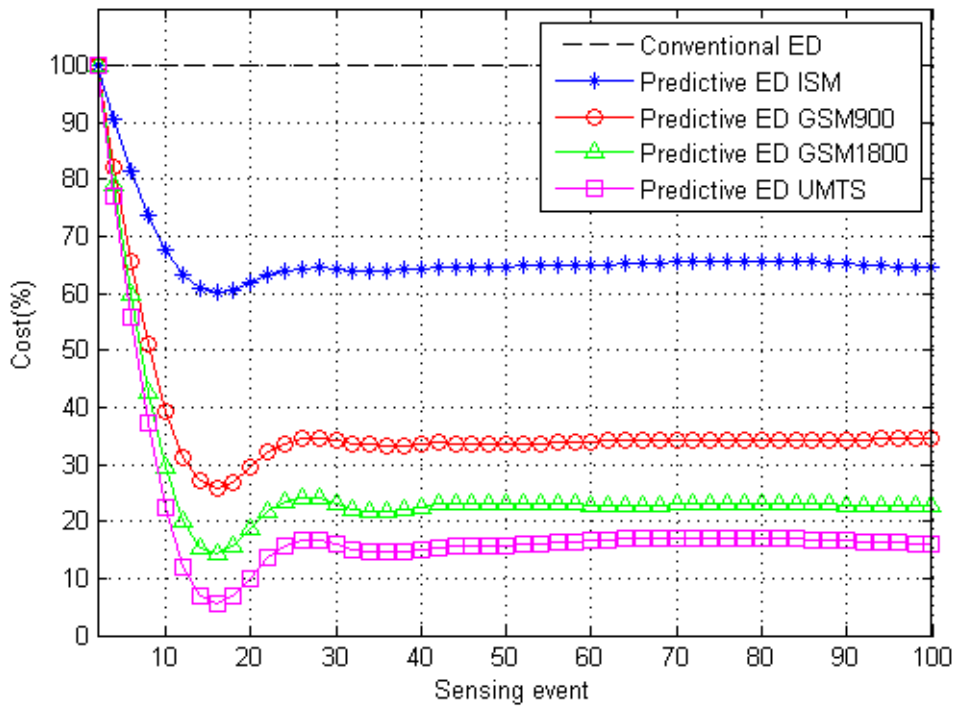

Figure 5.17: Spectrum sensing energy cost for conventional ED-based spectrum sensing and predictive ED-based spectrum sensing.

5.6 Summary

In this chapter the concept of predictive spectrum sensing as a smart sensing mechanism as a means of reducing the sensing cost of autonomous CR nodes has been introduced. The prediction performance of the proposed scheme has been evaluated through real-world spectrum activity measurements in different cellular frequency bands as well as in the 2.4 GHz ISM band. The proposed scheme is designed to perform real-time, short-term spectrum occupancy predictions by using short observation history. In summary, the HMM-based spectrum occupancy prediction has been found to outperform state-of-the-art prediction methods with up to 30% and 80% in terms of TPR and FPR, respectively. Furthermore, by applying the HMM-based spectrum occupancy prediction to spectrum sensing, an improvement between 45% and 84% is achieved on the sensing performance in terms of the required sensing time and sensing energy consumption.

Chapter 6

Channel Availability Modelling for the Polarisation Domain

6.1 Introduction

In this chapter a channel availability model for the polarisation domain is introduced. This model forms a statistical framework that describes channel availability in both vertical and horizontal polarisation for CR applications. The proposed channel availability model is developed and validated using empirical data obtained through a measurement campaign in the cellular bands within a realistic operational scenario. Such a probabilistic spectrum availability model can be employed for studying and improving the performance of CR systems operating in the defined scenario. A review of up to date channel availability models is presented in Section 6.2. In Section 6.3 the system model and problem formulation are presented by describing how the effects of polarisation affect the perceived spectrum availability, and hence degrade the performance of CR systems. A detailed description of the measurement campaign and methodology for capturing and processing the occupancy data is presented in Section 6.4. In Section 6.5 the effects of polarisation on the perceived channel availability are analysed, whereas in Section 6.6 the spectrum availability model for the polarisation domain is validated based on experimental data.

6.2 Related Work

Owing to the opportunistic nature of the DSA method, the network's performance is highly dependent on the PU spectrum occupancy statistics. As a result, accurate modelling of spectrum availability or occupancy is required in order to optimise the performance of CR systems in terms of energy and spectrum efficiency. Such probabilistic models are employed for either facilitating spectrum access or optimising spectrum sensing strategies.

For example, adaptive spectrum sensing based on prior knowledge of the spectrum occupancy statistics has been proposed in [127], [128]. More specifically, by using suitable statistical knowledge of the PU occupancy patterns, the sensing task can be prioritised and the amount of time for spectrum sensing and access can be partitioned accordingly. Given that spectrum occupancy statistics vary between different frequency bands, geographical locations and time periods, a method that relates these characteristics is required. To date, several statistical occupancy models have been proposed for time, frequency and space dimensions. Based on this classification, a review of these existing channel occupancy models follows.

In the frequency domain spectrum occupancy is described by the PSD of a received signal over a given resolution bandwidth. Frequency domain models are used to describe the probability distribution of occupied or available channels within a given frequency range. To this end, in [129] channel availability has been found to follow a Beta distribution whereas a Poisson-Normal approximation has been proposed to describe the number of available channels. The proposed model has been validated using real-time data obtained by an extensive measurement campaign in the frequency range 0-6 GHz in multiple indoor and outdoor locations around Europe [130].

Time domain models are used to model the average DC as well as the distribution of the duration of busy/idle periods. Two-state Markov chains are the most widely used statistical technique for describing spectrum occupancy in the time domain. The two states indicate a channel at a given time instant as

occupied or unoccupied. The average channel occupancy in the time domain is described in terms of the DC which expresses the fraction of time that the channel is occupied by a PU. Although DC is a straightforward metric, the duration of the busy and idle periods is an important metric for realistic spectrum occupancy modelling in the time domain.

Time-varying spectrum occupancy is a well investigated topic with different occupancy models for the time domain which have already been proposed. In [131] spectrum sensing has been evaluated by an exponential distribution to describe the busy periods of the primary system. In addition, a time-varying statistical model that can describe both the idle and busy periods of the primary system as two independent Poisson processes has also been proposed.

Spatial occupancy models are used to describe the spectrum occupancy patterns as perceived by the CR users at different geographic locations. This is a currently rich and extensive research area as it is closely related to radio propagation modelling. In the context of CR, radio environment maps have been proposed as a tool for improving the radio environment awareness particularly for cooperative spectrum sensing schemes [132]. In [133], spectrum occupancy has been analysed in terms of the spatial distribution of the PSD for a given frequency band. An alternative channel occupancy model for the spatial domain has been developed in [134] where a propagation model is first used to estimate the path loss between the PU transmitter and the CR user. Based on a set of parameters such as the PU transmission power, operating frequency and distance, the received power of the PU signal by the CR user in various locations is then calculated. By employing a detection threshold based on the receiver's noise power the received power level can be mapped to a binary busy/idle occupancy map at different locations. In addition, an analytical model based on a semivariogram has been fitted to average PSD values of different frequency band at various locations in [132].

All previous studies have provided accurate channel availability models for the frequency, temporal and spatial dimensions that constitute a valuable

tool for designing, evaluating and improving the performance of CR systems. However, in all the aforementioned studies only the vertical polarisation has been considered. Hence, the derived models are only applicable to CR nodes that perform spectrum sensing in a single polarisation, i.e. vertical. Therefore, the case of mobile SUs such as on-body sensors, mobile handsets or tablets are most likely to change their orientation and hence signal polarisation during spectrum sensing [135] has not been covered by the proposed models.

In such a scenario, the CR terminals may incorrectly sense an occupied channel as unoccupied and vice versa as the received signal power level may be significantly different between different polarisations (similar to the hidden PU problem) because of the propagation environment and the polarisation mismatch between the primary and secondary system. Furthermore, the concept of using polarisation as an additional degree of freedom for spectrum sharing has recently gained significant attention [136], [137] and has been found to enhance sensing efficiency. In this context, this work introduces an empirical channel availability model that describes the channel availability in both vertical and horizontal polarisation at the same time for mobile CR terminals.

6.3 System Model

Let a CR network use a frequency spectrum divided into $N_c h$ shared channels between the PU and SU system. The primary system is assumed to operate at a given polarisation, whereas the secondary system consists of mobile SUs that change their orientation during spectrum sensing, as shown in Figure 6.1a. With reference to ED-based spectrum sensing, the binary channel occupancy status, $S_{t,i}$, for the i^{th} channel at time instant t at the SU is obtained as,

$$S_{t,i} = \begin{cases} 1, & P_{i,t} \geq \lambda \\ 0, & P_{i,t} < \lambda, \end{cases} \tag{6.1}$$

where $P_{t,i}$ is the received signal's power and λ is the detection threshold. The temporal dependencies of the channel occupancy pattern at time instant t

varies as a function of time t, as shown in Figure 6.1b.

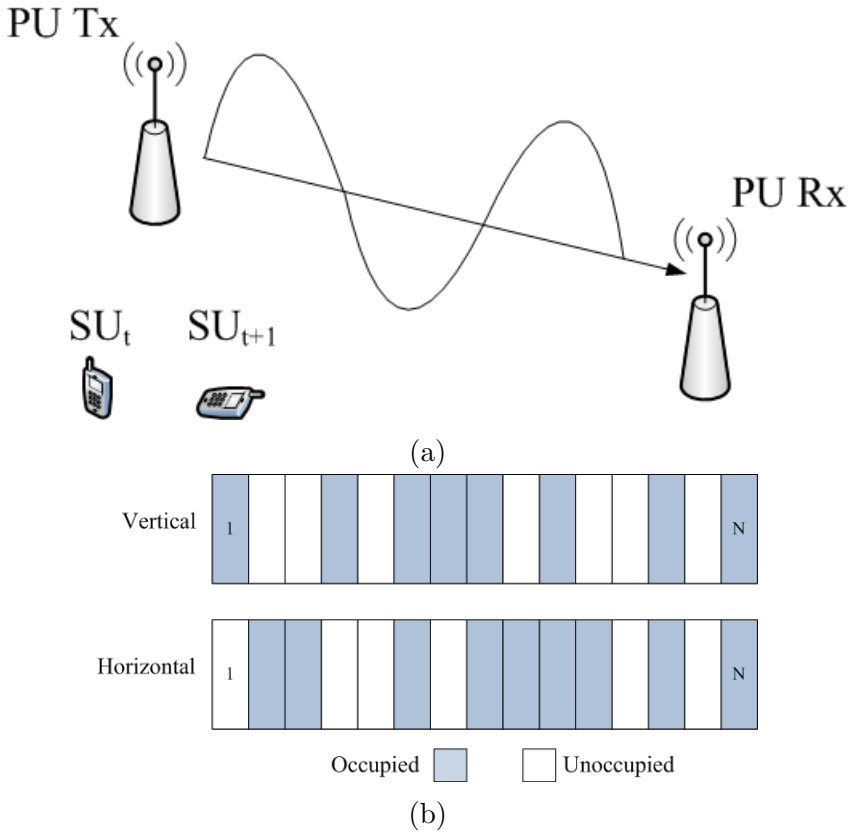

Figure 6.1: Problem formulation a) system model; b) example of spectrum occupancy of N channels at time instant t in both polarisations.

Under such conditions the missed detection and false alarm probabilities will increase, causing unwanted interference to the PU system and impairing the overall spectrum utilisation. Thus, in order to provide a framework for characterising this problem we propose a probabilistic model that describes the spectrum availability in both vertical and horizontal polarisations in terms of two different probabilistic metrics:

1. the distribution of available channels in both polarisations at the same time instant

2. the channel idleness probability in both polarisation at the same time instant.

Let N_{free} denote the total number of available channels in both polarisations at any given time. The probability distribution, mean and variance of N_{free} characterise spectrum availability. In addition, the channel idleness probability can be defined as the probability of the i^{th} channel to be unoccupied in both polarisations at the same time instant t and can be expressed mathematically as the joint probability,

$$p_{idleness} = P(S_{i,t_{vertical}} = 0, S_{i,t_{horizontal}} = 0), \tag{6.2}$$

where, $S_{i,t_{vertical}}$ and $S_{i,t_{horizontal}}$ denote the channel occupancy status by a vertically and a horizontally polarized receiving antenna, respectively.

6.4 Measurement Campaign

A measurement campaign was conducted in order to investigate the effects of polarisation on the perceived channel occupancy by an SU. To this end, the measurement equipment consisted of a Universal Software Radio Peripheral (USRP) platform, USRP-2922 and two omni-directional 3 dBi monopole antennas with a frequency range from 824 MHz to 980MHz and 1710 MHz to 1990 MHz with a Cross-polarisation Discrimination (XPD) of 8dB. The measurement set-up is depicted in Figure 6.2.

The NI USRP-2922 platform is an SDR transceiver with frequency coverage from 0.4 GHz to 4.4 GHz that covers a variety of popular bands and wireless standards such as cellular communication systems and the 2.4 GHz Wi-Fi [138]. Key specifications of the USRP platform's receiver are presented in Table 6.1. The USRP platform is connected to a host PC over a standard TCP/IP interface via 1 Gigabit Ethernet and is controlled by tailor-made software developed using LabView. A Graphical User Interface (GUI) accepts user defined parameter details such as start and stop frequency, number of sweeps and resolution bandwidth, and allows the USRP to collect PSD data in real-time, which is subsequently logged for post-processing. Owing to the Gigabit Ethernet connection, the I/Q real-time data is processed with a sampling rate

of up to 25 MSamples/s. This sampling rate corresponds to a real-time bandwidth of 20 MHz. Therefore, in order to sweep more than 20 MHz spectrum, a bandwidth aggregation technique is used. This technique allows the SDR to sense spectrum wider than 20 MHz by sensing chunks of 20 MHz, storing the corresponding I/Q data in a memory buffer and then perform the FFT to obtain the PSD of the entire bandwidth.

(a)

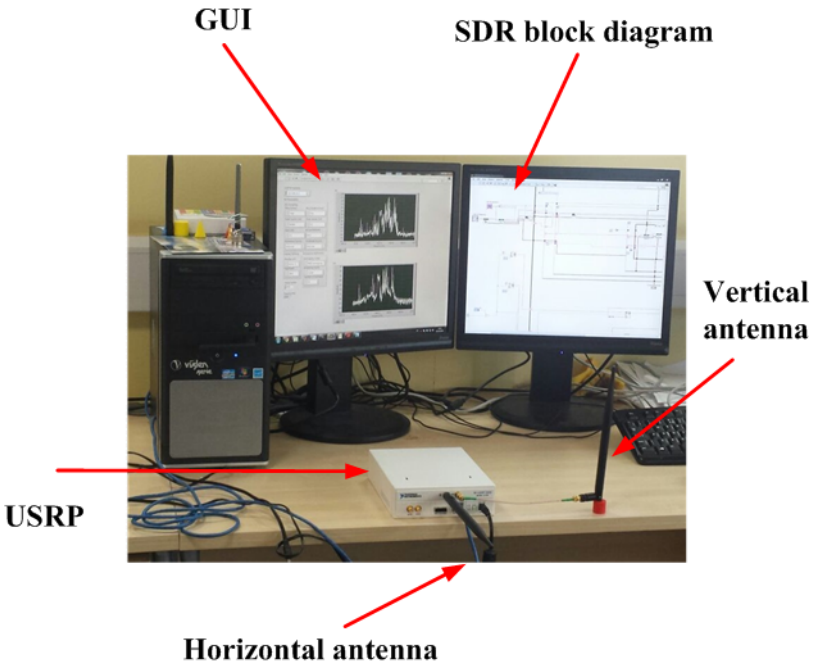

(b)

Figure 6.2: Measurement equipment a) block diagram; b) experimental set up.

The USRP platform was set to operate as an RMS detector with a resolution bandwidth of 200 kHz. The resolution bandwidth is equal to the channel bandwidth of GSM and the RMS detector has been chosen to obtain the average received signal power. In order to capture the polarisation diversity of the channel and avoid coupling between the receiving antennas, a spacing of half a wavelength was used, i.e. 16 cm for GSM 900 and 8 cm for GSM 1800.

Table 6.1: USRP-2922 specifications.

Parameter	Value
Frequency range	400 MHz-4.4 GHz
Rx Gain Range	0 dB-31.4 dB
Noise figure	5-7 dB
Max input power	0 dBm
Max real-time bandwidth	20 MHz
Max I/Q sample rate	25 MSamples/s
ADC	2 channels, 100 MSamples/s, 14 bit

The measurement campaign took place in an indoor environment in an office space on the first floor of an urban building at the University of Bedfordshire campus in Luton, UK. In most studies the measurement equipment had been placed at the rooftop of high buildings resulting in high power reception from all the transmitters [139], [140]. In this study, however, the measurement location has been chosen to mimic a more realistic situation for mobile CR terminals operating in an indoor environment, which is akin to the operational scenarios considered in this thesis. This campaign monitors the spectrum activity on the 900 MHz-1000 MHz and 1800 MHz-1900 MHz frequency bands that include the GSM 900 and GSM 1800 DL bands over 24 hours during a normal working day. The temporal power variation in the GSM 900 over 24 hours in the vertical and horizontal polarisation is shown in Figures 6.3a and 6.3b, respectively. Similarly, Figures 6.4a and 6.4b show the temporal power variation in the GSM 1800 band in both polarisations. With reference to Figure 6.4 and 6.5, it can be seen that the occupancy patterns on the different polarisations exhibit distinctive differences. A detailed analysis on the effects of polarisation on the channel occupancy is presented in the following section.

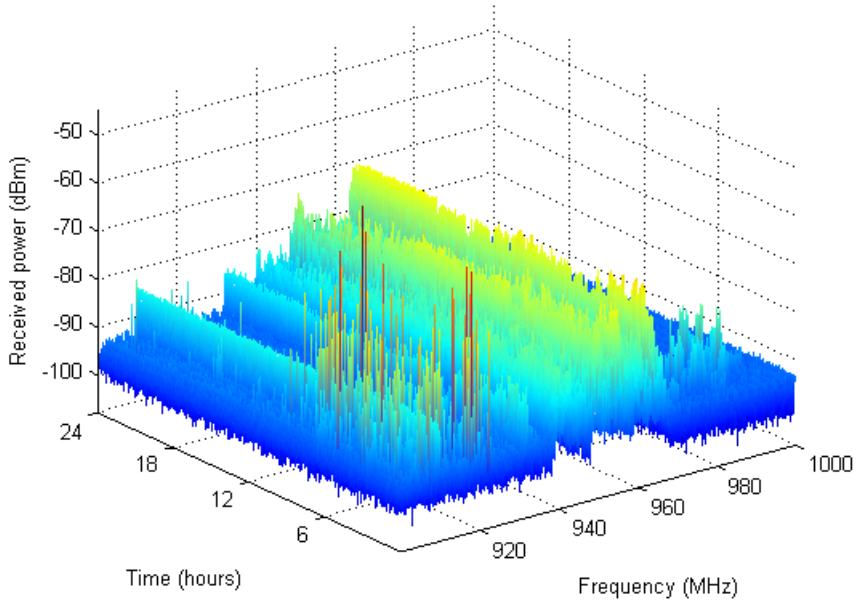

(a)

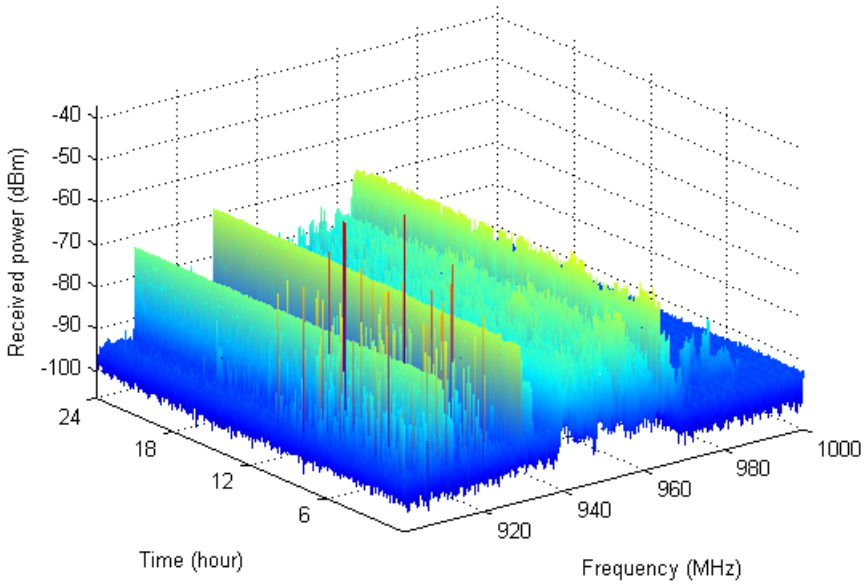

(b)

Figure 6.3: Temporal power variation in the GSM 900 frequency band on the: a) vertical polarisation; b) horizontal polarisation.

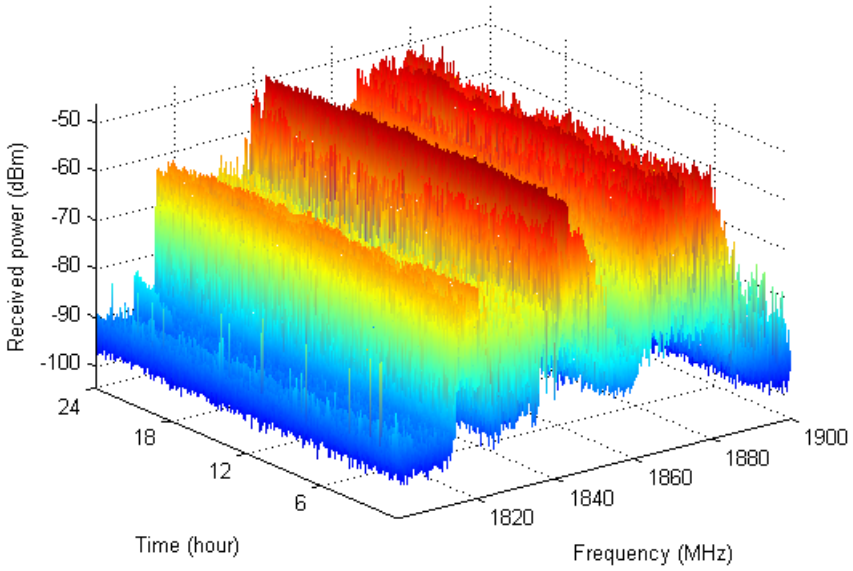

(a)

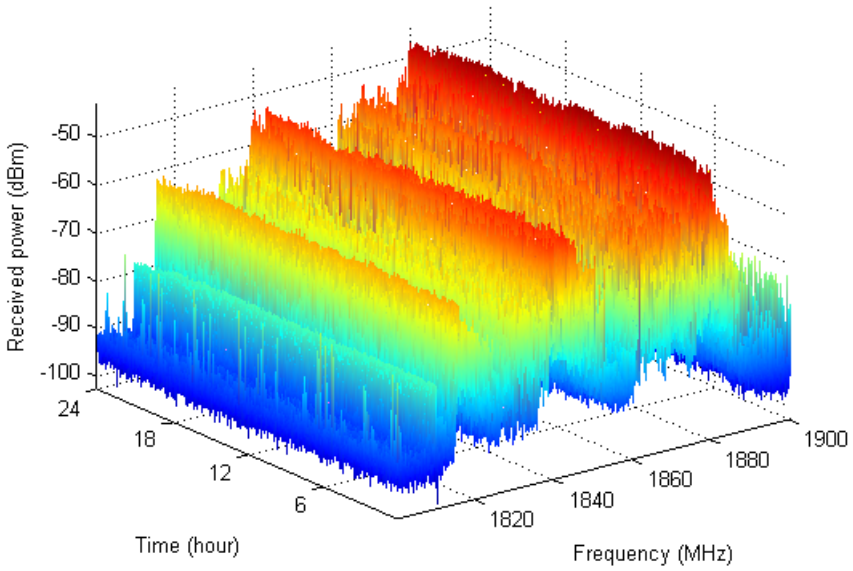

(b)

Figure 6.4: Temporal power variation in the GSM 1800 frequency band on the: a) vertical polarisation; b) horizontal polarisation.

6.4.1 Data post-processing

In order to develop and evaluate the proposed channel availability model, the obtained PSD data has been converted into binary occupancy data by applying a detection threshold, λ. The detection threshold is determined following the same procedure as described in Chapter 5. Thus, according to [133] for ED-based spectrum sensing the detection threshold is obtained by,

$$\lambda = Q^{-1}(P_{fa})\sigma_N, \tag{6.3}$$

where Q^{-1} and σ_N denote the inverse Q function and the equipment's noise variance, respectively.

The system's noise statistics have experimentally been obtained by replacing the antennas with a 50 Ω match load. Hence, from expression 6.3 and for a target $P_{fa} = 0.1$, as indicated by the IEEE 802.22 CR standard, and $\sigma_N = 2.2$ dB the detection threshold was set 5 dB above the equipment's noise floor of -100 dB. Hence, the detection threshold has been set to -95 dBm.

By applying the detection threshold to the captured PSD data, two different data-sets were created as shown in Figure 6.5:

1. received data for the vertical polarisation
2. received data for the horizontal polarisation.

The idleness probability, $p_{idleness}$, can now be obtained empirically by observing the channel availability ($S_i = 0$) of the i^{th} channel in both data-sets at the same time and averaging it over the duration of the measurement. In a similar way, the probability distribution of available channels in both polarisations was obtained.

V	Frequency channel *i*					
Time instant *t*	0	1	1	0	0	1
	1	0	0	1	1	1

H	Frequency channel *i*					
Time instant *t*	0	1	0	0	1	0
	0	0	0	1	1	1
	1	1	0	0	0	0
	1	0	0	0	1	0
	1	0	1	0	1	0
	0	1	1	1	1	1

Figure 6.5: Channel occupancy data-sets.

6.5 Effects of Polarisation

By observing the difference between the received power in the horizontal and vertical receiving branch $|P_{i,t_{horizontal}} - P_{i,t_{vertical}}|$, the effects of polarisation in the received signal can be evaluated. Figure 6.6 describes the difference between the received power in the horizontal and vertical receiving branch as a function of time and frequency. With reference to the obtained results a mean difference of 26 dB and 14 dB was observed in the GSM 900 and GSM 1800, respectively. This difference is clearly larger than the XPD of 8 dB and can be explained by the propagation environment and polarisation mismatch between the primary and secondary system. In turn, a difference of this order can significantly affect the sensing result between the vertical and horizontal branch.

Figure 6.7 presents two different spectrum sensing scenarios in terms of the noise and signal distribution in the vertical and horizontal polarisation. In the first scenario (Figure 6.7a), the received signal in both polarisations is above the detection and thus the sensed channel is perceived as occupied. On the other hand, in the second scenario (Figure 6.7b) the sensed channel is perceived as unoccupied in the horizontal polarisation whereas in the vertical polarisation is perceived as occupied.

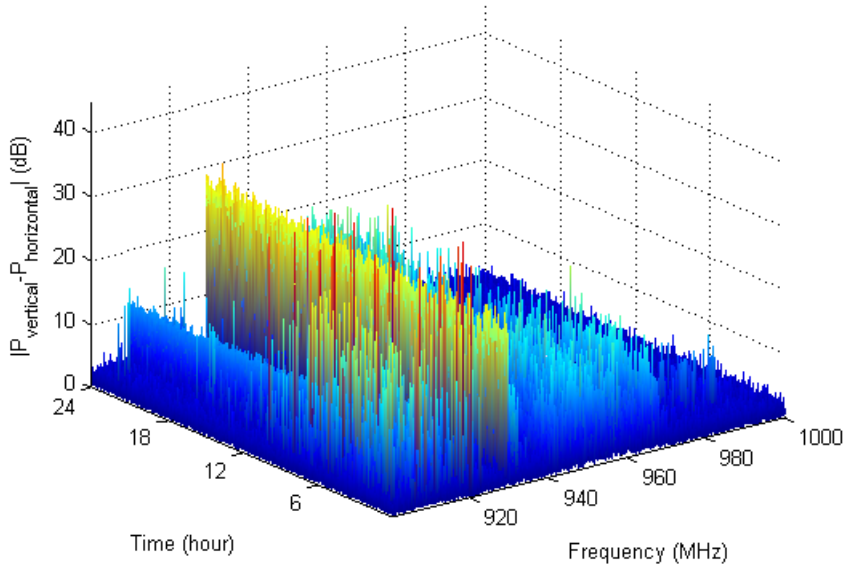

(a)

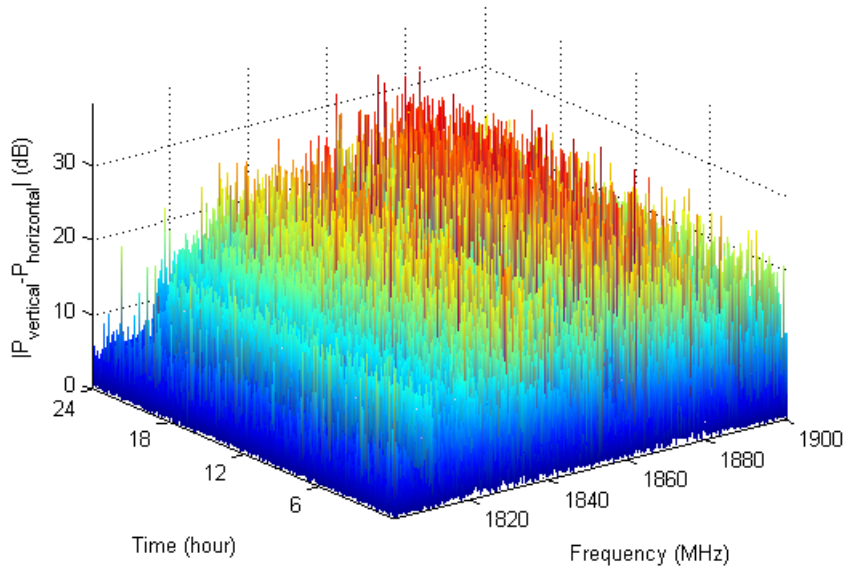

(b)

Figure 6.6: Difference in the received power between a vertically and horizontally polarised antenna in the: a) GSM 900 frequency band; b) GSM 1800 frequency band.

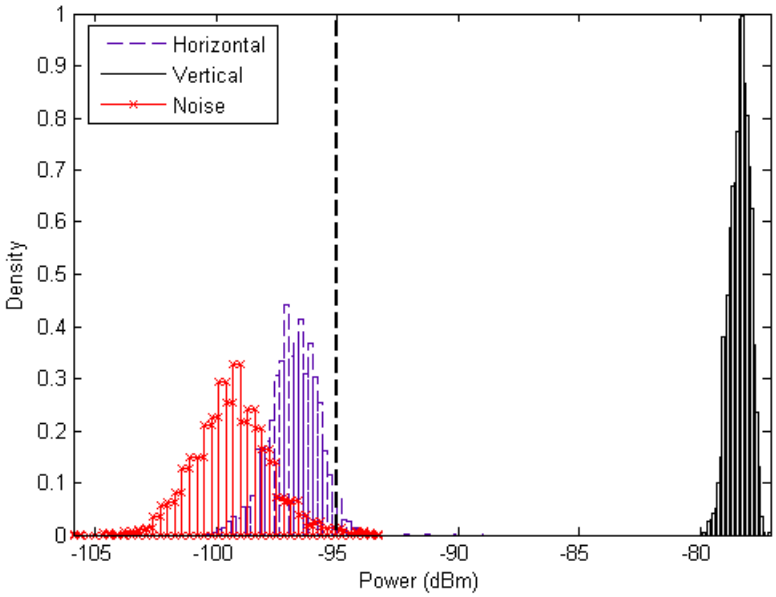

(a)

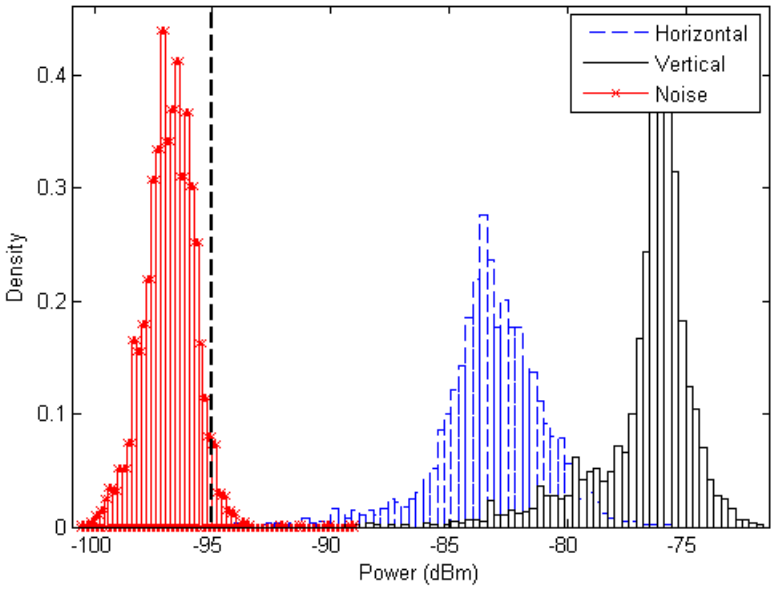

(b)

Figure 6.7: Distribution of the noise and the received signal in the vertical and horizontal polarisation for a) Scenario 1; b) Scenario 2.

Table 6.2 summarises the channel availability in the vertical and horizontal polarisation separately as well as on both polarisations at the same time. More specifically, it can be seen that there is up to 13% more channel availability in the vertical polarisation with an up to 70% difference when compared to both polarisations. This means that although the mean channel availability is not significantly different between the two polarisations there is a difference between the channels that are available at a given time instant.

Indicatively, Figure 6.8 depicts the received signal strength in each polarisation for four different channels over 20 continuous sensing slots (the black line represents the detection threshold). Therefore, it can be observed that the difference in the received signal's amplitude between different polarisations can be significant enough to affect the sensing output, resulting into up to 47% difference in the overall perceived channel availability.

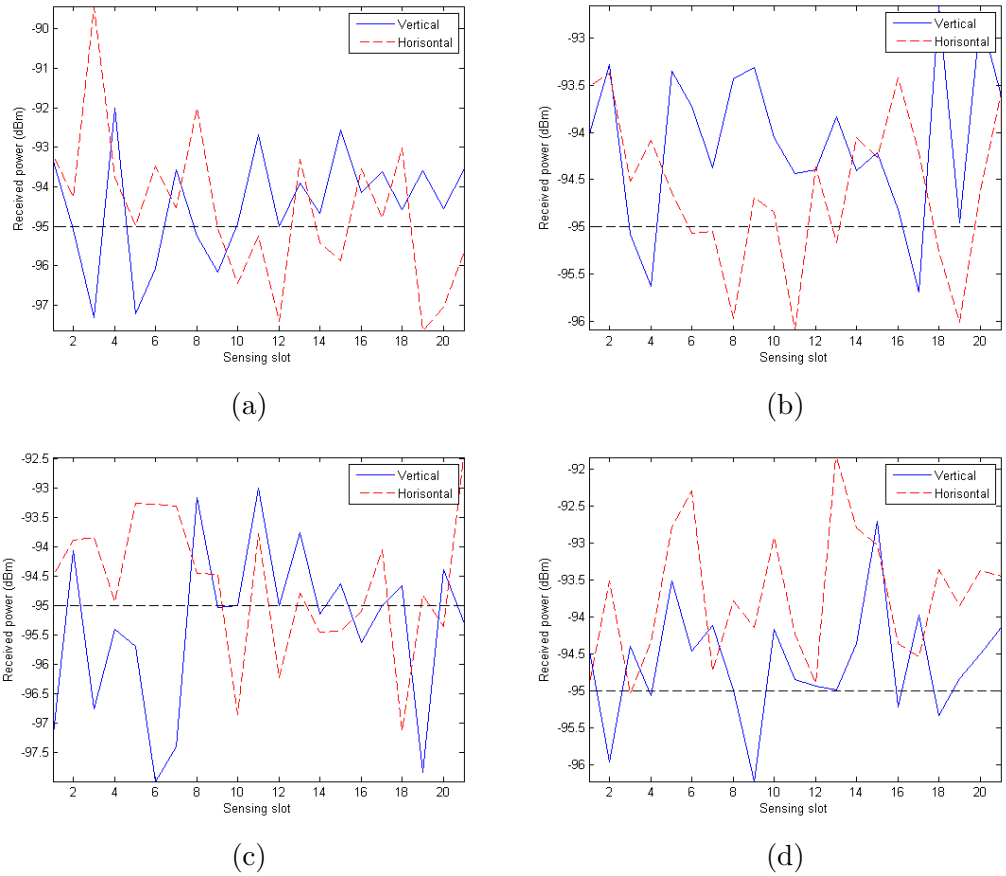

Figure 6.8: Time domain plots of the received PU signal by the SU in both the vertical and horizontal polarisation.

Table 6.2: Channel availability.

Parameter	GSM 900	GSM 1800
Vertical	280	170
Horizontal	255	150
$Vertical \wedge Horizontal$	236	100

6.6 Channel Availability Model

Let $\{x_1, x_2, ...x_N\}$ represent random variables of the PU system's channel occupancy status where $x_i = 1$ if the i^{th} channel is occupied by a PU and $x_i = 0$ if it is idle, with $i = 1, 2, ...N$ representing the channel index of a spectrum of N number of channels. In order to determine the channel availability a discrete random variable N_{free} that represents the total number of idle channels in both polarisations is also defined.

The CLT provides a well established baseline approach for approximating the limiting distribution of a sequence of variables [141]. Hence, let $\bar{N}_{free}$ and σ_N denote the mean and variance of the available channels in both polarisations at the same time, the probability of having k available channels in both polarisations can be approximated by a Gaussian distribution as,

$$P(N_{free} = k) \approx \frac{1}{\sqrt{2\pi\sigma_N}} e^{-\left(\frac{(x-\bar{N}_{free})^2}{2\sigma_N}\right)}, \tag{6.4}$$

where $k = 0, 1, ...N$.

Different statistical distributions that can reasonably represent the empirical distribution of N_{free} and $p_{idleness}$, including the Poisson, Binomial and Logistic distributions, were explored. The parameters of each distribution have been estimated by using the empirical data and by applying the maximum likelihood estimation (MLE) method. This method, selects a set of values as an estimate for which the observed sample is most likely to occur [142]. Based on the MLE method the Gaussian distribution was found to fit best to the observed data.

Having modelled the number of available channels as a Gaussian distribution, the channel idleness probability can also be approximated by a Gaussian distribution, which is expressed mathematically as,

$$P(S_{t,i_{vertical}} = 0, S_{t,i_{horizontal}} = 0) \approx \frac{1}{\sqrt{2\pi\sigma}} e^{-\left(\frac{(x-\mu)^2}{2\sigma}\right)}, \tag{6.5}$$

where μ is the mean and σ the standard deviation of the channel idleness probabilities.

Figures 6.9a and 6.9b show the empirical PDF plot of the available channels, $P(N_{free})$, for the GSM 900 DL and GSM 1800 DL frequency bands and its fit by the a Gaussian distribution. Similarly, Figures 6.10a and 6.10b show the empirical channel idleness probability distribution over its Gaussian approximation for the same frequency bands. Both figures indicate that there is a good agreement between the Gaussian Normal PDF and the empirical data that is confirmed by the Chi-squared goodness of fit validation test as presented in the following subsection.

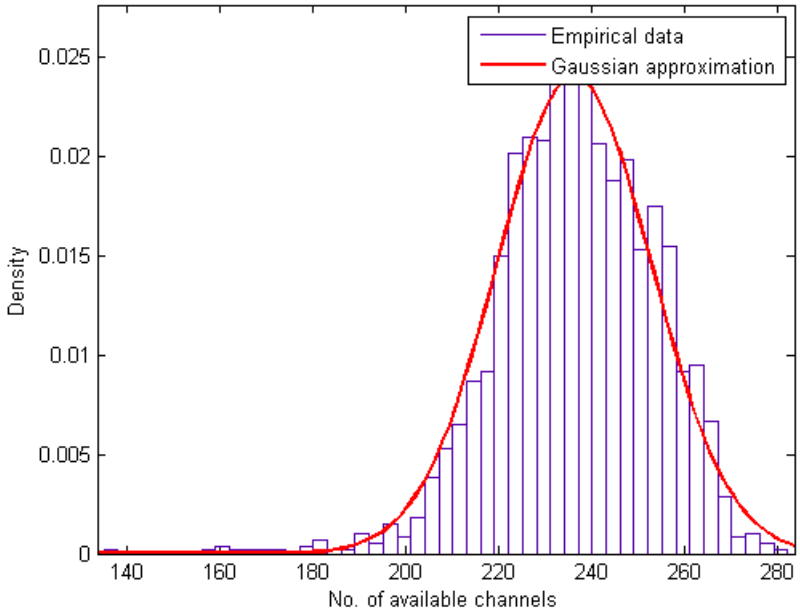

(a)

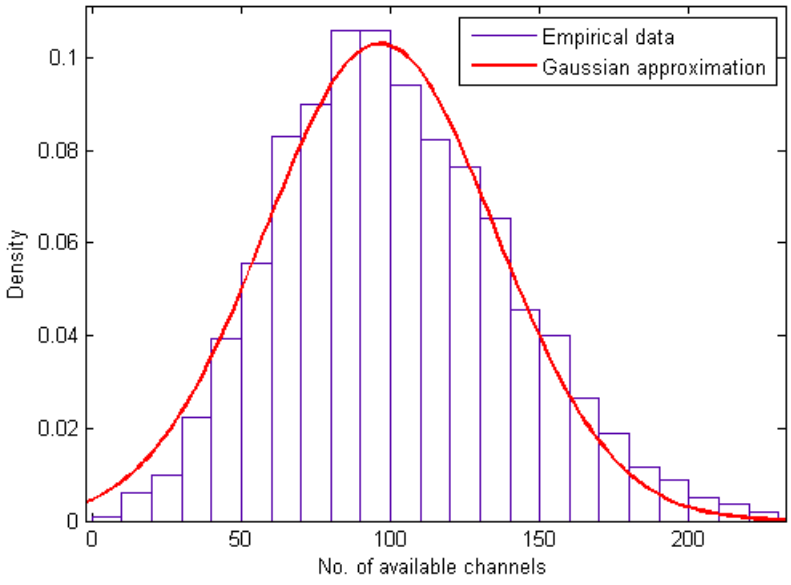

(b)

Figure 6.9: Normal approximation of number of available channels distribution over measured data for: a) GSM 900 DL; b) GSM 1800 DL.

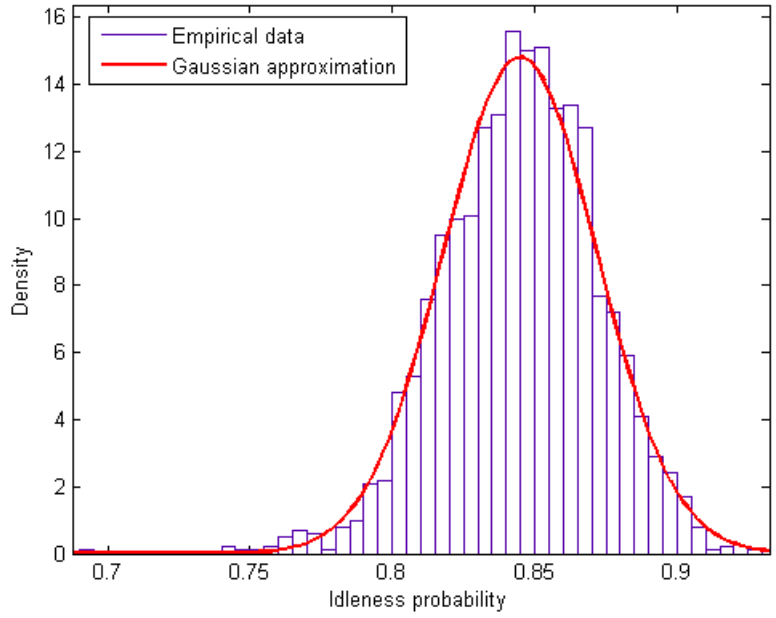

(a)

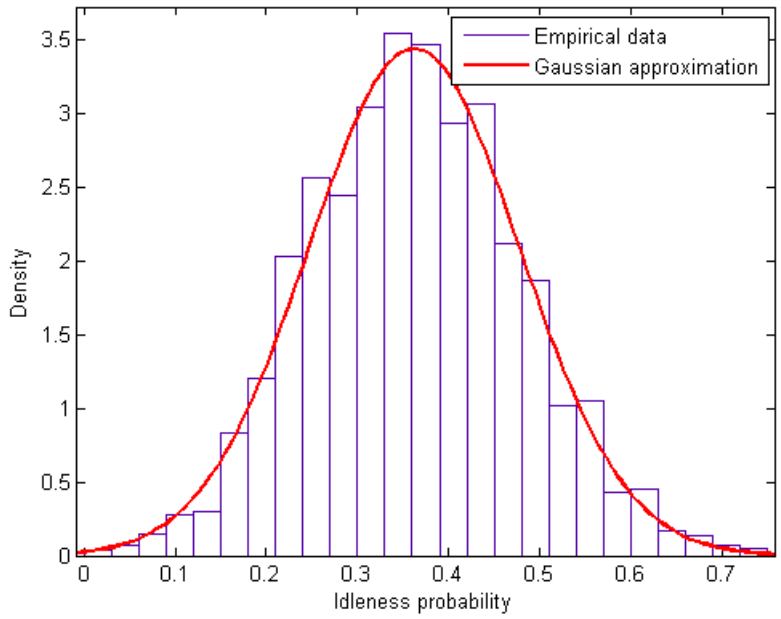

(b)

Figure 6.10: Normal approximation of number of available channels distribution over measured data for: a) GSM 900 DL; b) GSM 1800 DL.

6.6.1 Model Validation

Let y_i denote the empirically calculated probability values, known as the observed data, and $\bar{y_i}$ the expected probability values as obtained by the Gaussian model for the i^{th} frequency channel. The Chi-squared statistic, χ^2, is defined as the weighted difference between the observed and expected data [141]. Formally,

$$\chi^2 = \sum_{i=1}^{N} \frac{(y_i - \bar{y_i}^2)}{\bar{y_i}}. \tag{6.6}$$

Table 6.3 presents the estimated parameters μ and σ for the Gaussian approximation and the corresponding Chi-square goodness-of-fit validation test value. Given that the 5% critical value of χ^2 for a distribution with two degrees of freedom is 5.99 [129], both metrics of the channel idleness probability and channel availability can be modelled by a Gaussian distribution with 95% confidence bounds. Such confidence bounds in turn, suggest that the proposed model can estimate the channel availability with up to 95% accuracy which is inline with the IEEE 802.22 CR standard's requirements of identifying available channels with 90% accuracy.

Table 6.3: Gaussian approximation parameters.

Band	Parameter	μ	σ	χ^2
GSM 900	N_{free}	231	15.7	5.28
GSM 900	$p_{idleness}$	0.82	0.02	5.04
GSM 1800	N_{free}	96	3.87	4.83
GSM 1800	$p_{idleness}$	0.36	0.11	4.99

6.7 Summary

Accurate channel occupancy models are required in order to optimise the overall performance of CR networks. In this chapter a novel channel availability model for mobile CR terminals for the polarisation domain has been introduced. The channel availability has been described in terms of two different probabilistic metrics, the number of available channels and the idleness probability in both the vertical and horizontal polarisation at the same time. The proposed model has been validated using real-time measurements within realistic operational scenarios. Based on the obtained results it has been verified that the perceived channel occupancy by a CR terminal can be significantly different between different polarisations. To this end, the channel availability is approximated by a Gaussian distribution. Such a probabilistic availability model can assist in the optimisation of mobile CR terminals that change their orientation and can lead to performance improvement in terms of energy and spectrum efficiency.

Chapter 7

Conclusion and Further Work

7.1 Summary

As technology evolves, new wireless communication paradigms emerge, with new requirements and operational environments compared to traditional wireless systems. In this thesis the spectrum sensing process as a realisation of CR technology within M2M communication systems has been investigated. Initially, the problem of spectrum sensing over severe fading conditions that are expected to occur in the operational environments of wireless M2M communication systems has been addressed in order to study the feasibility of CR-based M2M systems. Furthermore, the use of statistical knowledge on channel occupancy as a means of "smart" sensing for minimising the time and energy cost of M2M cognitive nodes is investigated.

In Chapter 2 the concept of CR technology has been described and visions on future application of CR technology in the field of M2M systems and the IoT have been presented. With spectrum sensing being the focus of this work, the challenges regarding the operational environment and design requirements of M2M nodes are discussed. Amongst other theoretical notions, state-of-the-art spectrum sensing methods have been summarised. Furthermore, in this chapter the reader is being introduced to the concept of spectrum occupancy through a description of different prediction models and their applicability in CR.

In Chapter 3, simple yet accurate closed form expressions for the average probability of detection for ED-based spectrum sensing over TWDP fading channels have been derived and verified. These expressions facilitate the per-

formance evaluation of different ED-based spectrum sensing schemes for a variety of fading scenarios that include the well-known Rayleigh and Rician fading channels as well as a worse than Rayleigh fading channel which is characteristic of M2M nodes operating in confined environments. The obtained results provide a comprehensive performance analysis and identify the limits of ED-based spectrum sensing for emerging CR systems that are expected to operate in non conventional environments that cannot be adequately characterised by the traditional fading models. More specifically, the performance of ED-based spectrum sensing has been found to significantly degrade compared to Rician fading with the SNR requirements to increase by 137%. Hence, an ED-based CR system cannot meet the requirements and operate efficiently under such conditions. Therefore, appropriate mitigation techniques need to be applied in order for ED-based spectrum sensing to achieve the sensing requirements when operating in such environments. To this end, the performance improvement due to diversity reception and cooperative detection are investigated and are found to improve the sensing performance in terms of SNR requirements by up to 18 dB when cooperation is employed, whereas for diversity reception the overall detection improves by up to 95%. In addition to different sensing schemes an optimal threshold technique is proposed. The proposed technique dynamically adjusts the detection threshold subject to a minimum total detection error which allows to minimise both P_{fa} and P_{md}. The performance of ED-based spectrum sensing, and hence, spectrum efficiency has been found to be affected by TWDP fading at a higher extent than Rayleigh fading which is considered as the worst case fading. However, by applying different techniques as proposed, ED-based spectrum sensing can meet the requirements of CR standards for efficient spectrum usage.

In Chapter 4 the perceived spectrum occupancy in the temporal domain has been formulated as an HMM. The PU transmission patterns are modelled as a 2-state Markov chain, whereas the sensing output is described as a binary random variable being observed through a Gaussian channel. The HMM is used to estimate and predict the PU channel occupancy states at future time

instants based on a history of past sensing outputs.

By incorporating spectrum occupancy prediction to ED-based spectrum sensing, in Chapter 5 a "smart" sensing multi-channel scheme has been proposed as a means of reducing the sensing time of CR systems. The performance of the proposed spectrum sensing approach is evaluated using both real spectrum measurement data and simulated data obtained by the spectrum activity measurements. With reference to the obtained results, the HMM-based approach was found to accurately estimate the occupancy parameters and outperform other prediction methods, particularly in scenarios with less correlated occupancy statistics as well as in low SNR regions. Furthermore, by using longer observation history the prediction performance of the proposed approach was found to improve for multiple step ahead predictions. In addition, the proposed sensing method leads to up to 84% reduction of the sensing cost expressed by the sensing time and energy consumption when compared to conventional ED-based spectrum sensing. As a result, by using appropriate history length and prediction span in order to optimise the prediction performance with respect to complexity, the proposed scheme can significantly reduce the energy consumption of energy-constrained CR terminals.

The effects of polarisation in the perceived channel occupancy are investigated in Chapter 6. With reference to the obtained results it can be verified that the perceived channel occupancy by a CR terminal can vary significantly between different polarisations. Such differences in the sensing results between the vertical and horizontal polarisation can affect sensing performance akin to the hidden PU problem by increasing the P_{fa} and P_d. Therefore, accurate channel availability modelling for the polarisation domain is required. To this end, this work proposes a statistical framework for modelling the available channles in both polarisations at the same time. The proposed model characterises the channel availability in terms of two different probabilistic metrics, the number of available channels and the idleness probability in both the vertical and horizontal polarisation at the same time and is validated using real-time measurements within realistic operational scenarios.

7.2 Conclusions

The key conclusions for the research presented in this study can be summarised as follows:

- Under hyper-Rayleigh fading conditions single user spectrum sensing cannot achieve the required sensing performance that ensures efficient spectrum access without interfering to the primary system for cognitive M2M systems.

- Cooperative spectrum sensing with up to 6 cooperative SUs can improve the sensing performance by up to 45% and reduce the SNR requirements by up to 11.5 dB within environments that exhibit worse than Rayleigh fading conditions.

- Under the same fading conditions, diversity reception with up to Cooperative spectrum sensing with up to 5 diversity branches can improve the sensing performance by up to 38%.

- Threshold optimisation for ED-based spectrum sensing can significantly improve the sensing performance by achieving an up to 13 dB SNR gain.

- Temporal spectrum occupancy can be efficiently modelled and estimated in terms of transmission probabilities using a 2-state HMM.

- HMM-based spectrum occupancy prediction outperforms state-of-the-art prediction methods and can achieve up to 93% and 8% prediction accuracy in terms of TPR and FPR, respectively. Such values suggest that prediction can infer the channel occupancy with comparable performance of detection.

- Predictive spectrum sensing can significantly reduce the sensing cost in terms of sensing energy and time by up to 84% based on the occupancy statistics of the primary frequency band of interest.

- Signal polarisation can affect the sensing output. To this end, channel availability on the polarisation domain can be modelled as a Gaussian approximation with 95% confidence bounds.

7.3 Limitations

Throughout this thesis ED is considered owing to its low implementation complexity and computational needs. However, the assumption of using ED is that the noise variance may always be accurately estimated which is not always achievable in practice. The noise uncertainty is expected to degrade the system's performance even for cooperative or diversity reception spectrum sensing strategies. In addition, in order to provide closed form solutions for the integrals regarding the average probability of detection over TWDP fading channels, a time-bandwidth product $u = 1$ is assumed. Therefore, the obtained expressions are limited for the case of $u = 1$. They give however an insight into the performance over worse than Rayleigh fading conditions when compared to benchmark results for the same time bandwidth parameters. This limitation can be overcome by using the Moment Generation Function (MGF) of the TWPD fading model to obtain analytical expressions for the average probability of detection over TWDP for different time-bandwidth values. However, owing to the integrals under evaluation including the MGF, the obtained expressions would be in the form of a series expansions rather than in a closed form. Furthermore, spectrum sensing is considered as a binary decision problem and hence the prediction performance as well as the channel availability model depend on the detection threshold. In addition, PU activity is modelled as a two-state discrete time first order Markov chain in order to ensure minimal complexity. However, by considering higher order HMMs may capture a more complete description of the temporal correlation.

7.4 Further Work

Although this thesis has offered some new insights on cognitive M2M systems and on spectrum sensing in particular, there is still a number of open problems that need to be solved to enable the development of fully cognitive M2M communication systems. Owing to the cognitive nature of such systems, integration and convergence among different wireless communication systems is expected. Therefore, standardisation and regularisation is an important aspect for future M2M systems. In addition, accurate traffic characterisation of M2M networks is fundamental to the design and optimisation of such infrastructures. Furthermore, although the proposed predictive spectrum sensing scheme enables energy efficiency for CR M2M nodes, by reducing the sensing cost, current SDR solutions have processing requirements, which may delay the operation of such a scheme. However, as CR is an emerging technology, it is expected that future SDR platforms will be optimised and this issue will be resolved. Based on the presented findings this work can be further extended by considering the following research directions for future work:

- Investigate the performance of ED-based spectrum sensing over composite fading i.e. multipath and shadowing. In addition, for a comprehensive analysis on the performance of diversity reception different diversity schemes such as Maximal Ratio Combining (MRC), Equal Gain Combining (EGC) should be considered.

- Modify the HMM-based spectrum occupancy prediction scheme to include more than 2 states such as the possibility of a channel to be at a "fuzzy" state (SU is undetermined whether the channel is occupied or unoccupied).

- Extend the proposed predictive spectrum sensing scheme to account for cooperative prediction where predictions from multiple SUs will be combined into improving the overall performance.

- Use the proposed spectrum occupancy prediction scheme for predicting the activity of other SUs as a means of efficient spectrum sharing.
- Investigate the optimal length of history for accurate and efficient multi-step ahead predictions.
- The use of the derived channel availability model to identify the probability of an adjacent channel to be unoccupied in a different polarisation could be exploited for polarisation diversity.
- The proposed model can be further extended to account for tri-polar antennas for CR systems with additional degrees of freedom as a means of improving spectrum sensing and hence spectrum efficiency.

References

[1] G. Staple and K. Werbach, "The end of spectrum scarcity [spectrum allocation and utilization]," *Spectrum, IEEE*, vol. 41, no. 3, pp. 48–52, March 2004.

[2] *The UK Frequency Allocations*, 2007, [Online]. Available: http://www.roke.co.uk/resources/datasheets/uk-frequency-allocations.pdf, (accessed October 31, 2014).

[3] M. A. McHenry, "NSF spectrum occupancy measurements project summary," Shared spectrum company, Tech. Report, August 2005.

[4] "Spectrum policy task force report (ed docket no. 02-135)," Federal Communications Commission, Tech. Report, 2002.

[5] "Cisco visual networking index: Global mobile data traffic forecast update, 2013 - 2018," February 2014, White Paper.

[6] B. Hochwald and S. Ten Brink, "Achieving near-capacity on a multiple-antenna channel," *Communications, IEEE Transactions on*, vol. 51, no. 3, pp. 389–399, March 2003.

[7] C. Y. Wong, R. Cheng, K. Lataief, and R. Murch, "Multiuser ofdm with adaptive subcarrier, bit, and power allocation," *Selected Areas in Communications, IEEE Journal on*, vol. 17, no. 10, pp. 1747–1758, Oct 1999.

[8] I. F. Akyildiz, W.-Y. Lee, M. C. Vuran, and S. Mohanty, "Next generation/dynamic spectrum access/cognitive radio wireless networks:

A survey," *Comput. Netw.*, vol. 50, no. 13, pp. 2127–2159, Sep. 2006. [Online]. Available: http://dx.doi.org/10.1016/j.comnet.2006.05.001

[9] J. Mitola and J. Maguire, G.Q., "Cognitive radio: making software radios more personal," *Personal Communications, IEEE*, vol. 6, no. 4, pp. 13–18, Aug 1999.

[10] H.-K. Lee, D. M. Kim, Y. Hwang, S. M. Yu, and S.-L. Kim, "Feasibility of cognitive machine-to-machine communication using cellular bands," *Wireless Communications, IEEE*, vol. 20, no. 2, pp. 97–103, April 2013.

[11] S. Haykin, "Cognitive radio: brain-empowered wireless communications," *Selected Areas in Communications, IEEE Journal on*, vol. 23, no. 2, pp. 201–220, Feb 2005.

[12] L. Berlemann and S. Mangold, *Cognitive Radio and Dynamic Spectrum Access*. Wiley, 2009. [Online]. Available: http://books.google.co.uk/books?id=XUGN9tKTIiYC

[13] C. Stevenson, G. Chouinard, Z. Lei, W. Hu, S. Shellhammer, and W. Caldwell, "IEEE 802.22: The first cognitive radio wireless regional area network standard," *Communications Magazine, IEEE*, vol. 47, no. 1, pp. 130–138, January 2009.

[14] J. Wang, M. Ghosh, and K. Challapali, "Emerging cognitive radio applications: A survey," *Communications Magazine, IEEE*, vol. 49, no. 3, pp. 74–81, March 2011.

[15] V. Chandrasekhar, J. Andrews, and A. Gatherer, "Femtocell networks: a survey," *Communications Magazine, IEEE*, vol. 46, no. 9, pp. 59–67, September 2008.

[16] G. Gur, S. Bayhan, and F. Alagoz, "Cognitive femtocell networks: an overlay architecture for localized dynamic spectrum access [dynamic spectrum management]," *Wireless Communications, IEEE*, vol. 17, no. 4, pp. 62–70, August 2010.

[17] T. Doumi, "Spectrum considerations for public safety in the united states," *Communications Magazine, IEEE*, vol. 44, no. 1, pp. 30–37, Jan 2006.

[18] E. Hossain and V. K. Bhargava, *Cognitive wireless communication networks*. Springer, 2007.

[19] S. Whitehead, "Adopting wireless machine-to-machine technology," *Computing Control Engineering Journal*, vol. 15, no. 5, pp. 40–46, Oct 2004.

[20] E. Tragos and V. Angelakis, "Cognitive radio inspired m2m communications," in *Wireless Personal Multimedia Communications (WPMC), 2013 16th International Symposium on*, June 2013, pp. 1–5.

[21] K. Chang, A. Soong, M. Tseng, and Z. Xiang, "Global wireless machine-to-machine standardization," *Internet Computing, IEEE*, vol. 15, no. 2, pp. 64–69, March 2011.

[22] W. Webb, *Understanding Weightless: Technology, Equipment, and Network Deployment for M2M Communications in White Space*. Cambridge University Press, 2012.

[23] Y. Zhang, R. Yu, M. Nekovee, Y. Liu, S. Xie, and S. Gjessing, "Cognitive machine-to-machine communications: visions and potentials for the smart grid," *Network, IEEE*, vol. 26, no. 3, pp. 6–13, May 2012.

[24] H. Karimi, "Geolocation databases for white space devices in the uhf tv bands: Specification of maximum permitted emission levels," in *New Frontiers in Dynamic Spectrum Access Networks (DySPAN), 2011 IEEE Symposium on*, May 2011, pp. 443–454.

[25] M. Nekovee, T. Irnich, and J. Karlsson, "Worldwide trends in regulation of secondary access to white spaces using cognitive radio," *Wireless Communications, IEEE*, vol. 19, no. 4, pp. 32–40, August 2012.

[26] H. Urkowitz, "Energy detection of unknown deterministic signals," *Proceedings of the IEEE*, vol. 55, no. 4, pp. 523–531, April 1967.

[27] D. Cabric, S. Mishra, and R. Brodersen, "Implementation issues in spectrum sensing for cognitive radios," in *Signals, Systems and Computers, 2004. Conference Record of the Thirty-Eighth Asilomar Conference on*, vol. 1, Nov 2004, pp. 772–776 Vol.1.

[28] A. Dandawate and G. Giannakis, "Statistical tests for presence of cyclostationarity," *Signal Processing, IEEE Transactions on*, vol. 42, no. 9, pp. 2355–2369, Sep 1994.

[29] S. Mishra, A. Sahai, and R. Brodersen, "Cooperative sensing among cognitive radios," in *Communications, 2006. ICC '06. IEEE International Conference on*, vol. 4, June 2006, pp. 1658–1663.

[30] J. Ma, G. Li, and B.-H. Juang, "Signal processing in cognitive radio," *Proceedings of the IEEE*, vol. 97, no. 5, pp. 805–823, May 2009.

[31] S. M. Kay, *Fundamentals of statistical signal processing: detection theory.* Prentice-hall, 1998.

[32] T. Yucek and H. Arslan, "A survey of spectrum sensing algorithms for cognitive radio applications," *Communications Surveys Tutorials, IEEE*, vol. 11, no. 1, pp. 116–130, First 2009.

[33] J. Dong, S. Zhang, and X. Wu, "Cross-correlation processing based an energy detection algorithm for non-carrier uwb radar," in *Geoscience and Remote Sensing Symposium (IGARSS), 2013 IEEE International*, July 2013, pp. 1537–1540.

[34] A. Rabbachin, T. Quek, P. Pinto, I. Oppermann, and M. Win, "Uwb energy detection in the presence of multiple narrowband interferers," in *Ultra-Wideband, 2007. ICUWB 2007. IEEE International Conference on*, Sept 2007, pp. 857–862.

[35] S. Haykin, D. Thomson, and J. Reed, "Spectrum sensing for cognitive radio," *Proceedings of the IEEE*, vol. 97, no. 5, pp. 849–877, May 2009.

[36] J. G. Proakis, "Digital communications," 1995.

[37] D. Cabric, A. Tkachenko, and R. Brodersen, "Spectrum sensing measurements of pilot, energy, and collaborative detection," in *Military Communications Conference, 2006. MILCOM 2006. IEEE*, Oct 2006, pp. 1–7.

[38] W. A. Gardner, A. Napolitano, and L. Paura, "Cyclostationarity: Half a century of research," *Signal processing*, vol. 86, no. 4, pp. 639–697, 2006.

[39] J. Lunden, V. Koivunen, A. Huttunen, and H. Poor, "Collaborative cyclostationary spectrum sensing for cognitive radio systems," *Signal Processing, IEEE Transactions on*, vol. 57, no. 11, pp. 4182–4195, Nov 2009.

[40] S. Chaudhari, V. Koivunen, and H. Poor, "Autocorrelation-based decentralized sequential detection of ofdm signals in cognitive radios," *Signal Processing, IEEE Transactions on*, vol. 57, no. 7, pp. 2690–2700, July 2009.

[41] S. Mishra, S. Ten Brink, R. Mahadevappa, and R. Brodersen, "Cognitive technology for ultra-wideband/wimax coexistence," in *New Frontiers in Dynamic Spectrum Access Networks, 2007. DySPAN 2007. 2nd IEEE International Symposium on*, April 2007, pp. 179–186.

[42] E. Axell and E. Larsson, "Optimal and sub-optimal spectrum sensing of ofdm signals in known and unknown noise variance," *Selected Areas in Communications, IEEE Journal on*, vol. 29, no. 2, pp. 290–304, February 2011.

[43] A. Tkachenko, D. Cabric, and R. Brodersen, "Cyclostationary feature detector experiments using reconfigurable bee2," in *New Frontiers in Dynamic Spectrum Access Networks, 2007. DySPAN 2007. 2nd IEEE International Symposium on*, April 2007, pp. 216–219.

[44] P. D. Sutton, J. Lotze, K. E. Nolan, and L. E. Doyle, "Cyclostationary signature detection in multipath rayleigh fading environments," in *Cognitive Radio Oriented Wireless Networks and Communications, 2007. CrownCom 2007. 2nd International Conference on*, Aug 2007, pp. 408–413.

[45] E. Axell and E. Larsson, "A unified framework for glrt-based spectrum sensing of signals with covariance matrices with known eigenvalue multiplicities," in *Acoustics, Speech and Signal Processing (ICASSP), 2011 IEEE International Conference on*, May 2011, pp. 2956–2959.

[46] R. Couillet and M. Debbah, "A bayesian framework for collaborative multi-source signal sensing," *Signal Processing, IEEE Transactions on*, vol. 58, no. 10, pp. 5186–5195, Oct 2010.

[47] Y. Zeng and Y.-C. Liang, "Spectrum-sensing algorithms for cognitive radio based on statistical covariances," *Vehicular Technology, IEEE Transactions on*, vol. 58, no. 4, pp. 1804–1815, May 2009.

[48] ——, "Eigenvalue-based spectrum sensing algorithms for cognitive radio," *Communications, IEEE Transactions on*, vol. 57, no. 6, pp. 1784–1793, June 2009.

[49] Z. Tian and G. Giannakis, "A wavelet approach to wideband spectrum sensing for cognitive radios," in *Cognitive Radio Oriented Wireless Networks and Communications, 2006. 1st International Conference on*, June 2006, pp. 1–5.

[50] D. Thomson, "Spectrum estimation and harmonic analysis," *Proceedings of the IEEE*, vol. 70, no. 9, pp. 1055–1096, Sept 1982.

[51] B. Farhang-Boroujeny, "Filter bank spectrum sensing for cognitive radios," *Signal Processing, IEEE Transactions on*, vol. 56, no. 5, pp. 1801–1811, May 2008.

[52] Z. Fanzi, C. Li, and Z. Tian, "Distributed compressive spectrum sensing in cooperative multihop cognitive networks," *Selected Topics in Signal Processing, IEEE Journal of*, vol. 5, no. 1, pp. 37–48, Feb 2011.

[53] C. Han, T. Harrold, S. Armour, I. Krikidis, S. Videv, P. M. Grant, H. Haas, J. Thompson, I. Ku, C.-X. Wang, T. A. Le, M. Nakhai, J. Zhang, and L. Hanzo, "Green radio: radio techniques to enable energy-efficient wireless networks," *Communications Magazine, IEEE*, vol. 49, no. 6, pp. 46–54, June 2011.

[54] Y. Pei, Y.-C. Liang, K. Teh, and K. H. Li, "Energy-efficient design of sequential channel sensing in cognitive radio networks: Optimal sensing strategy, power allocation, and sensing order," *Selected Areas in Communications, IEEE Journal on*, vol. 29, no. 8, pp. 1648–1659, September 2011.

[55] K. W. Choi, W. S. Jeon, and D. G. Jeong, "Sequential detection of cyclostationary signal for cognitive radio systems," *Wireless Communications, IEEE Transactions on*, vol. 8, no. 9, pp. 4480–4485, September 2009.

[56] Q. Zou, S. Zheng, and A. Sayed, "Cooperative sensing via sequential detection," *Signal Processing, IEEE Transactions on*, vol. 58, no. 12, pp. 6266–6283, Dec 2010.

[57] S. Appadwedula, V. Veeravalli, and D. Jones, "Decentralized detection with censoring sensors," *Signal Processing, IEEE Transactions on*, vol. 56, no. 4, pp. 1362–1373, April 2008.

[58] K. Yamasaki and T. Ohtsuki, "Design of energy-efficient wireless sensor networks with censoring, on-off, and censoring and on-off sensors based on mutual information," in *Vehicular Technology Conference, 2005. VTC 2005-Spring. 2005 IEEE 61st*, vol. 2, May 2005, pp. 1312–1316 Vol. 2.

[59] S. Maleki, A. Pandharipande, and G. Leus, "Energy-efficient distributed spectrum sensing for cognitive sensor networks," *Sensors Journal, IEEE*, vol. 11, no. 3, pp. 565–573, March 2011.

[60] C. Tekin, S. Hong, and W. Stark, "Enhancing cognitive radio dynamic spectrum sensing through adaptive learning," in *Military Communications Conference, 2009. MILCOM 2009. IEEE*, Oct 2009, pp. 1–7.

[61] E. Chatziantoniou, B. Allen, and V. Velisavljevic, "An hmm-based spectrum occupancy predictor for energy efficient cognitive radio," in *Personal Indoor and Mobile Radio Communications (PIMRC), 2013 IEEE 24th International Symposium on*, Sept 2013, pp. 601–605.

[62] S. Yarkan and H. Arslan, "Binary time series approach to spectrum prediction for cognitive radio," in *Vehicular Technology Conference, 2007. VTC-2007 Fall. 2007 IEEE 66th*, Sept 2007, pp. 1563–1567.

[63] Z. Wen, T. Luo, W. Xiang, S. Majhi, and Y. Ma, "Autoregressive spectrum hole prediction model for cognitive radio systems," in *Communications Workshops, 2008. ICC Workshops '08. IEEE International Conference on*, May 2008, pp. 154–157.

[64] M. Feder, N. Merhav, and M. Gutman, "Universal prediction of individual sequences," in *Electrical and Electronics Engineers in Israel, 1991. Proceedings., 17th Convention of*, Mar 1991, pp. 223–226.

[65] L. Rabiner, "A tutorial on hidden markov models and selected applications in speech recognition," *Proceedings of the IEEE*, vol. 77, no. 2, pp. 257–286, Feb 1989.

[66] Q.-J. Zhang, K. C. Gupta, and V. K. Devabhaktuni, "Artificial neural networks for rf and microwave design-from theory to practice," *Microwave Theory and Techniques, IEEE Transactions on*, vol. 51, no. 4, pp. 1339–1350, 2003.

[67] P. Werbos, "Backpropagation through time: what it does and how to do it," *Proceedings of the IEEE*, vol. 78, no. 10, pp. 1550–1560, Oct 1990.

[68] V. Tumuluru, P. Wang, and D. Niyato, "A neural network based spectrum prediction scheme for cognitive radio," in *Communications (ICC), 2010 IEEE International Conference on*, May 2010, pp. 1–5.

[69] G. E. P. Box and G. Jenkins, *Time Series Analysis, Forecasting and Control*. Holden-Day, Incorporated, 1990.

[70] P. J. Brockwell and R. A. Davis, *Time Series: Theory and Methods*. New York, NY, USA: Springer-Verlag New York, Inc., 1986.

[71] Z. Wang and S. Salous, "Time series arima model of spectrum occupancy for cognitive radio," in *Cognitive Radio and Software Defined Radios: Technologies and Techniques, 2008 IET Seminar on*, Sept 2008, pp. 1–4.

[72] ——, "Spectrum occupancy statistics and time series models for cognitive radio," *Journal of Signal Processing Systems*, vol. 62, no. 2, pp. 145–155, 2011. [Online]. Available: http://dx.doi.org/10.1007/s11265-009-0352-5

[73] Z. Lin, X. Jiang, L. Huang, and Y. Yao, "A energy prediction based spectrum sensing approach for cognitive radio networks," in *Wireless Communications, Networking and Mobile Computing, 2009. WiCom '09. 5th International Conference on*, Sept 2009, pp. 1–4.

[74] A. Molisch, L. Greenstein, and M. Shafi, "Propagation issues for cognitive radio," *Proceedings of the IEEE*, vol. 97, no. 5, pp. 787–804, May 2009.

[75] F. Digham, M.-S. Alouini, and M. K. Simon, "On the energy detection of unknown signals over fading channels," *Communications, IEEE Transactions on*, vol. 55, no. 1, pp. 21–24, Jan 2007.

[76] S. Herath and N. Rajatheva, "Analysis of equal gain combining in energy detection for cognitive radio over nakagami channels," in *Global Telecommunications Conference, 2008. IEEE GLOBECOM 2008. IEEE*, Nov 2008, pp. 1–5.

[77] S. Atapattu, C. Tellambura, and H. Jiang, "Performance of an energy detector over channels with both multipath fading and shadowing," *Wireless Communications, IEEE Transactions on*, vol. 9, no. 12, pp. 3662–3670, December 2010.

[78] P. Sofotasios, E. Rebeiz, L. Zhang, T. Tsiftsis, D. Cabric, and S. Freear, "Energy detection based spectrum sensing over κ-μ and κ-μ extreme fading channels," *Vehicular Technology, IEEE Transactions on*, vol. 62, no. 3, pp. 1031–1040, March 2013.

[79] O. Akan, O. Karli, and O. Ergul, "Cognitive radio sensor networks," *Network, IEEE*, vol. 23, no. 4, pp. 34–40, July 2009.

[80] J. Frolik, "On appropriate models for characterizing hyper-rayleigh fading," *Wireless Communications, IEEE Transactions on*, vol. 7, no. 12, pp. 5202–5207, December 2008.

[81] I. Sen, D. Matolak, and W. Xiong, "Wireless channels that exhibit "worse than rayleigh" fading: Analytical and measurement results," in *Military Communications Conference, 2006. MILCOM 2006. IEEE*, Oct 2006, pp. 1–7.

[82] D. Kim, M.-A. Ingram, and J. Smith, W.W., "Measurements of small-scale fading and path loss for long range rf tags," *Antennas and Propagation, IEEE Transactions on*, vol. 51, no. 8, pp. 1740–1749, Aug 2003.

[83] V. Sipal, J. Gelabert, B. Allen, C. Stevens, and D. Edwards, "Frequency-selective fading of ultrawideband wireless channels in confined environments," *Microwaves, Antennas Propagation, IET*, vol. 5, no. 11, pp. 1328–1335, August 2011.

[84] T. S. Rappaport *et al.*, *Wireless communications: principles and practice*. prentice hall PTR New Jersey, 1996, vol. 2.

[85] J. Frolik, "A case for considering hyper-rayleigh fading channels," *Wireless Communications, IEEE Transactions on*, vol. 6, no. 4, pp. 1235–1239, April 2007.

[86] M. K. Simon and M.-S. Alouini, *Digital communication over fading channels*. John Wiley & Sons, 2005, vol. 95.

[87] G. Durgin, T. Rappaport, and D. A. De Wolf, "New analytical models and probability density functions for fading in wireless communications," *Communications, IEEE Transactions on*, vol. 50, no. 6, pp. 1005–1015, Jun 2002.

[88] A. Coulson, A. Williamson, and R. Vaughan, "A statistical basis for lognormal shadowing effects in multipath fading channels," *Communications, IEEE Transactions on*, vol. 46, no. 4, pp. 494–502, Apr 1998.

[89] R. Subadar and A. Singh, "Performance of sc receiver over twdp fading channels," *Wireless Communications Letters, IEEE*, vol. 2, no. 3, pp. 267–270, June 2013.

[90] M. Abramowitz and I. A. Stegun, *Handbook of mathematical functions: with formulas, graphs, and mathematical tables*. Courier Dover Publications, 1972, no. 55.

[91] J. Marcum, "A statistical theory of target detection by pulsed radar," 1948.

[92] A. Nuttall, "Some integrals involving the q-function," Naval Underwater Systems Center (NUSC), Tech. Rep., 04 1972.

[93] A. Ghasemi and E. Sousa, "Impact of user collaboration on the performance of sensing-based opportunistic spectrum access," in *Vehicular Technology Conference, 2006. VTC-2006 Fall. 2006 IEEE 64th*, Sept 2006, pp. 1–6.

[94] D. Duan, L. Yang, and J. Principe, "Cooperative diversity of spectrum sensing for cognitive radio systems," *Signal Processing, IEEE Transactions on*, vol. 58, no. 6, pp. 3218–3227, June 2010.

[95] W. Zhang, R. Mallik, and K. Letaief, "Cooperative spectrum sensing optimization in cognitive radio networks," in *Communications, 2008. ICC '08. IEEE International Conference on*, May 2008, pp. 3411–3415.

[96] K. Letaief and W. Zhang, "Cooperative communications for cognitive radio networks," *Proceedings of the IEEE*, vol. 97, no. 5, pp. 878–893, May 2009.

[97] S. Herath, N. Rajatheva, and C. Tellambura, "Unified approach for energy detection of unknown deterministic signal in cognitive radio over fading channels," in *Communications Workshops, 2009. ICC Workshops 2009. IEEE International Conference on*, June 2009, pp. 1–5.

[98] E. Neasmith and N. Beaulieu, "New results on selection diversity," *Communications, IEEE Transactions on*, vol. 46, no. 5, pp. 695–704, May 1998.

[99] W. Zhang, R. Mallik, and K. Letaief, "Optimization of cooperative spectrum sensing with energy detection in cognitive radio networks," *Wireless Communications, IEEE Transactions on*, vol. 8, no. 12, pp. 5761–5766, December 2009.

[100] Y. Wang, C. Feng, C. Guo, and F. Liu, "Optimization of parameters for spectrum sensing in cognitive radios," in *Wireless Communications, Networking and Mobile Computing, 2009. WiCom '09. 5th International Conference on*, Sept 2009, pp. 1–4.

[101] C. Fitzhugh, J. Frolik, R. Ketcham, J. Covell, and T. Meyer, "Multipath fading in airframes at 2.4 ghz," in *Wireless and Microwave Technology, 2005. WAMICON 2005. The 2005 IEEE Annual Conference*, 2005, pp. 4 pp.–.

[102] S. Herath, N. Rajatheva, and C. Tellambura, "Energy detection of unknown signals in fading and diversity reception," *Communications, IEEE Transactions on*, vol. 59, no. 9, pp. 2443–2453, September 2011.

[103] M. Lopez-Benitez and F. Casadevall, "Signal uncertainty in spectrum sensing for cognitive radio," *Communications, IEEE Transactions on*, vol. 61, no. 4, pp. 1231–1241, April 2013.

[104] C. Ghosh, C. Cordeiro, D. Agrawal, and M. Rao, "Markov chain existence and hidden markov models in spectrum sensing," in *Pervasive Computing and Communications, 2009. PerCom 2009. IEEE International Conference on*, March 2009, pp. 1–6.

[105] I. Akbar and W. Tranter, "Dynamic spectrum allocation in cognitive radio using hidden markov models: Poisson distributed case," in *SoutheastCon, 2007. Proceedings. IEEE*, March 2007, pp. 196–201.

[106] Z. Chen, N. Guo, Z. Hu, and R. Qiu, "Experimental validation of channel state prediction considering delays in practical cognitive radio," *Vehicular Technology, IEEE Transactions on*, vol. 60, no. 4, pp. 1314–1325, May 2011.

[107] Z. Sun, G. Bradford, and J. Laneman, "Sequence detection algorithms for phy-layer sensing in dynamic spectrum access networks," *Selected Topics in Signal Processing, IEEE Journal of*, vol. 5, no. 1, pp. 97–109, Feb 2011.

[108] Y. Ephraim and N. Merhav, "Hidden markov processes," *Information Theory, IEEE Transactions on*, vol. 48, no. 6, pp. 1518–1569, Jun 2002.

[109] G. Grimmett and D. Stirzaker, *Probability and random processes*. Oxford Univ Press, 1992, vol. 2.

[110] A. J. Goldsmith and L. J. Greenstein, *Principles of Cognitive Radio*. Cambridge University Press, 2012.

[111] S. Geirhofer, L. Tong, and B. Sadler, "Cognitive radios for dynamic spectrum access - dynamic spectrum access in the time domain: Modeling and exploiting white space," *Communications Magazine, IEEE*, vol. 45, no. 5, pp. 66–72, May 2007.

[112] K. Haghighi, E. Strom, and E. Agrell, "On optimum causal cognitive spectrum reutilization strategy," *Selected Areas in Communications, IEEE Journal on*, vol. 30, no. 10, pp. 1911–1921, November 2012.

[113] T. Nguyeny, B. Mark, and Y. Ephraim, "Hidden markov process based dynamic spectrum access for cognitive radio," in *Information Sciences and Systems (CISS), 2011 45th Annual Conference on*, March 2011, pp. 1–6.

[114] L. E. Baum, J. Eagon *et al.*, "An inequality with applications to statistical estimation for probabilistic functions of markov processes and to a model for ecology," *Bull. Amer. Math. Soc*, vol. 73, no. 3, pp. 360–363, 1967.

[115] L. E. Baum and G. Sell, "Growth transformations for functions on manifolds," *Pacific Journal of Mathematics*, vol. 27, no. 2, pp. 211–227, 1968.

[116] H. Si, Y. Wang, J. Yuan, and X. Shan, "Mobility prediction in cellular network using hidden markov model," in *Consumer Communications and Networking Conference (CCNC), 2010 7th IEEE*, Jan 2010, pp. 1–5.

[117] J. Forney, G.D., "The viterbi algorithm," *Proceedings of the IEEE*, vol. 61, no. 3, pp. 268–278, March 1973.

[118] A. J. Viterbi, "Error bounds for convolutional codes and an asymptotically optimum decoding algorithm," *Information Theory, IEEE Transactions on*, vol. 13, no. 2, pp. 260–269, 1967.

[119] L. E. Baum and T. Petrie, "Statistical inference for probabilistic functions of finite state markov chains," *The annals of mathematical statistics*, pp. 1554–1563, 1966.

[120] L. E. Baum, T. Petrie, G. Soules, and N. Weiss, "A maximization technique occurring in the statistical analysis of probabilistic functions of markov chains," *The annals of mathematical statistics*, pp. 164–171, 1970.

[121] Q. Zhao and A. Swami, "A decision-theoretic framework for opportunistic spectrum access," *Wireless Communications, IEEE*, vol. 14, no. 4, pp. 14–20, August 2007.

[122] D. Datla, R. Rajbanshi, A. M. Wyglinski, and G. Minden, "Parametric adaptive spectrum sensing framework for dynamic spectrum access networks," in *New Frontiers in Dynamic Spectrum Access Networks, 2007. DySPAN 2007. 2nd IEEE International Symposium on*, April 2007, pp. 482–485.

[123] M. Wellens, J. Riihijarvi, and P. Mahonen, "Evaluation of adaptive mac-layer sensing in realistic spectrum occupancy scenarios," in *New Frontiers in Dynamic Spectrum, 2010 IEEE Symposium on*, April 2010, pp. 1–12.

[124] M. Wellens, A. de Baynast, and P. Mahonen, "Exploiting historical spectrum occupancy information for adaptive spectrum sensing," in *Wireless Communications and Networking Conference, 2008. WCNC 2008. IEEE*, March 2008, pp. 717–722.

[125] ——, "Performance of dynamic spectrum access based on spectrum occupancy statistics," *Communications, IET*, vol. 2, no. 6, pp. 772–782, July 2008.

[126] J. Davis and M. Goadrich, "The relationship between precision-recall

and roc curves," in *Proceedings of the 23rd international conference on Machine learning*. ACM, 2006, pp. 233–240.

[127] H. Kim and K. G. Shin, "Efficient discovery of spectrum opportunities with mac-layer sensing in cognitive radio networks," *IEEE Transactions on Mobile Computing*, vol. 7, no. 5, pp. 533–545, May 2008. [Online]. Available: http://dx.doi.org/10.1109/TMC.2007.70751

[128] J. Ma, X. Zhou, and G. Li, "Probability-based periodic spectrum sensing during secondary communication," *Communications, IEEE Transactions on*, vol. 58, no. 4, pp. 1291–1301, April 2010.

[129] C. Ghosh, S. Roy, and M. B. Rao, "Modeling and validation of channel idleness and spectrum availability for cognitive networks," *Selected Areas in Communications, IEEE Journal on*, vol. 30, no. 10, pp. 2029–2039, November 2012.

[130] M. Wellens and P. Mahonen, "Lessons learned from an extensive spectrum occupancy measurement campaign and a stochastic duty cycle model," in *Testbeds and Research Infrastructures for the Development of Networks Communities and Workshops, 2009. TridentCom 2009. 5th International Conference on*, April 2009, pp. 1–9.

[131] C. Ghosh, S. Pagadarai, D. Agrawal, and A. M. Wyglinski, "A framework for statistical wireless spectrum occupancy modeling," *Wireless Communications, IEEE Transactions on*, vol. 9, no. 1, pp. 38–44, January 2010.

[132] M. Wellens, J. Riihijarvi, M. Gordziel, and P. Mahonen, "Spatial statistics of spectrum usage: From measurements to spectrum models," in *Communications, 2009. ICC '09. IEEE International Conference on*, June 2009, pp. 1–6.

[133] M. Lopez-Benitez and F. Casadevall, "Statistical prediction of spectrum occupancy perception in dynamic spectrum access networks," in *Com-*

munications (ICC), 2011 IEEE International Conference on, June 2011, pp. 1–6.

[134] M. Lopez-Benitez and F. Casadevall, "Spatial duty cycle model for cognitive radio," in *Personal Indoor and Mobile Radio Communications (PIMRC), 2010 IEEE 21st International Symposium on*, Sept 2010, pp. 1631–1636.

[135] R. Chavez-Santiago, K. Nolan, O. Holland, L. De Nardis, J. Ferro, N. Barroca, L. Borges, F. Velez, V. Goncalves, and I. Balasingham, "Cognitive radio for medical body area networks using ultra wideband," *Wireless Communications, IEEE*, vol. 19, no. 4, pp. 74–81, August 2012.

[136] S. Sharma, S. Chatzinotas, and B. Ottersten, "Spectrum sensing in dual polarized fading channels for cognitive satcoms," in *Global Communications Conference (GLOBECOM), 2012 IEEE*, Dec 2012, pp. 3419–3424.

[137] F. Liu, C. Feng, C. Guo, Y. Wang, and D. Wei, "Polarization spectrum sensing scheme for cognitive radios," in *Wireless Communications, Networking and Mobile Computing, 2009. WiCom '09. 5th International Conference on*, Sept 2009, pp. 1–4.

[138] *NI USRP-292x/293x Datasheet*, 2009, [Online]. Available: http://www.ni.com/datasheet/pdf/en/ds-355.

[139] T. Harrold, R. Cepeda, and M. Beach, "Long-term measurements of spectrum occupancy characteristics," in *New Frontiers in Dynamic Spectrum Access Networks (DySPAN), 2011 IEEE Symposium on*, May 2011, pp. 83–89.

[140] A. Palaios, J. Riihijarvi, O. Holland, and P. Mahonen, "A week in london: Spectrum usage in metropolitan london," in *Personal Indoor and Mobile Radio Communications (PIMRC), 2013 IEEE 24th International Symposium on*, Sept 2013, pp. 2522–2527.

[141] A. Law, *Simulation Modeling and Analysis*, ser. McGraw-Hill series in industrial engineering and management science. McGraw-Hill, 2007. [Online]. Available: http://books.google.co.uk/books?id=0S1TngEACAAJ

[142] R. Ash, *Real analysis and probability*, ser. Probability and mathematical statistics. Academic Press, 1972. [Online]. Available: http://books.google.co.uk/books?id=0iTvAAAAMAAJ

Appendix A | *Derivations*

A.1 Derivation of expression (3.19)

For the first order i.e., $M = 1$, the average probability of detection is expressed as

$$\begin{aligned}\bar{P}_{d_{TWDP}} = a_i \frac{K+1}{2\bar{\gamma}} \Bigg[& exp(K(a_i-1)) \int_0^\infty Q_u(\sqrt{2\gamma}, \sqrt{\lambda}) \\ & exp\bigg(- \frac{(K+1)\gamma}{\bar{\gamma}} \bigg) I_0 \bigg(2\sqrt{\frac{K(K+1)(1-a_i)\gamma}{\bar{\gamma}}} \bigg) d\gamma \\ & + exp(-K(a_i+1)) \int_0^\infty Q_u(\sqrt{2\gamma}, \sqrt{\lambda}) \\ & exp\bigg(- \frac{(K+1)\gamma}{\bar{\gamma}} \bigg) I_0 \bigg(2\sqrt{\frac{K(K+1)(1+a_i)\gamma}{\bar{\gamma}}} \bigg) d\gamma \end{aligned} \tag{A.1}$$

By substituting for $x = \sqrt{2\gamma}$ (A.1) can be rewritten

$$\begin{aligned}\bar{P}_{d_{TWDP}} = a_i \frac{K+1}{2\bar{\gamma}} \Bigg[& exp(K(a_i-1)) \int_0^\infty Q_u(x, \sqrt{\lambda}) \\ & exp\bigg(- \frac{(K+1)\gamma}{\bar{\gamma}} \bigg) I_0 \bigg(2\sqrt{\frac{K(K+1)(1-a_i)\gamma}{\bar{\gamma}}} \bigg) x dx \\ & + exp(-K(a_i+1)) \int_0^\infty Q_u(x, \sqrt{\lambda}) \\ & exp\bigg(- \frac{(K+1)\gamma}{\bar{\gamma}} \bigg) I_0 \bigg(2\sqrt{\frac{K(K+1)(1+a_i)\gamma}{\bar{\gamma}}} \bigg) x dx \end{aligned} \tag{A.2}$$

For $u = 1$ the integrals in (A.2) can be solved according to [92, eq. (45)] following that

$$\int_0^\infty Q_u(ax, b) exp\left(- \frac{p^2 x^2}{2} \right) I_0(cx) x dx = \left(\frac{c^2}{2p^2} \right) Q\left(\frac{ac}{p\sqrt{p^2 + a^2}}, \frac{bp}{\sqrt{p^2 + a^2}} \right) \tag{A.3}$$

with $a = 1$, $b = \sqrt{\lambda}$, $p = \sqrt{\frac{K+1}{\bar{\gamma}}}$, and $c = 2\sqrt{\frac{K(K+1)(1 \pm a_i)}{2\bar{\gamma}}}$

For all approximation orders M, the average probability of detection is given as a summation by

$$\bar{P}_{d_{TWPD}} = \sum_{i=1}^{M} \frac{1}{2} a_i \left[Q\left(\sqrt{\frac{2K\bar{\gamma}(1 - a_i)}{K + \bar{\gamma} + 1}}, \sqrt{\frac{\lambda(K+1)}{K + \bar{\gamma} + 1}} \right) + Q\left(\sqrt{\frac{2K\bar{\gamma}(1 + a_i)}{K + \bar{\gamma} + 1}}, \sqrt{\frac{\lambda(K+1)}{K + \bar{\gamma} + 1}} \right) \right] \tag{A.4}$$

A.2 Derivation of expression (3.42)

Based on [92, eq. (9)],

$$\frac{\partial Q_m(a, b)}{\partial b} = -b \left(\frac{b}{a} \right)^{m-1} exp\left(- \frac{a^2 + b^2}{2} \right) I_{m-1}(ab) \tag{A.5}$$

For $m = 1$, (A.5) can be rewritten as

$$\frac{\partial Q_m(a, b)}{\partial b} = -b exp\left(- \frac{a^2 + b^2}{2} \right) I_0(ab) \tag{A.6}$$

From (3.42) $a = \sqrt{\frac{2K\bar{\gamma}(1-a_i)}{K+\bar{\gamma}+1}}$ and $b = \sqrt{\frac{\lambda(K+1)}{K+\bar{\gamma}+1}}$. By applying the chain rule yields,

$$\begin{aligned}
&\frac{\partial P_d}{\partial \lambda} = -\frac{(K+1)}{2\big(\frac{\lambda(K+1)}{K+\bar{\gamma}+1}\big)^{\frac{1}{2}}(K+\bar{\gamma}+1)} \\
&\sum_{i=1}^{M} \frac{1}{2} a_i \Bigg[exp\Bigg(-\frac{2K\bar{\gamma}(1-a_i)+\lambda(K+1)}{2(K+\bar{\gamma}+1)} \Bigg) \\
&I_0\Bigg(\frac{2K\bar{\gamma}\lambda(K+1)(1-a_i)}{(K+\bar{\gamma}+1)^2} \Bigg) + \\
&exp\Bigg(-\frac{2K\bar{\gamma}(1+a_i)+\lambda(K+1)}{2(K+\bar{\gamma}+1)} \Bigg) \\
&I_0\Bigg(\frac{2K\bar{\gamma}\lambda(K+1)(1+a_i)}{(K+\bar{\gamma}+1)^2} \Bigg) \Bigg]
\end{aligned} \tag{A.7}$$